

General Disclaimer

One or more of the Following Statements may affect this Document

- This document has been reproduced from the best copy furnished by the organizational source. It is being released in the interest of making available as much information as possible.
- This document may contain data, which exceeds the sheet parameters. It was furnished in this condition by the organizational source and is the best copy available.
- This document may contain tone-on-tone or color graphs, charts and/or pictures, which have been reproduced in black and white.
- This document is paginated as submitted by the original source.
- Portions of this document are not fully legible due to the historical nature of some of the material. However, it is the best reproduction available from the original submission.

DOE/NASA/0167-81/2 ✓
NASA CR-165329 ✓
GARRETT NO. 31-3725(2)

**ADVANCED GAS TURBINE (AGT)
POWERTRAIN SYSTEM DEVELOPMENT
FOR AUTOMOTIVE APPLICATIONS**

**SECOND SEMIANNUAL PROGRESS REPORT
(JULY 1980 - DECEMBER 1980)**

Engineering Staff of
Garrett Turbine Engine Company
A Division of The Garrett Corporation

July 1981

(NASA-CR-165329) ADVANCED GAS TURBINE (AGT)
POWERTRAIN SYSTEM DEVELOPMENT FOR AUTOMOTIVE
APPLICATIONS Semiannual Progress Report,
Jul. - Dec. 1980 (Garrett Turbine Engine
Co.) 151 p HC A08/MF A01

N83-13038

Unclass
00872

Prepared for

CSCI 13F G3/85

**NATIONAL AERONAUTICS AND SPACE ADMINISTRATION
Lewis Research Center
Cleveland, Ohio 44135
Under Contract DEN3-167**



**for
U.S. DEPARTMENT OF ENERGY
Office of Transportation Programs
Division of Automotive Technology Development
Washington D.C. 20585**

DOE/NASA/0167—81/2

NASA CR-165329

GARRETT NO. 31-3725(2)

**ADVANCED GAS TURBINE (AGT)
POWERTRAIN SYSTEM DEVELOPMENT
FOR AUTOMOTIVE APPLICATIONS**

**SECOND SEMIANNUAL PROGRESS REPORT
(JULY 1980 - DECEMBER 1980)**

Engineering Staff of
Garrett Turbine Engine Company
A Division of The Garrett Corporation

July 1981

Prepared for
NATIONAL AERONAUTICS AND SPACE ADMINISTRATION
Lewis Research Center
Cleveland, Ohio 44135
Under Contract DEN3-167

**for
U.S. DEPARTMENT OF ENERGY
Office of Transportation Programs
Division of Automotive Technology Development
Washington D.C. 20585**

TABLE OF CONTENTS

	<u>Page</u>
1.0 SUMMARY	1
2.0 INTRODUCTION	10
3.0 POWERTRAIN DEVELOPMENT	17
3.1 Reference Powertrain Design (RPD)	18
3.2 Performance	21
3.3 Fabrication	26
3.4 Contractor's Vehicle	27
4.0 COMPONENT/SUBSYSTEM DEVELOPMENT	28
4.1 Compressor Development	29
4.2 Turbine Development	34
4.3 Combustion System	43
4.4 Regenerator	48
4.5 Gearbox/Transmission	54
4.6 Ceramic Structures	56
4.7 Ceramic Component Development	58
4.8 Foil Gas Bearing	91
4.9 Bearings and Seals	95
4.10 Rotor Dynamics Development	98
4.11 Controls and Accessories	102
APPENDIX I FORD MOTOR COMPANY ADVANCED GAS TURBINE (AGT) POWERTRAIN PROGRAM SECOND SEMI-ANNUAL TECHNICAL PROGRESS REPORT	107
APPENDIX II AIRESEARCH CASTING COMPANY (ACC) ADVANCED GAS TURBINE (AGT) POWERTRAIN PROGRAM SECOND SEMI-ANNUAL TECHNICAL PROGRESS REPORT	127
APPENDIX III CARBORUNDUM COMPANY ADVANCED GAS TURBINE (AGT) POWERTRAIN PROGRAM SECOND SEMI-ANNUAL TECHNICAL PROGRESS REPORT, COMMON WORK	134
APPENDIX IV CARBORUNDUM COMPANY ADVANCED GAS TURBINE (AGT) POWERTRAIN PROGRAM SECOND SEMI-ANNUAL TECHNICAL PROGRESS REPORT, UNIQUE WORK	142
APPENDIX V PURE CARBON COMPANY ADVANCED GAS TURBINE (AGT) POWERTRAIN PROGRAM SECOND SEMI-ANNUAL TECHNICAL PROGRESS REPORT	148
REFERENCES PROCEEDINGS FROM SEMI-ANNUAL MEETINGS	150

1.0 SUMMARY

This report describes progress and work performed by the Garrett/Ford team to develop an Advanced Gas Turbine (AGT) powertrain system for automotive applications, for the period July through December 1980. The work was performed for the Department of Energy under NASA Contract DEN3-167. This is the second in a series of planned reports. Work performed during the first period (Reference 1) initiated design and analysis, ceramic development and component testing.

During this reporting period, accomplishments included:

- o Completion of Mod I, Build 1 (1600°F, all metal engine) component detail design and associated component test rigs
- o Completion of Mod I engine (2100°F, metal turbine rotor, ceramic structures) detail design
- o Initiation of hardware procurement and fabrication of the Mod I, Build 1 powertrain (engine, gearbox, transmission)
- o Completion of regenerator cold flow testing (low pressure and high pressure), single foil bearing and VSTC testing
- o Initiation of testing on the combustor autoignition/element rig, Ford regenerator static seal leakage rig and ceramic test bars
- o Spin test of the initial ceramic simulated turbine rotor (provided by Carborundum)
- o Continuation of ceramic subcontractor efforts to develop material strengths and fabrication processes for the ceramic turbine rotor and ceramic structures
- o Continuation of associated planning, management and reporting

As noted herein, progress through December 1980 indicates that all contract goals, objectives, and milestones will be achieved on schedule, including first test of the Mod 1, Build 1 powersection in July 1981.

Salient features of the AGT powertrain system, as noted in Reference 1, are repeated in the remainder of this section as a ready summary for the reader. No significant changes have been made to the design, or performance predictions, during this reporting period.

The AGT101 Powertrain, pictorially shown in Figure 1, consists of a regenerated single-shaft gas turbine engine power section (flat-rated at 100 horsepower), a split differential gearbox, and a Ford Automatic Overdrive (AOD) production transmission. The powertrain is controlled by an electronic digital microprocessor and associated actuators, instrumentation, and sensors. Standard automotive accessories are driven by engine power provided by an accessory pad on the gearbox.

The AGT101 power section, Figure 2, is characterized by a single-stage, 5:1, backward-swept centrifugal compressor and single-stage ceramic radial inflow turbine mounted on a common shaft. This rotating group is supported at the output pinion gear by an angular-contact ball bearing and an air-lubricated foil bearing located between the compressor and turbine. Maximum rotor speed of the AGT101 is 100,000 rpm. Ceramic combustor and hot-section structural components are utilized in conjunction with the ceramic radial turbine rotor. This allows engine operation at turbine inlet temperatures (TIT) of 2500°F (maximum power) and 2150°F (idle) to maintain maximum thermodynamic efficiency over the operating range. Variable geometry has been utilized in the compressor and combustion sections to vary engine airflow and control combustion primary-zone temperatures to approximately 3000°F. Table 1 summarizes the power section salient features.

The gearbox, Figure 3, is a split-path differential design accepting power directly from the output pinion gear. Power is split in the differential planetary gears with a portion taken through an output gear on the planetary carrier directly to the AOD transmission. The remaining power continues via the same differential planetary to a rotating ring gear and associated gear train to the variable stator torque converter (VSTC). The VSTC provides a variable speed ratio output that is fed back to the planetary carrier and combines with the power delivered to the transmission.

AGT101 powertrain development was initiated in October 1979 through detail design activities based on prior studies. Design efforts on the reference powertrain design (RPD) were approved in January 1980 by NASA. Evolutionary progress toward realization of the RPD continued with design approval of the Mod I powertrain concept in April 1980.

As shown in Figure 4, AGT101 evolution begins with the Mod I, Build 1 all-metallic (except regenerator) engine version. As ceramic hot-section structural components are qualified in dedicated test

ORIGINAL PAGE IS
OF POOR QUALITY

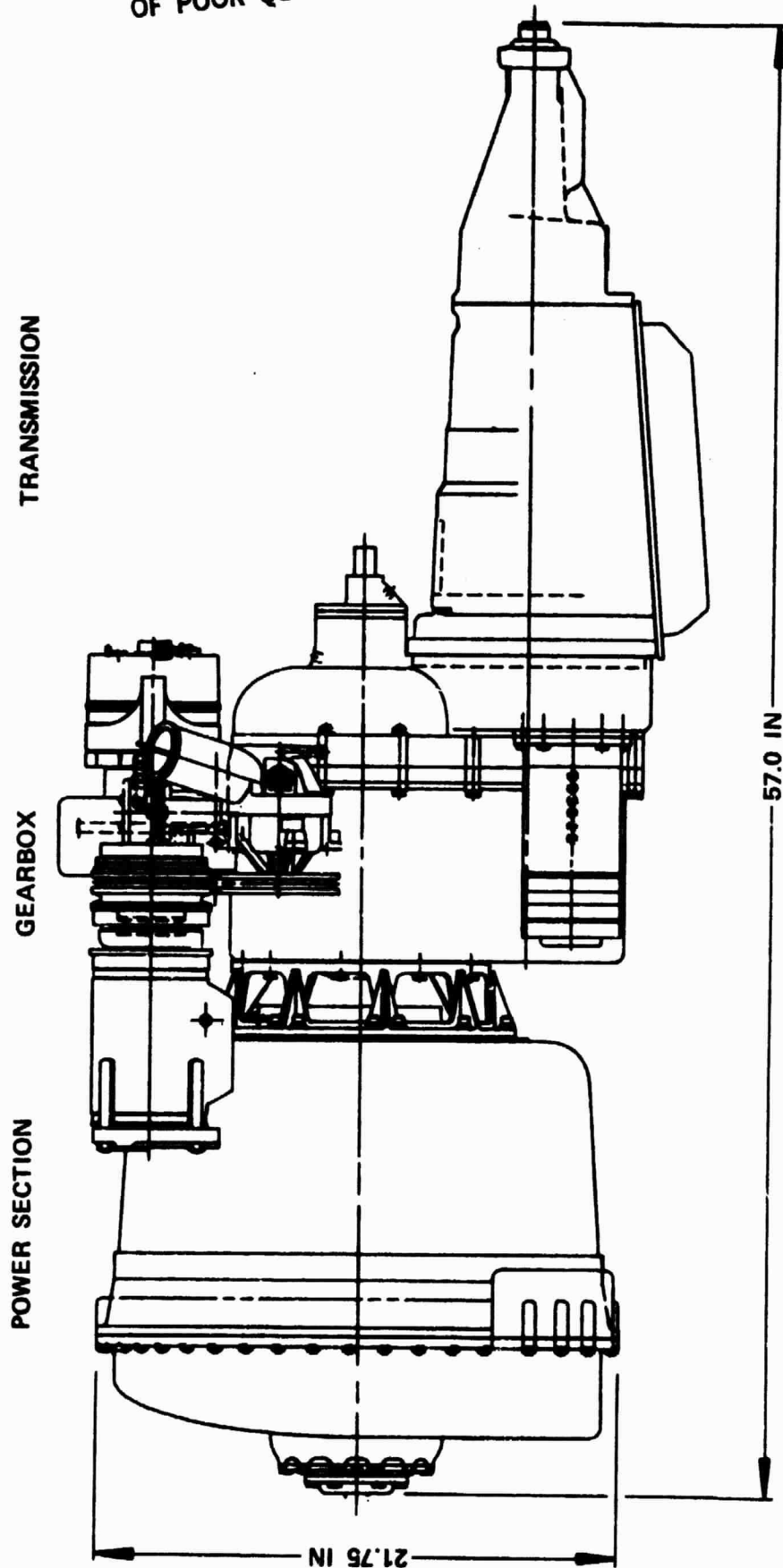


Figure 1. AGT101 Powertrain.

ORIGINAL PAGE IS
OF POOR QUALITY

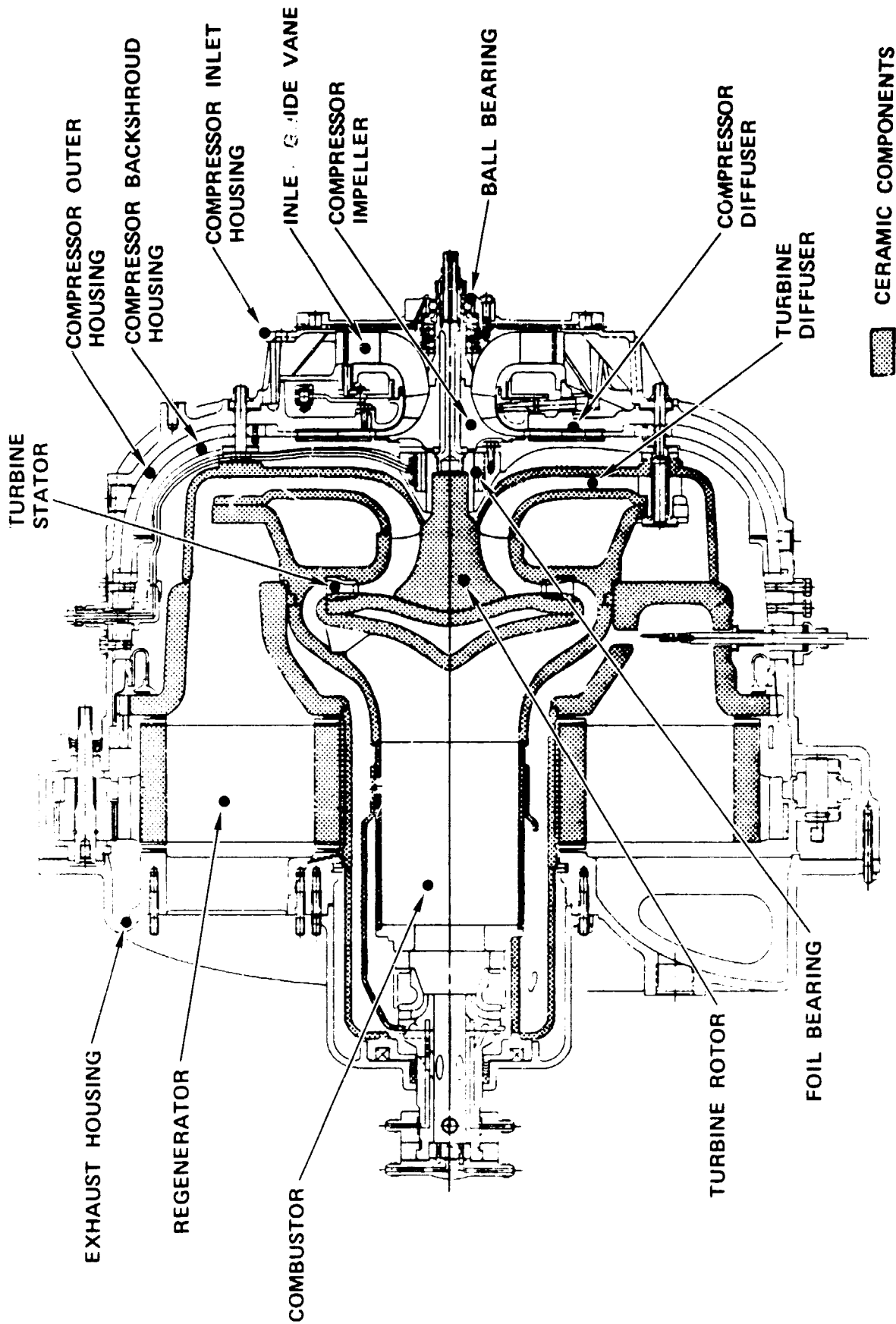


Figure 2. AGT101 Power Section Layout.

TABLE 1. AGT101 MOD II DESIGN SUMMARY (MAXIMUM POWER)

COMPRESSOR - CENTRIFUGAL

Material	Aluminum
Design flow, lbs/sec	0.85
Number of blades/splitters	12/12
Backward curvature, degrees	50
VIGV type, number of vanes	Articulated, 17
Diffuser type	2D vane island, cascade deswirl
Predicted stage efficiency, percent	80.5

TURBINE - RADIAL INFLOW

Material	SiC or Si ₃ N ₄
Maximum inlet temperature, °F	2500
Maximum tip speed, fps	2300
Number of blades	13
Stator type, number of vanes	Radial, 19
Diffuser type	Radial
Predicted stage efficiency, percent	90.1

REGENERATOR - ROTARY

Material, fabrication process	AS or MAS, extruded
Active matrix diameter, in	18.2
Matrix thickness, in	3.3
Hydraulic diameter, in	0.020
Support type, drive	Rim, rim drive
Predicted effectiveness, percent	92.9
Predicted seal leakage, percent	3.6

COMBUSTOR - PILOTED, VARIABLE GEOMETRY

Material	Ceramic
Outlet temperature, °F	2150 to 2500
Maximum primary zone temperature, °F	3000

BALL BEARING - SPLIT INNER RACE, ANGULAR CONTACT

Material	52100
Size, mm	15
Maximum load - radial/axial, lbs	9/255

FOIL BEARING

Number of foils	7
Diameter, in	1.35
Length, in	1.075
Maximum load - steady state, lbs	3
Maximum load - shock, g's	X6

ORIGINAL PAGE IS
OF POOR QUALITY

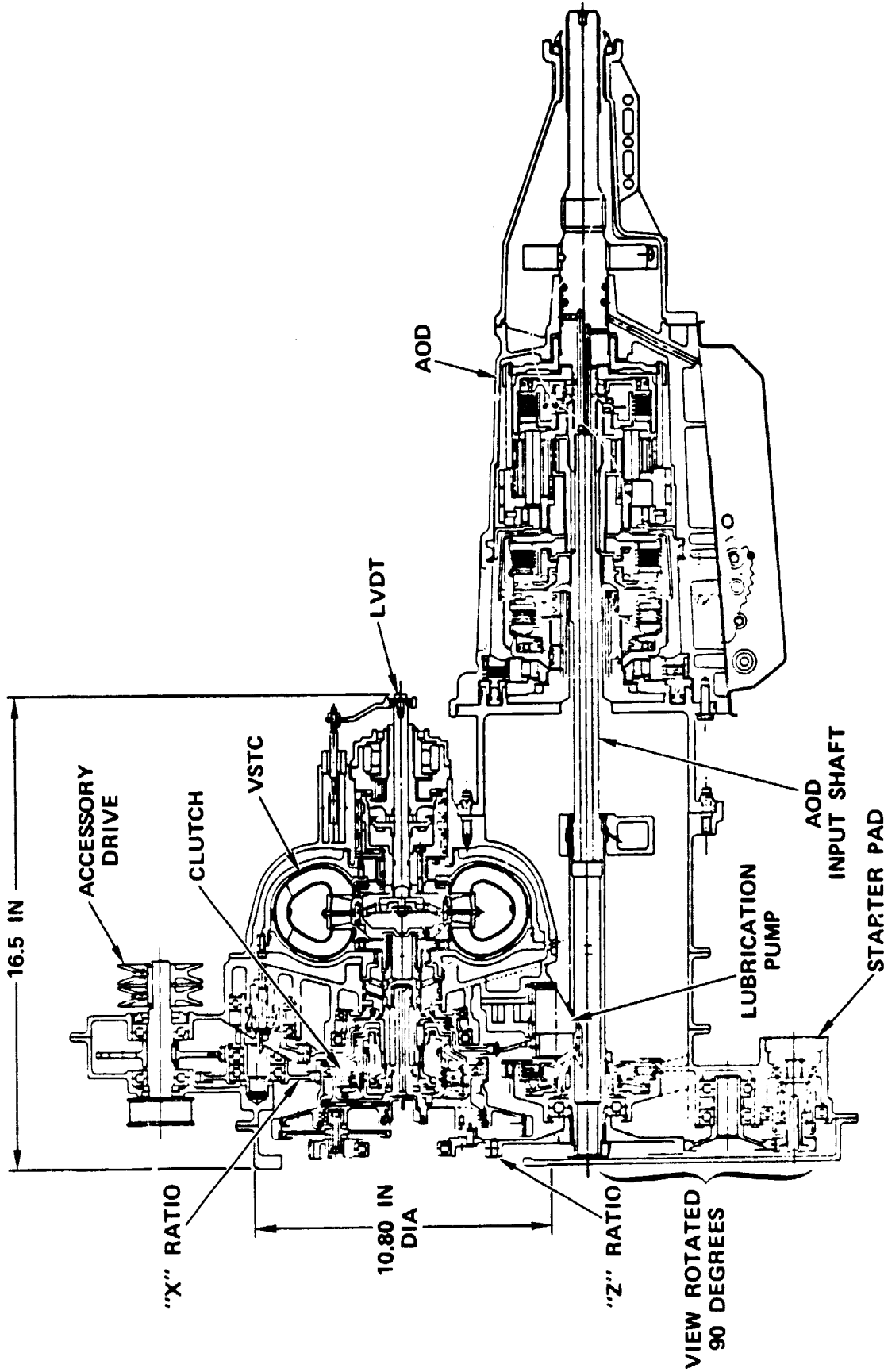


Figure 3. AGT101 Gearbox and Transmission Layout.

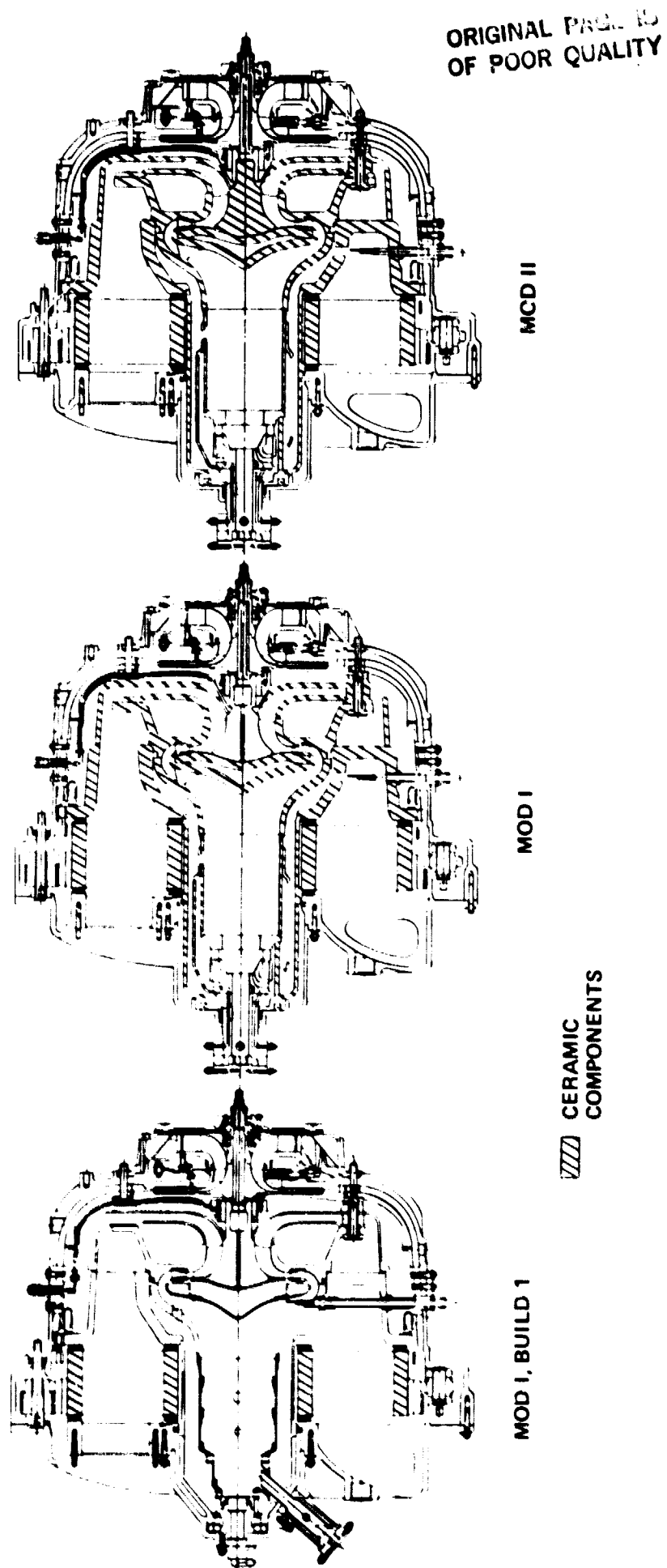


Figure 4. ACT101 Ceramic Evolution.

rigs, the Mod I, Build 1 is selectively upgraded to the Mod I concept (2100°F TIT, metal rotor, ceramic structures). This stepwise evolutionary process enables early verification of component technology development, controls interface, and validation of computer programs used to predict engine performance. In addition, based on "systems design" philosophy wherein distinct recognition is given to the AGT101 operating range over the combined federal driving cycle (CFDC), an interactive component/engine design feedback loop is established to further optimize program goals (i.e., fuel economy, driveability, emissions, etc.). The evolutionary process continues with the introduction of the ceramic radial turbine rotor into the Mod I powertrain. This configuration, entitled Mod II, currently is equivalent to the RPD. Incorporation of the ceramic rotor will allow TIT to be increased to 2500°F. Mod I equipped vehicles will be delivered to EPA prior to July 1984 for evaluation and demonstration of progress toward program goals. Mod II equipped vehicles will be delivered prior to July 1985 for final evaluation. Table 2 shows the AGT101 powertrain performance summary and salient component configuration.

ORIGINAL PAGE IS
OF POOR QUALITY

TABLE 2. AGT101 POWERTRAIN SUMMARY

	MOD I BUILD I	MOD I	MOD II	RPD
CFDC (MPG), (DF-2, 50°F, SEA LEVEL)	N/A	34	42.8	42.8
CRUISE SFC	0.503	0.388	0.329	0.329
RPM (MAX)	100,000	100,000	86,829	86,829
MAXIMUM POWER (HP NET)	50.0	83.6	100.0	100.0
TURBINE INLET MAX TEMP (°F)	1,800	2,100	2,500	2,500
REGENERATOR MAX TEMP (°F)	1,441	1,837	2,000	2,000
POWERSECTION CONFIGURATION				
COMPRESSOR	2219 T6	P M ALUM	P M ALUM	P M ALUM
COMBUSTOR	DIFF FLAME	VAR GEOM	VAR GEOM	VAR GEOM
TURBINE	METAL	METAL	CERAMIC	CERAMIC
REGENERATOR	NGK-THICK*	CORNING THIN	THIN*	THIN*
STRUCTURES	METAL	CERAMIC	CERAMIC	CERAMIC
CONTROLS CONFIGURATION	ANALOG	DIGITAL	DIGITAL	DIGITAL

*EXTRUDED CORE

2.0 INTRODUCTION

This report is the second in a series of Semi-Annual Technical Summary reports for the Advanced Gas Turbine (AGT) Powertrain System Development Project, authorized under NASA Contract DEN3-167 and sponsored by The Department of Energy. This report has been prepared by the Garrett Turbine Engine Company (hereinafter referred to as Garrett), a Division of The Garrett Corporation, and includes information provided by Ford Motor Company, The Carborundum Company, AiResearch Casting Company, and The Pure Carbon Company. The project is administered by Mr. Roger Palmer, Project Manager, NASA-Lewis Research Center, Cleveland, Ohio. This report presents plans and progress from July 1980 through December 1980.

Project effort conducted under this contract is part of the DOE Gas Turbine Highway Vehicle System Program. This program is oriented at providing the United States automotive industry the technology base necessary to produce gas turbine powertrains for automobiles that will have reduced fuel consumption and reduced environmental impact. It is intended that technology resulting from this program be capable of reaching the marketplace by the early 1990's.

The project goal is to develop and demonstrate, by July 1985, an advanced automotive gas turbine powertrain system which, when installed in a 1985 production vehicle of the Ford Fairmont class (3000 pounds inertia weight), meets the following objectives:

- o A CFDC fuel economy of 42.8 miles per gallon based on Environmental Protection Agency (EPA) test procedures and diesel No. 2 fuel. The AGT-powered vehicle shall give substantially the same overall vehicle driveability and performance as a comparable 1985 production vehicle powered by a conventional spark-ignition powertrain system (baseline system)

- o Gaseous emissions and particulate levels less than:

$$\text{NO}_x = 0.4 \text{ gm/mile}$$

$$\text{HC} = 0.41 \text{ gm/mile}$$

$$\text{CO} = 3.4 \text{ gm/mile}$$

and a total particulate of 0.2 gm/mile, using the same fuel as used for fuel economy measurements

- o Ability to use a variety of alternate fuels

Progress toward achieving these objectives will be demonstrated in dynamometer and vehicle testing of AGT powertrains at several points during the project. In addition to the demonstratable objectives, the following are system design objectives:

- o Reliability and life equal to or better than powertrains currently on the market
- o A competitive initial cost and a life cycle cost no greater than that of a comparable conventionally powered vehicle
- o Acceleration suitable for safety and consumer considerations
- o Noise and safety characteristics that meet currently legislated federal standards and those projected for 1984

The following are major contract milestones:

- o Complete initial RPD and Mod I powertrain preliminary design review (completed April 30, 1980)
- o Complete dynamometer characterization and assessment of first-build Mod I powertrain by July 31, 1982
- o Complete dynamometer characterization and assessment of Mod I powertrain by July 31, 1983
- o Complete vehicle testing of fuel economy and emissions using the Mod I powertrain system by July 31, 1984 (testing to be performed by the EPA on two vehicles)
- o Complete dynamometer characterization and assessment of Mod II powertrain prior to July 31, 1984
- o Complete vehicle testing of fuel economy and emissions using the Mod II powertrain system by July 31, 1985 (testing to be performed by the EPA on two vehicles)

The Advanced Automotive Gas Turbine Powertrain System has been designated the AGT101 and is shown installed in a 1980 Ford Fairmont in Figure 5. The AGT101 represents a significant advancement in gas turbine state-of-the-art. A significant quantity of ceramic parts are employed to enhance high-temperature operation and provide low-cost manufacturing potential for automotive application.

The AGT101 program team is depicted in Figure 6. Garrett is the prime contractor responsible for overall powertrain design and development and project management. Ford Motor Company, as a major subcontractor, is responsible for providing the vehicle-related tasks

ORIGINAL PAGE IS
OF POOR QUALITY

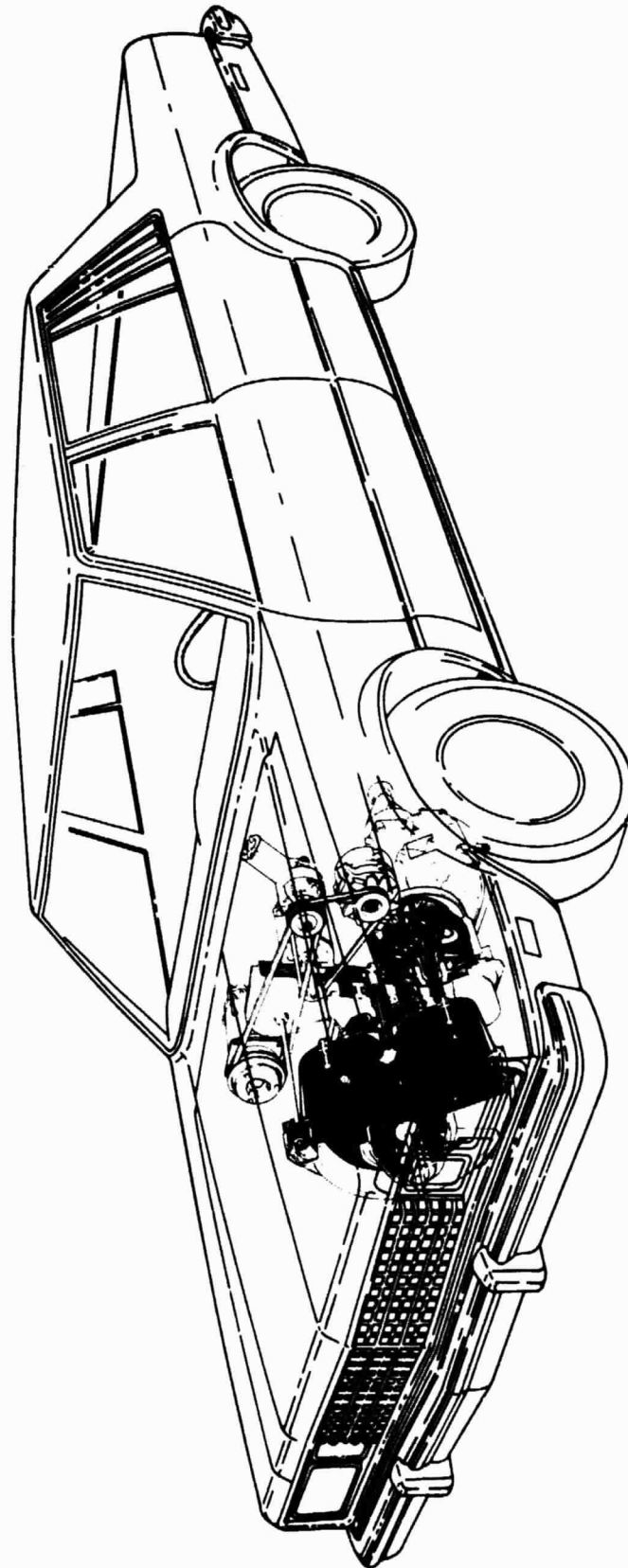


Figure 5. AGT Powertrain Installed in 1980 Ford Fairmont Vehicle.

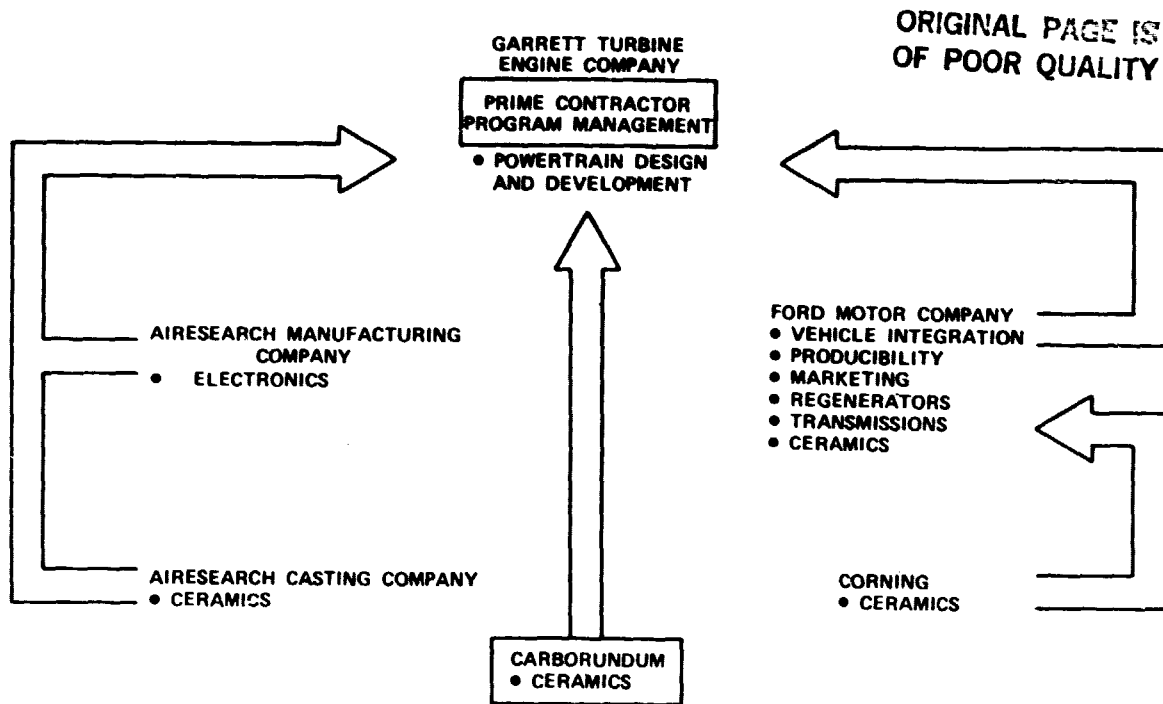


Figure 6. AGT101 Program Team.

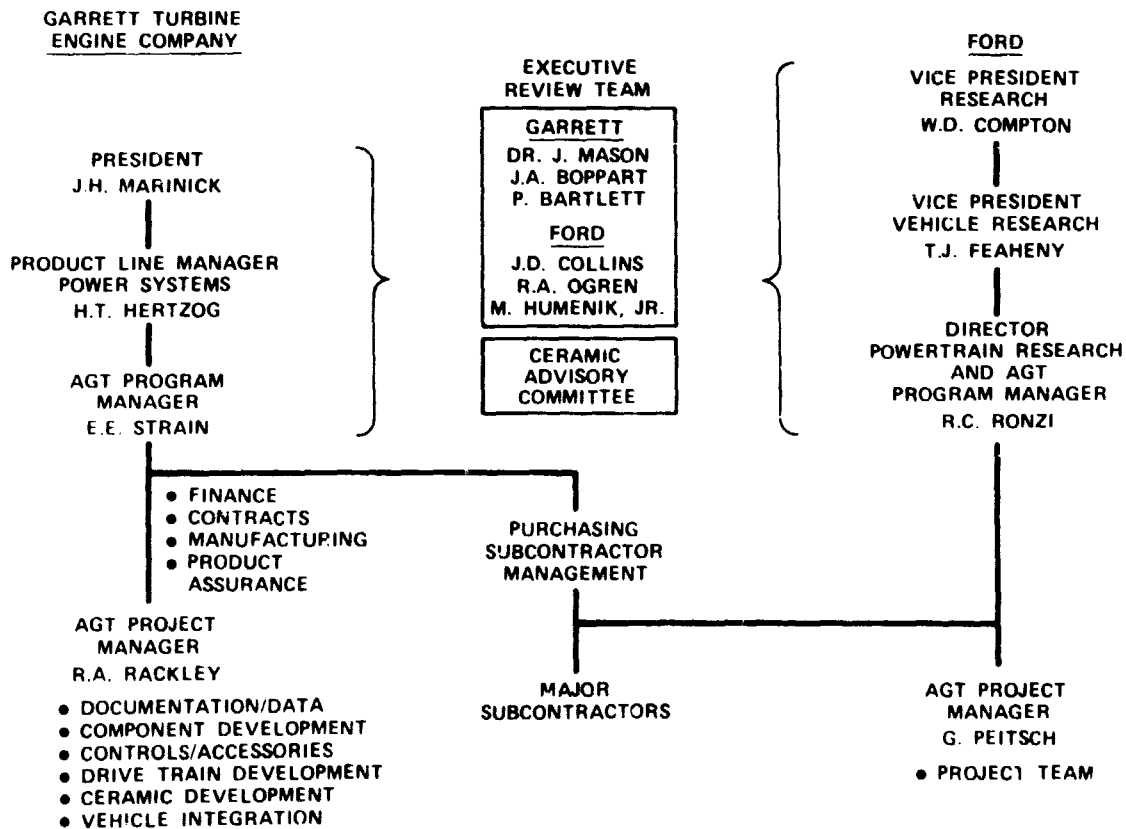


Figure 7. Garrett/Ford AGT101 Program Organization.

(i.e., production manufacturing and marketing studies), transmissions, regenerator technology, and major ceramic development efforts. The Corning Company is providing ceramic regenerator cores and one of the major ceramic structural components, under subcontract to Ford Motor Company. As shown in Figure 6, there are three other major subcontractors:

- o The Carborundum Company, a Division of Kennecott, located in Niagara Falls, New York, developing and providing ceramic components
- o AiResearch Casting Company, located in Torrance, California, also developing and providing ceramic components
- o AiResearch Manufacturing Company, located in Torrance, California, developing and providing the electronic control system

The Garrett/Ford AGT101 project team organization is shown on Figure 7. The Garrett organization falls under the Power Systems Product Line in Phoenix, Arizona while the Ford organization is located in the Research Department at Dearborn, Michigan. Both companies provide upper management visibility via an executive review team which meets on a quarterly basis to review progress. The team is comprised of three executives of various disciplines from each organization providing guidance to help assure the success of the AGT101 Project. In addition, a Ceramic Advisory Committee, comprised of members of both organizations, meets on a periodic basis to review ceramic development progress.

The AGT101 project schedule, shown in Figure 8, includes eight project tasks and six major contract milestones. Project duration is 70 months, comprised of Phase I (47 months) and Phase II (23 months). At the conclusion of Phase I, DOE and NASA will evaluate progress of the AGT project prior to initiating Phase II.

The RPD design (Task 1, Figure 8) reflects the ultimate powertrain configuration to be achieved at the end of this project. Ford may utilize the RPD as a baseline to proceed into automotive preproduction and production phases, which is the overall goal of the DOE Gas Turbine Highway Vehicle Systems Program. Mod I and Mod II are sequential development versions of the ultimate RPD powertrain. The Mod I engine begins with an all-metallic power section. As Mod I development progresses, ceramic structural parts will be integrated into the Mod I power section until, at the end of Phase I, all hot-section components will be ceramic except for the turbine rotor.

Mod II development begins with the inclusion of the ceramic turbine rotor into the final Mod I and continues through development to the end of Phase II.

ORIGINAL PAGE IS
OF POOR QUALITY

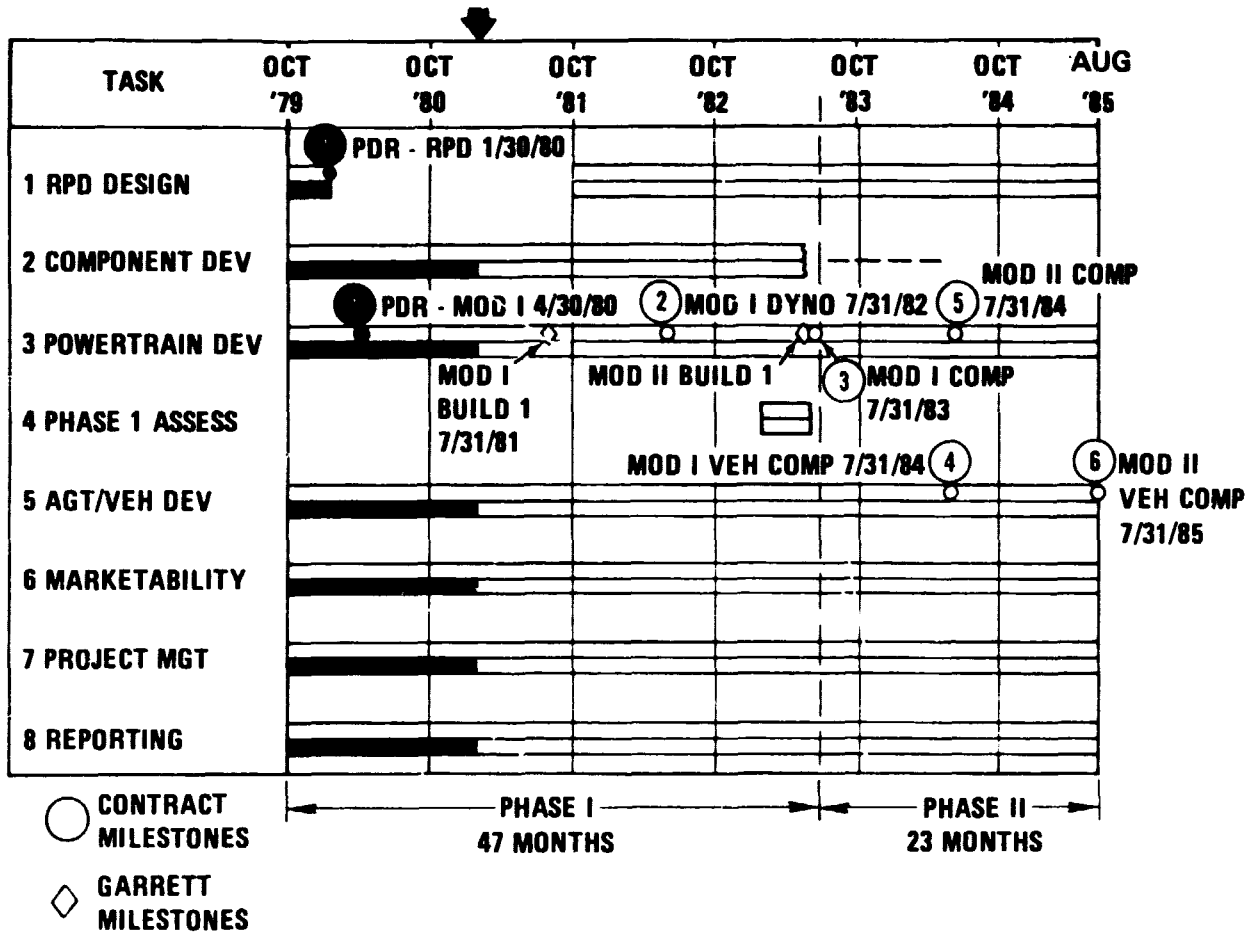


Figure 8. AGT101 Project Schedule.

Extensive component development is planned throughout the project (Task 2, Figure 8) and is discussed in Section 4 of this report. Powertrain development (Task 3) includes engine, gearbox, and transmission testing and is discussed in Section 3 herein. Vehicle development (Task 5) incorporates powertrains from Task 3 into production-styled vehicles, and provides for testing by Garrett and Ford and ultimately by the EPA. This task is also discussed in Section ..

3.0 POWERTRAIN DEVELOPMENT

Development of the AGT101 involves a series of sequential and parallel tasks as described in Reference 1. The first task was the analytical design of various components and subsystems. This task, which included preparation of the detail drawings, has been completed for the Mod I power sections (metallic and ceramic versions).

3.1 Mod I, Build 1 Powertrain Description

The power section shown in Figure 9 for the Mod I, Build 1 powertrain is structurally very similar to the Mod II power section except that simple symmetrical metal structures have been used in lieu of their ceramic counterparts in the Mod II design.

The structural load path for the Mod I replicates the Mod II load path, as shown in Figure 10. As in the Mod II power section design, a mechanical spring load (nominally 125 pounds) is applied to the combustor dome and holds the structural components in position when the engine is not operating.

The aerodynamic flow path for the Mod I, Build 1 power section, shown in Figure 10, is similar to the Mod II flow path. The major difference between the two designs is that the Mod I, Build 1 will incorporate a diffusion-flame combustor, whereas the Mod II will use a premixed/prevaporized variable-geometry combustor. Both designs include a pilot combustor to facilitate engine starting.

In summary the Mod I, Build 1 power section replicates the Mod II power section, with housings of similar configuration, identical mechanical load paths, and identical aerodynamic flow paths except for the combustion system.

ORIGINAL PAGE IS
OF POOR QUALITY

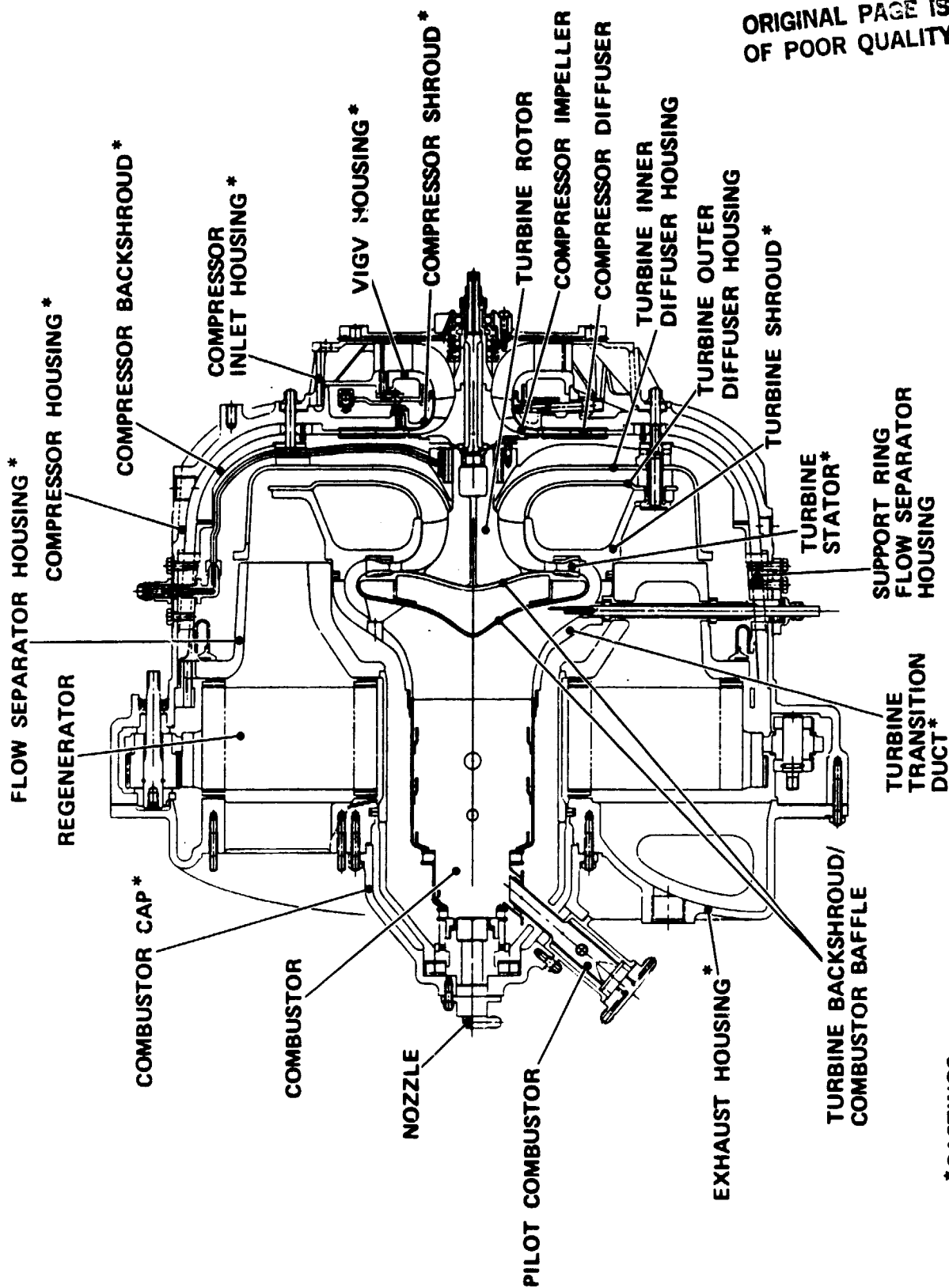


Figure 9. Mod I, Build 1 Power Section.

ORIGINAL PAGE IS
OF POOR QUALITY

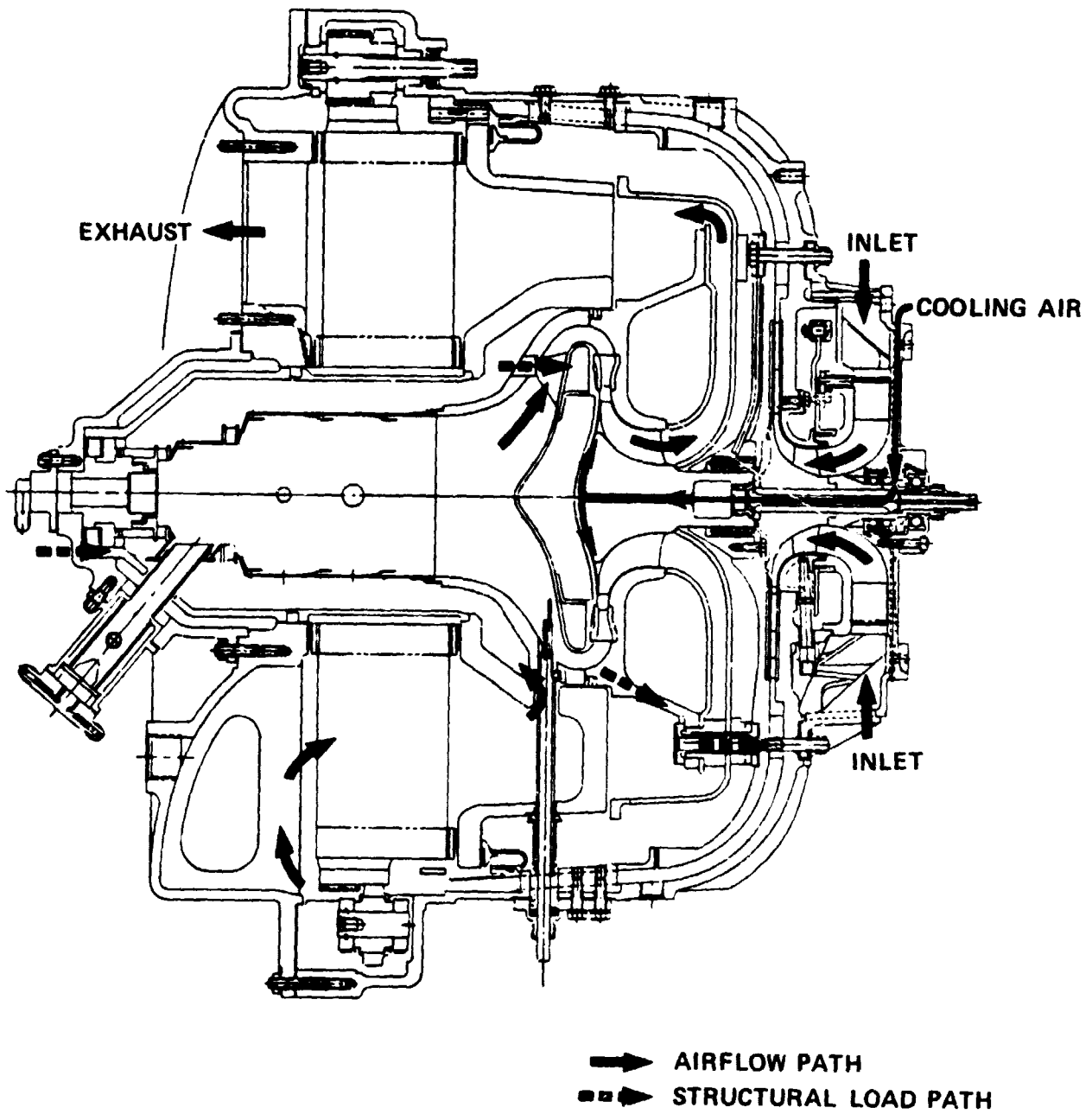


Figure 10. Mod I, Build 1 Power Section.

3.2 Performance

The engine and vehicle performance models are unchanged from those described in Reference 1, except that the gross vehicle weight (GVW) for the baseline vehicle is now 3000 pounds compared to 3163 pounds previously reported. Table 3 summarizes vehicle performance with the Mod II engine. Power schematics are shown in Figures 11 and 12 for the Mod II and Mod I engines respectively and are identical to those in Reference 1.

Figure 13 presents the revised optimization of engine idle and clutch engagement speeds. This revised optimization includes effects of correcting ambient conditions (59°F, sea level) and the GVW of 3000 pounds. At an engine idle speed of 48,900 rpm with a clutch engagement speed of 65,000 rpm, the AGT101 meets the 2-, 3-, and 4-second distance criteria while providing optimum fuel economy. These idle and clutch engagement speeds have minimal effect on 1-second distance.

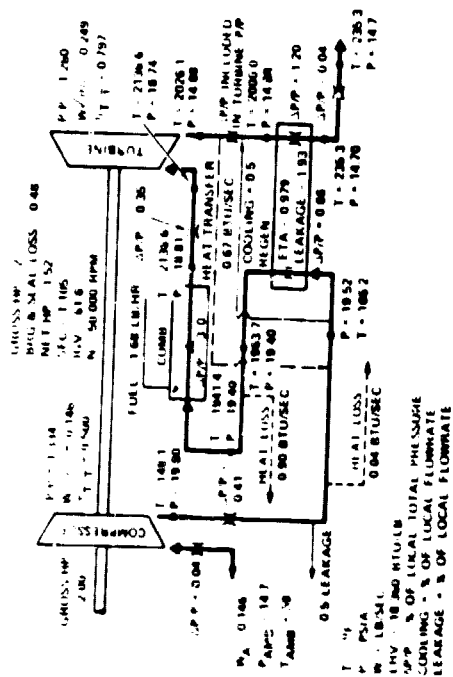
Figure 14 shows the predicted steady-state cruise mileage for the conditions of Table 3 for each gear range of the AOD.

TABLE 3. AGT101 VEHICLE PERFORMANCE WITH MOD II ENGINE
(DCER 5187, FLAT-RATED)

Gross Vehicle Weight - lb	3,000
Ambient Temperature - °F	59
Elevation	Sea level
2-Second Distance - ft	8.0
Idle Speed - krpm	48.9
Fuel	DF-2
LHV - Btu/lb	18,360
LHV - Btu/gal	130,650
CFDC Mileage - mpg	42.8

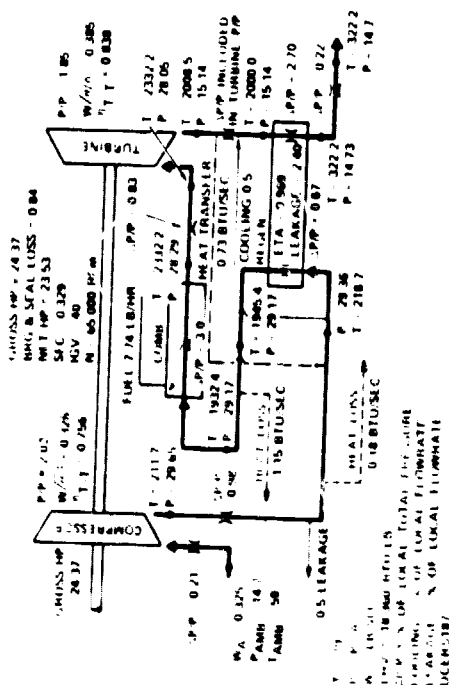
ORIGINAL PAGE IS
OF POOR QUALITY

IDLE



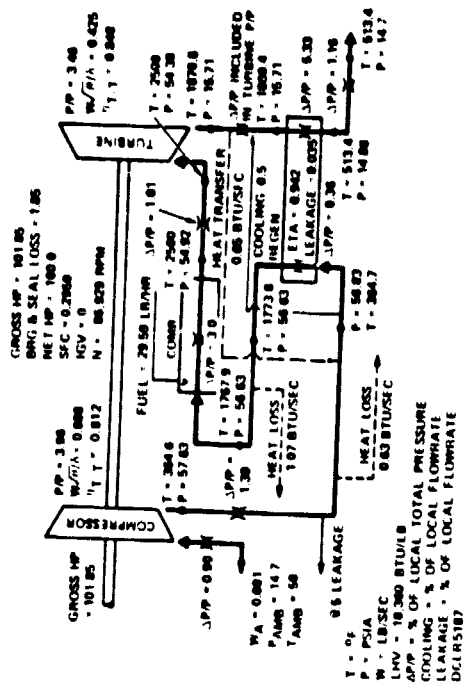
(a)

CRUISE



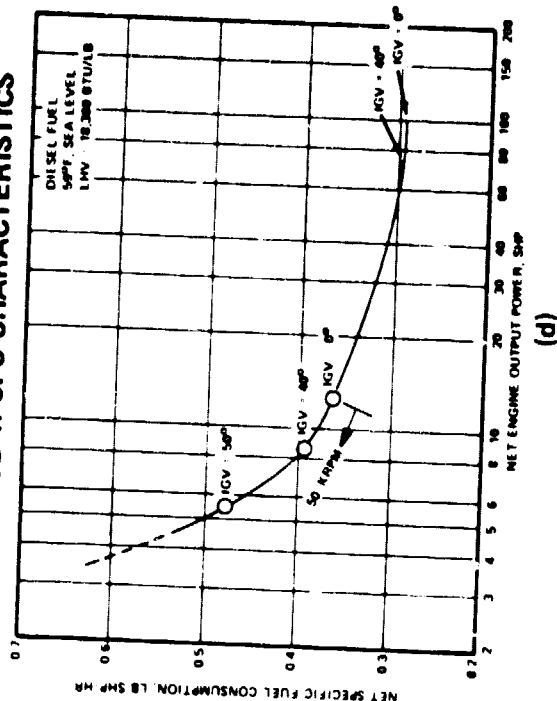
(c)

MAXIMUM POWER



(b)

AGT MOD II SFC CHARACTERISTICS



(d)

Figure 11. AGT101 Mod II Performance (59°F, Sea Level, Diesel Fuel No. 2).

ORIGINAL PAGE IS
OF POOR QUALITY

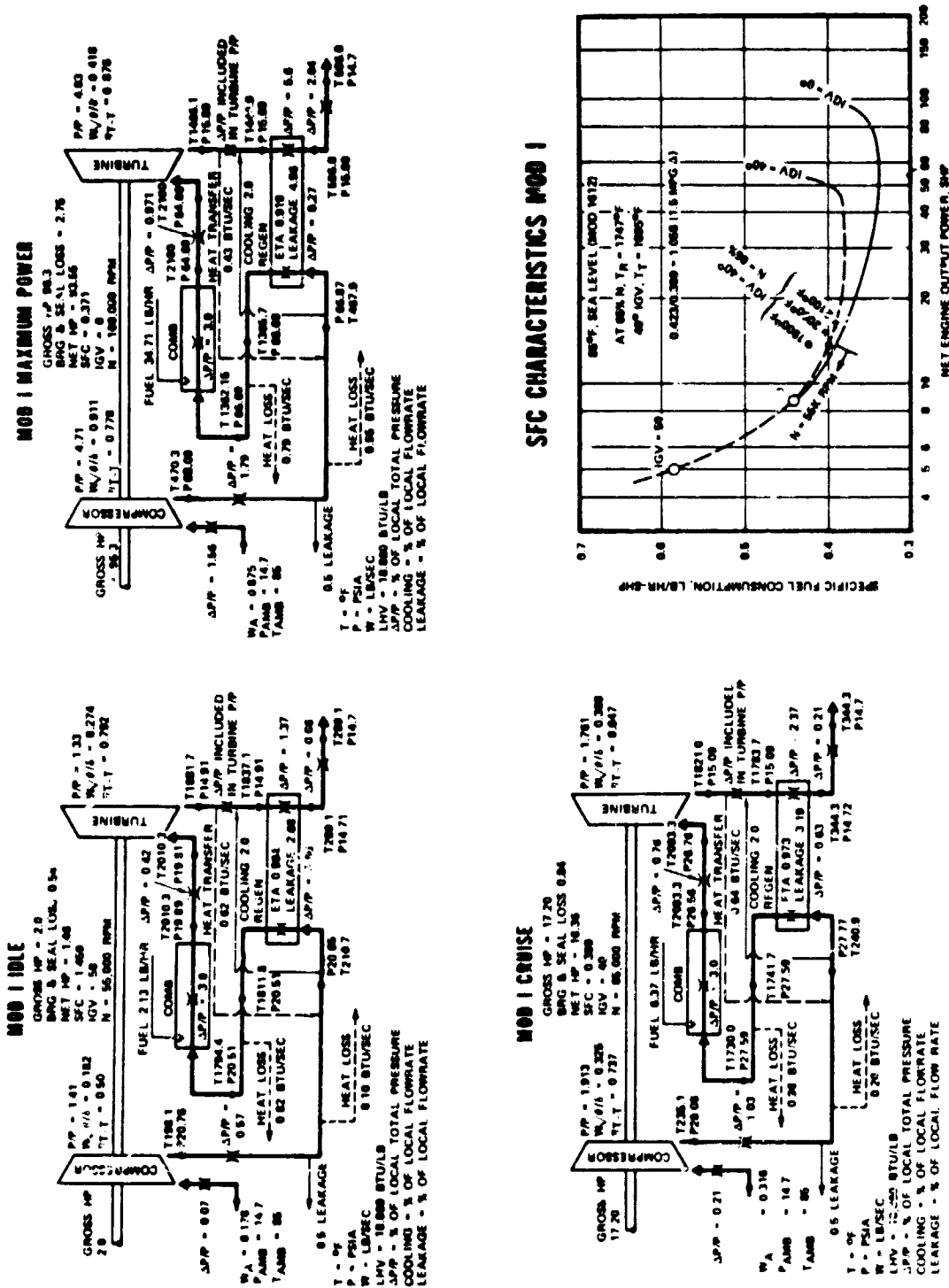


Figure 12. AGT101 Mod I Performance (85°F, Sea Level, Gasoline).

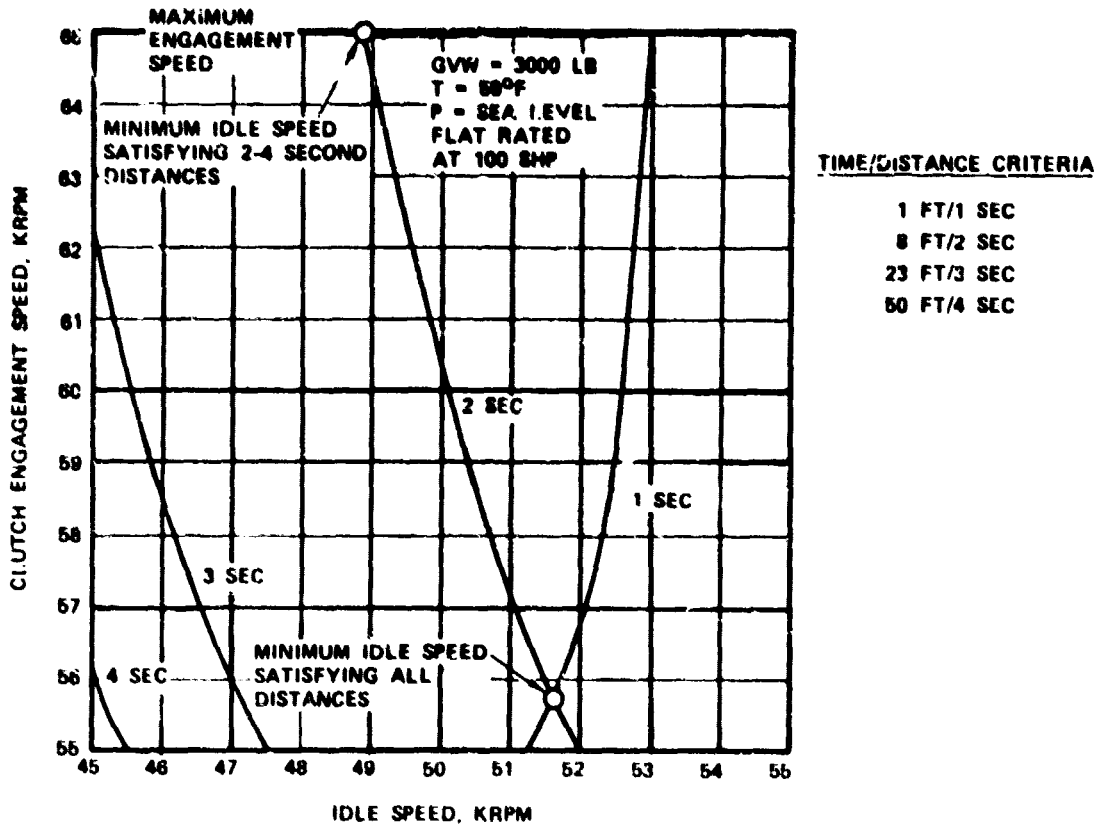


Figure 13. AGT101 Mod 11 Idle and Clutch Engagement Speeds.

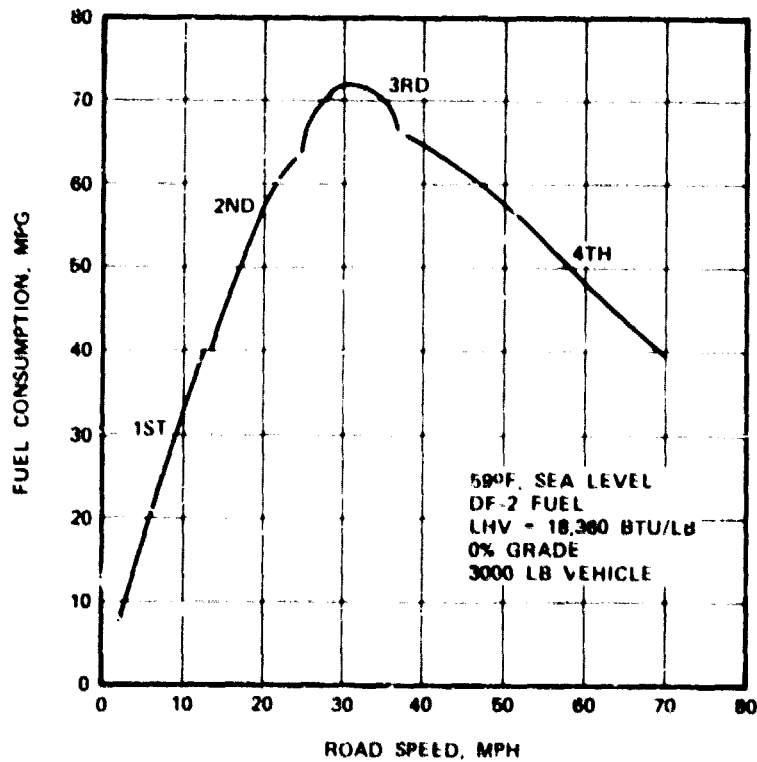


Figure 14. AGT101 Mod 11 Steady State Performance (Mileage Versus Road Speed).

3.3 Fabrication

Procurement of Mod I, Build 1 power section hardware was initiated as required to meet the planned start of test in July, 1981. Initial procurement efforts for the eleven major castings, shown in Figure 9, involved canvassing potential supplier foundry work loads, costs, and scheduling. Selected supplier comments were solicited with reference to simplified casting approaches, machining tolerances, and in-process fabrication techniques. All orders were placed by mid-September, 1980. Remaining power section hardware was placed on order during the reporting period and scheduled to meet the July, 1981 testing.

3.4 Contractor's Vehicle

The vehicle selected for the contractor's initial installation of the AGT101 will be a 1982 Fairmont, 4-door sedan, with a 2.73 axle ratio. Vehicle options include AM/FM radio, power steering, air conditioning, and a group special decor. For a GVW comparison, this vehicle will be 3002 pounds versus 3000 pounds for the reference vehicle with a 3.3 liter internal combustion engine.

The AGT101 passenger comfort system will obtain heat from the engine oil flow to the existing heater core. The heater plenum will be modified to include and auxiliary diesel- (or gasoline-) fired heater to supplement engine oil heat, when required in extremely cold weather.

4.0 COMPONENT/SUBSYSTEM DEVELOPMENT

Task 2, Component Subsystem Development, activities comprise the design, test, and developmental efforts for each major component and/or subsystem. Development of each component will be undertaken with dedicated test rigs specifically designed to fully evaluate the component both for performance and mechanical integrity. Distinct design iterations have been planned for each component/subsystem, so that, as test data from Tasks 2 and 3 (Component Development and Powertrain Development) becomes available, an interactive rig/engine feedback loop is realized. This allows further optimization of the "system design" philosophy as related to program goals (e.g., fuel economy manufacturing compromises, marketability, packaging, etc.).

This section discusses the major efforts and accomplishments during this reporting period for each component/subsystem.

4.1 Compressor Development

Aerodynamic detail designs for the compressor-stage hardware were completed as reported in Reference 1. To date, activities have encompassed fabrication of test rig hardware, powder metal material evaluation, and preparation for test and evaluation of the VIGV system and stage hardware.

4.1.1 Test Rig Hardware Fabrication

All test rig aerodynamic hardware fabrication has been initiated. Two compressor impellers were machined from Al2219 for initial evaluation. Figure 15 shows the impeller. Airfoil and hub and shroud contour inspection is complete, and both impellers have been accepted. Figure 16 shows the compressor diffuser for test rig evaluation. Diffuser inspection is complete and has been accepted. All other flow-path hardware has been fabricated and is being instrumented for testing.

Hardware fabrication of the compressor test rig and IGV flow rig has progressed. Major structural hardware and associated shafting components are nearing completion as scheduled for test initiation in February and March for the IGV rig and compressor rig, respectively.

4.1.2 Powder Metal Aluminum

As discussed in Reference 1, Novamet (INCO) IN-9081 and ALCOA Al-Fe-Ce are two of the advanced aluminum alloy systems selected as candidate materials for the compressor impeller. Essentially produced by powder metallurgical (P/M) techniques, the systems derive high-temperature strength (400 to 650°F) from stable secondary-phase dispersions.

Preliminary studies indicated that the mechanical property response of Novamet IN-9081 is dependent on thermomechanical processing (TMP) variables, e.g., the deformation rate. Since the current primary mode of fabricating the impeller is by forging and machining, a forging evaluation program was conducted to define the TMP parameters needed to develop the maximum potential strength of the alloy.

The forging iteration results, conducted during this reporting period, failed to establish optimum TMP conditions and did not yield acceptable mechanical properties. As shown in Figure 17, the forging data generated are lower than the baseline extrusion data and below the AGT101 design criteria. The poor forging response was attributed partly to subtle variations in powder processing and the influence of the dispersion ratio between the oxide and carbide phases, which primarily strengthen the alloy.

ORIGINAL PAGE IS
OF POOR QUALITY

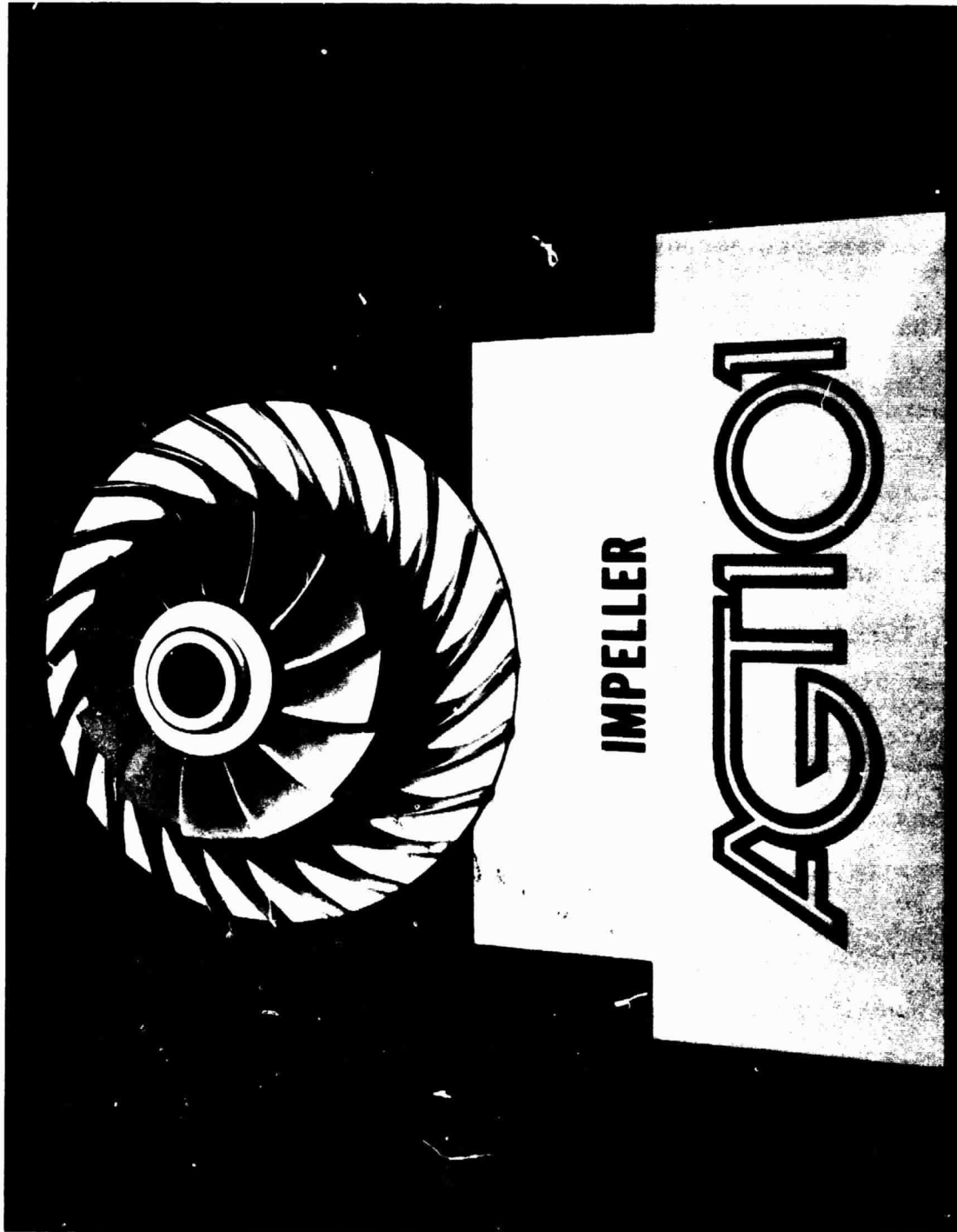


Figure 15. Compressor Impeller (Al2219 Material).

ORIGINAL PAGE IS
OF POOR QUALITY

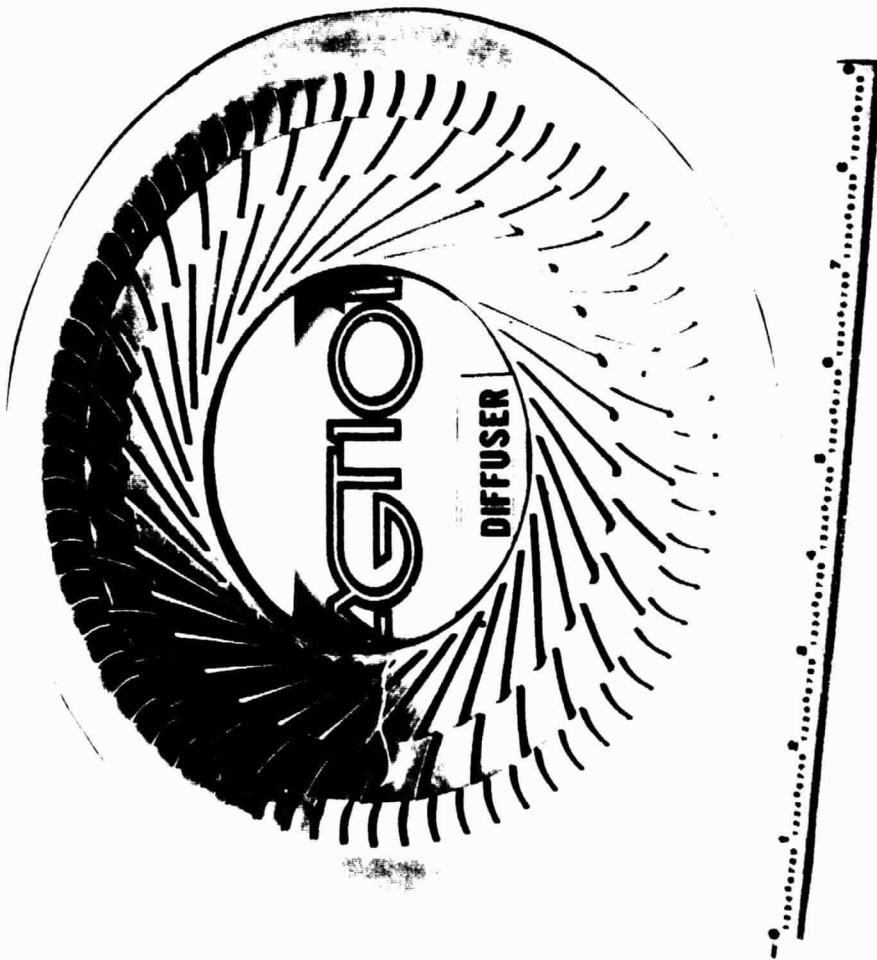


Figure 16. AGT101 Diffuser.

ORIGINAL PAGE IS
OF POOR QUALITY.

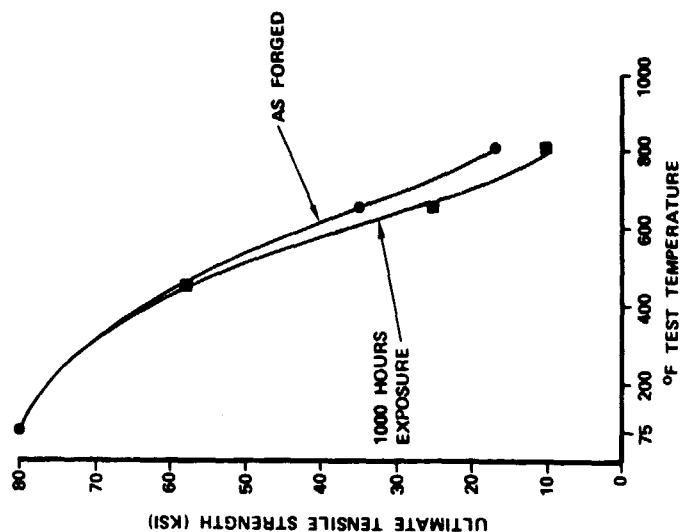


Figure 19. Effect of 1000-Hour Thermal Exposure on Forged Alcoa Al-Fe-Ce.

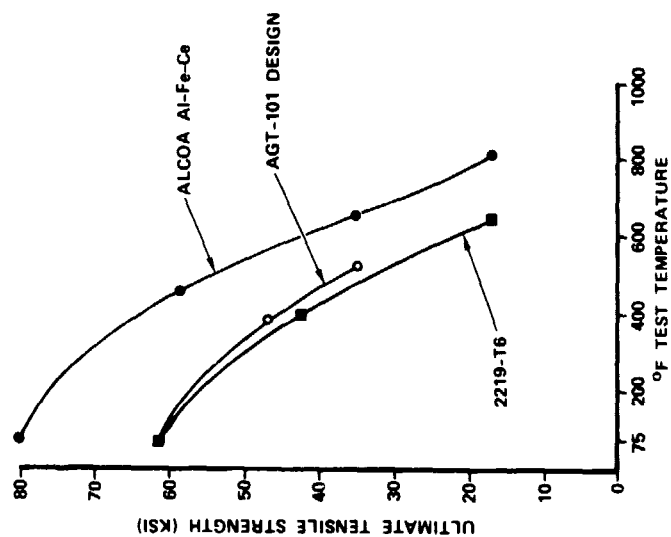


Figure 18. Tensile Properties of Forged Alcoa Al-Fe-Ce.

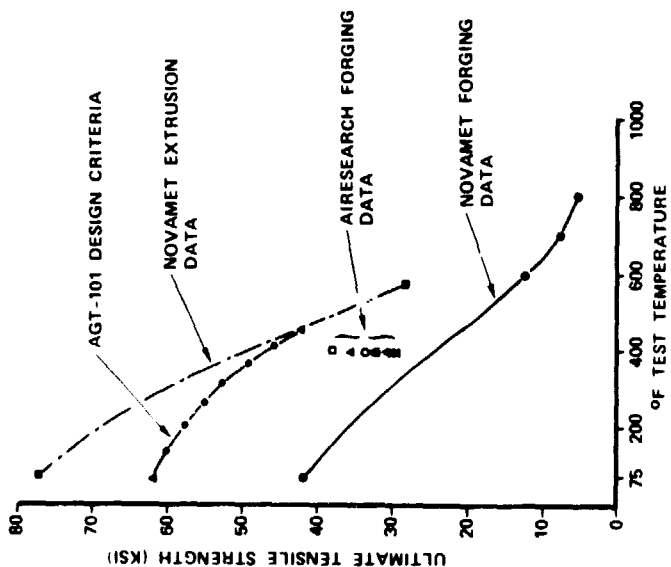


Figure 17. Tensile Properties of Forged and Extruded Novamet IN-9081.

Following discussions between Garrett, Novamet, and INCO, a decision was made to place the IN-9081 on hold for the AGT101 program. By agreement, resolution of the TMP problems and/or the necessary chemistry modifications are to be undertaken by Novamet.

Concurrent with the Novamet alloy characterization work, sub-size pancake forgings of the ALCOA Al-Fe-Ce were being evaluated under a Garrett IR&D program. Room- and elevated-temperature tensile tests demonstrated superior strength capability over wrought 2219-T6 aluminum alloy, and results exceeded the preliminary design requirement of the AGT101 compressor rotor at the 450°F temperature level (Figure 18). To evaluate alloy response to phase-coarsening under thermal soak-back conditions, forged samples were aged under various temperatures for 1000 hours and tensile-tested at those temperatures. No property degradation was evident up to a temperature of 450°F (Figure 19). Some degradation, as expected, occurred at 650 and 850°F.

With the favorable results obtained from the ALCOA forgings and the less-than-satisfactory response from the Novamet IN-9081, the ALCOA alloy was transitioned into the AGT101 compressor impeller program. Ten full-size wheel blank forgings (4.5 inches in diameter by 3 inches high) were procured to extensively characterize the alloy in terms of tensile, creep rupture, LCF and HCF properties. Based on material property testing, prototype impellers will be machined to provide hardware for spin-pit and future rig testing.

4.2 Turbine Development

Aerodynamic detail design activities for turbine-stage hardware were completed and reported in Reference 1. To date, activities have encompassed fabrication of the turbine cold-air test rig, dual-alloy rotor processing and preparation for test, and evaluation of turbine-stage hardware.

4.2.1 Rotor Design Modification

The blade-thickness distribution was modified to decrease the transient blade stresses for the ceramic rotors. The goal was to decrease maximum principal stresses below 30 ksi for all transient operation. Thickness changes were limited to local regions of high stress.

With the recontoured blades, transient stresses were computed for both sintered SiC and Si₃N₄. Figure 20 shows the temperature distribution at the time point for the worst-case start-up transient that produces the highest blade stresses. Figures 21 and 22 depict the maximum principal stress distributions for this case (20 seconds after start-up) for the sintered SiC and Si₃N₄, respectively. For the SiC wheel, the maximum blade stress was reduced from 47 to 32 ksi by recontouring the blades. Because of the additional blade structure, maximum disk stress was increased slightly from 37.7 to 38.2 ksi. Blade stresses for the sintered Si₃N₄ wheel were reduced from 31 to 22 ksi.

The temperature distribution for the time point that produces the highest blade stresses during a worst-case shutdown is illustrated in Figure 23. The stress distributions for the two materials at 40 seconds after shutdown are shown in Figures 24 and 25. The resulting blade stresses are below 30 ksi for both materials except for a small region at the trailing-edge blade fillet for SiC. Thickness changes were not made to this region because of a possible detrimental impact on aerodynamic performance.

4.2.2 Dual-Alloy Fabrication

Fabrication and processing studies were initiated for the Mod I dual-alloy turbine rotor. The rotor is comprised of a cast MAR M-247 blade ring, HIP-bonded to a consolidated powder LC Astroloy hub.

A surrogate part was utilized to determine processing parameters required to achieve directionally solidified (DS) inducer blading. TRW poured four castings of the Garrett GTP36-50 turbine rotor using different process controls to achieve the DS blade grain morphology. As shown in Figure 26, initial trials were successful on some blades, while unsuccessful on others. Effort is being directed at optimization of the processing parameters to affect full DS grain structure on all blades.

ORIGINAL PAGE IS
OF POOR QUALITY

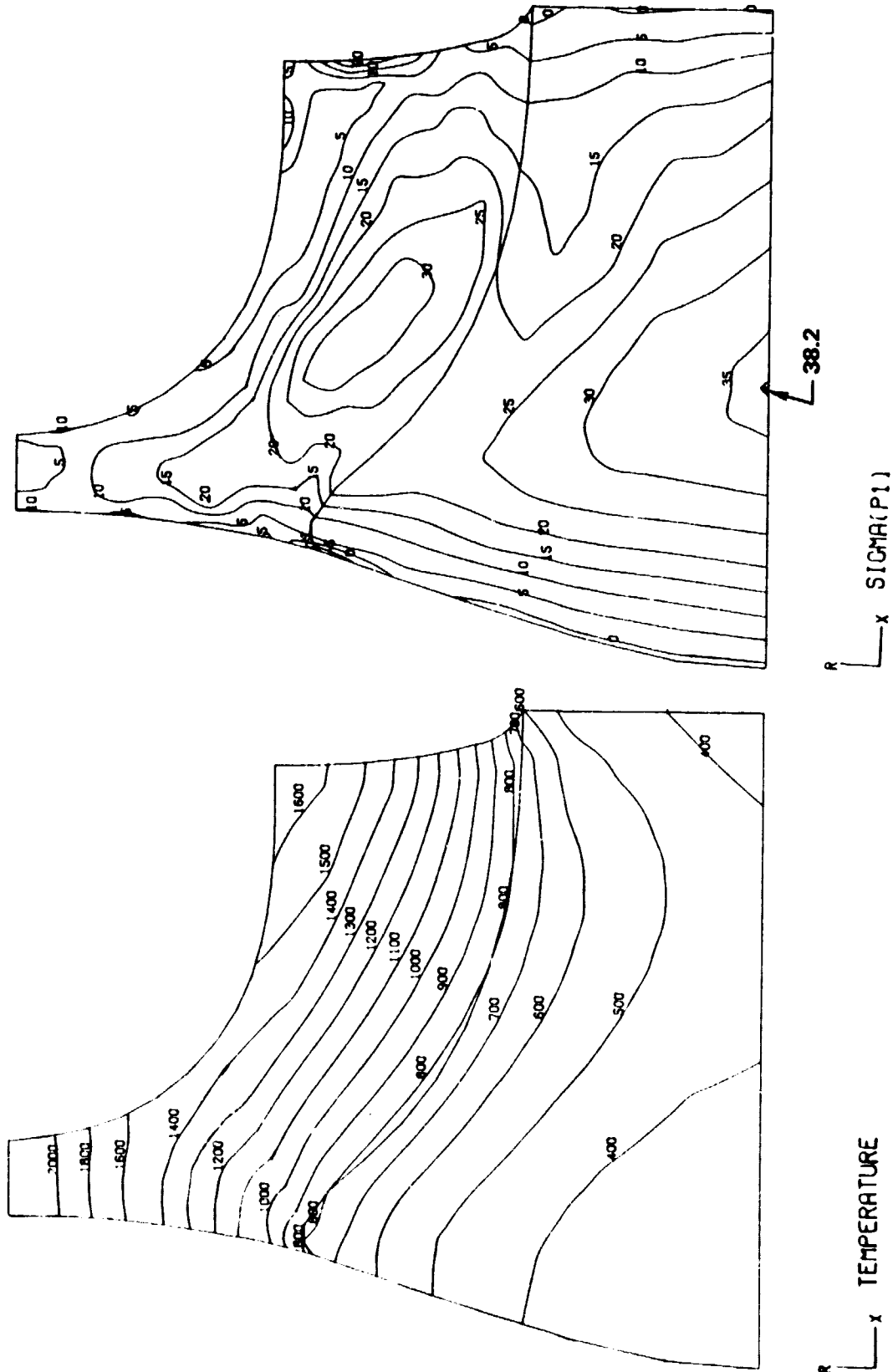


Figure 20. Worst Case Startup Transient Temperature Map.

Figure 21. Sintered SiC Worst Case Startup Maximum Principle Stress.

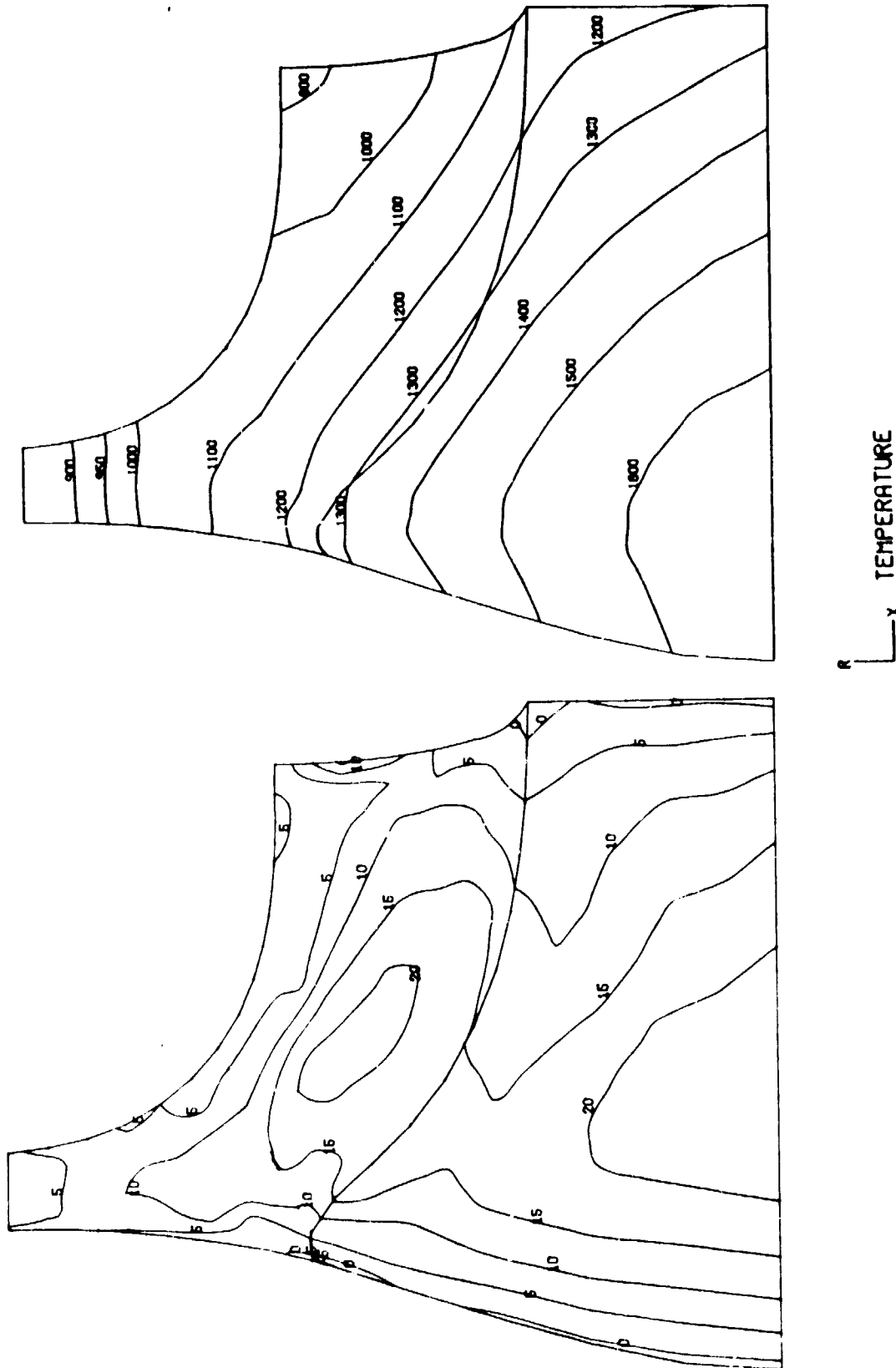


Figure 23. Worst Case Shutdown
Transient Temperature
Map.

Figure 22. Si_3N_4 Worst Case
Startup Maximum
Principle Stress

ORIGINAL PAGE IS
OF POOR QUALITY

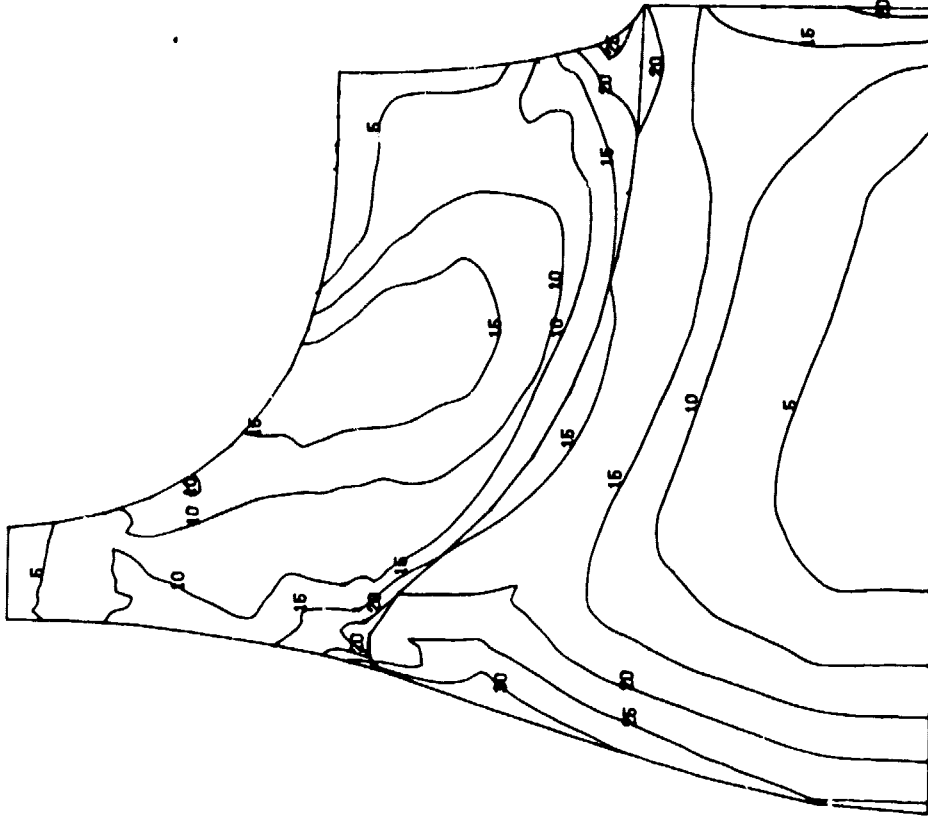


Figure 25. Si₃N₄ Worst Case Shutdown Stress Distribution.

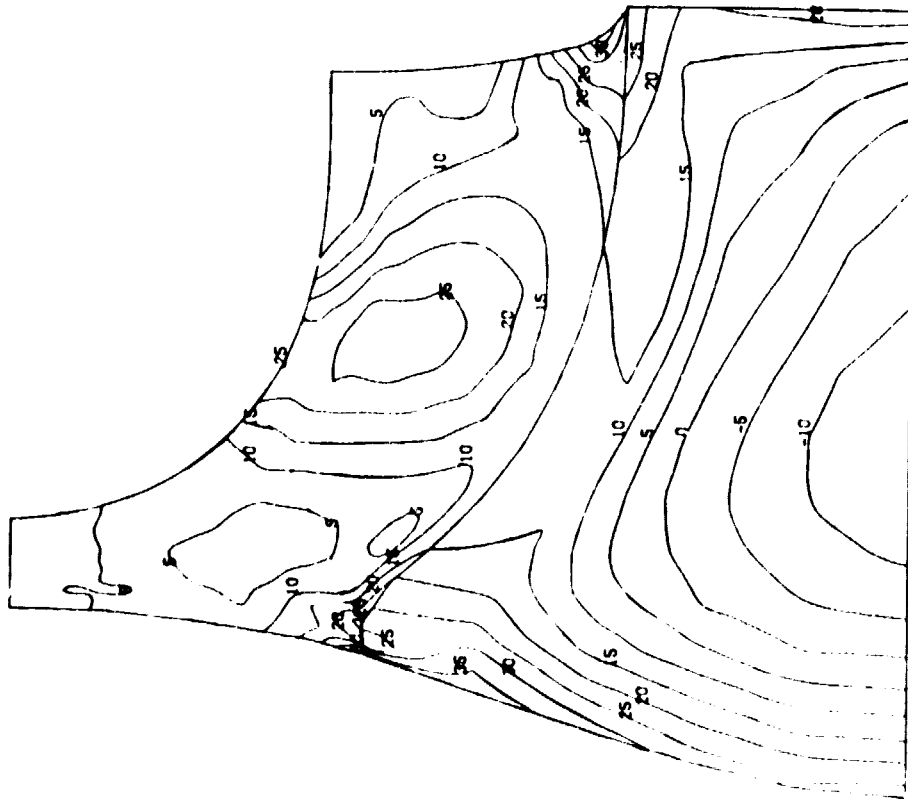


Figure 24. Sintered SiC Worst Case Shutdown Stress Distribution.

σ_x SIGMA(P1)

ORIGINAL PAGE
BLACK AND WHITE PHOTOGRAPH



Figure 26. Mod I Dual-Alloy Turbine rotor.

Trial HIP-bonding and heat-treat studies were initiated on specimens to define the processing control required for AGT fabrication.

4.2.3 Test-Rig Hardware Fabrication

All cold turbine test-rig and aerodynamic hardware fabrication activities were initiated. The first turbine rotor machined from Astroloy was received and is shown in Figure 27. The rotor is currently in inspection. Other test rig and flow-path hardware fabrication is nearing completion on schedule for initiation of tests.

Fabrication and development of the high-speed, direct-reading torque-meter progressed. At the close of this reporting period, preliminary testing had been accomplished by the supplier, Torquemeters, Ltd., Ravensthorpe, England with Delivery scheduled to support the testing program.

4.2.4 Test Results

During the low pressure (LP) Cold Flow Regenerator Test Program (Section 4.4), a 1.85 area ratio turbine exhaust diffuser was evaluated. This configuration was preliminary and not analyzed in detail prior to fabrication deadlines for procurement of LP rig hardware. Subsequent detailed 2-D boundary layer analysis (Reference 1) indicated a 1.75 area ratio diffuser was desirable. Due to timing, hardware, and scheduling, LP testing was initiated using the 1.85 area ratio diffuser.

Figure 28 presents the measured static pressure recovery, as a function of meridional distance, for maximum power and uniform inlet flow (100-percent open area screen) conditions. As shown, the measured overall static pressure recovery under these conditions is 0.468. When the diffuser was evaluated with a 70.6-percent open area screen (approximates rotor exit total pressure gradient), the overall diffuser recovery decreased to 0.42, (Figure 29). These values compare to the estimated diffuser recovery factor of 0.40 used in overall turbine performance predictions. Since, test data indicated significant static pressure recovery was still occurring even at an area ratio of 1.85 a detailed analytical model was established based on total pressure loss consistent. As shown in Figure 28, the analytical predictions for hub and shroud static pressure recovery and the measured static pressure recovery agree very well. The 1.85 analysis was extended to encompass a non-uniform inlet total pressure gradient (70.6-percent open area screen) and as shown in Figure 29 agreement is not as good as shown in Figure 28 due to the inability to account for total pressure mixing in the duct.

ORIGINAL PAGE IS
OF POOR QUALITY



AGT101

Figure 27. Astroloy Turbine Rotor.

ORIGINAL PAGE IS
OF POOR QUALITY

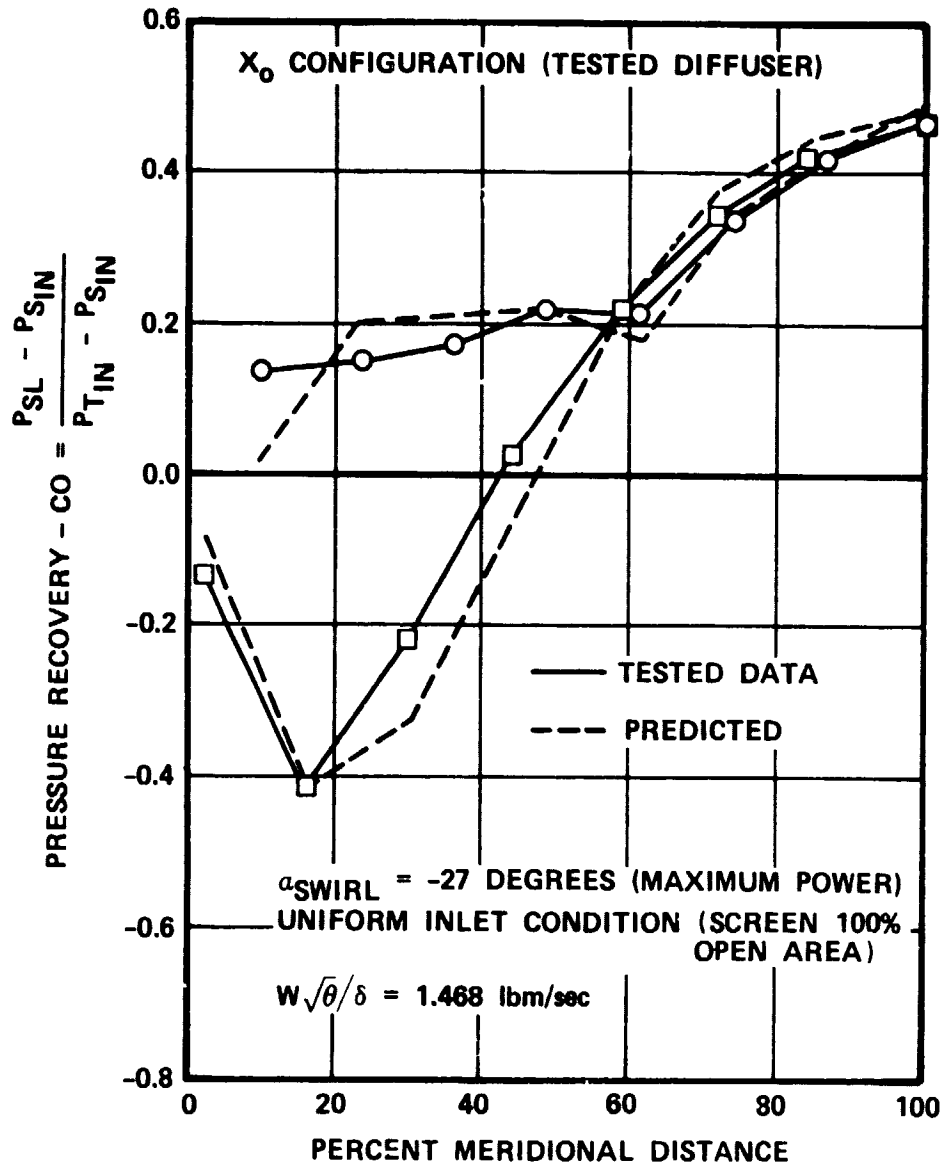


Figure 28. Turbine Exhaust Diffuser Characteristics at -27.0 Degrees Exit Swirl.

ORIGINAL PAGE IS
OF POOR QUALITY

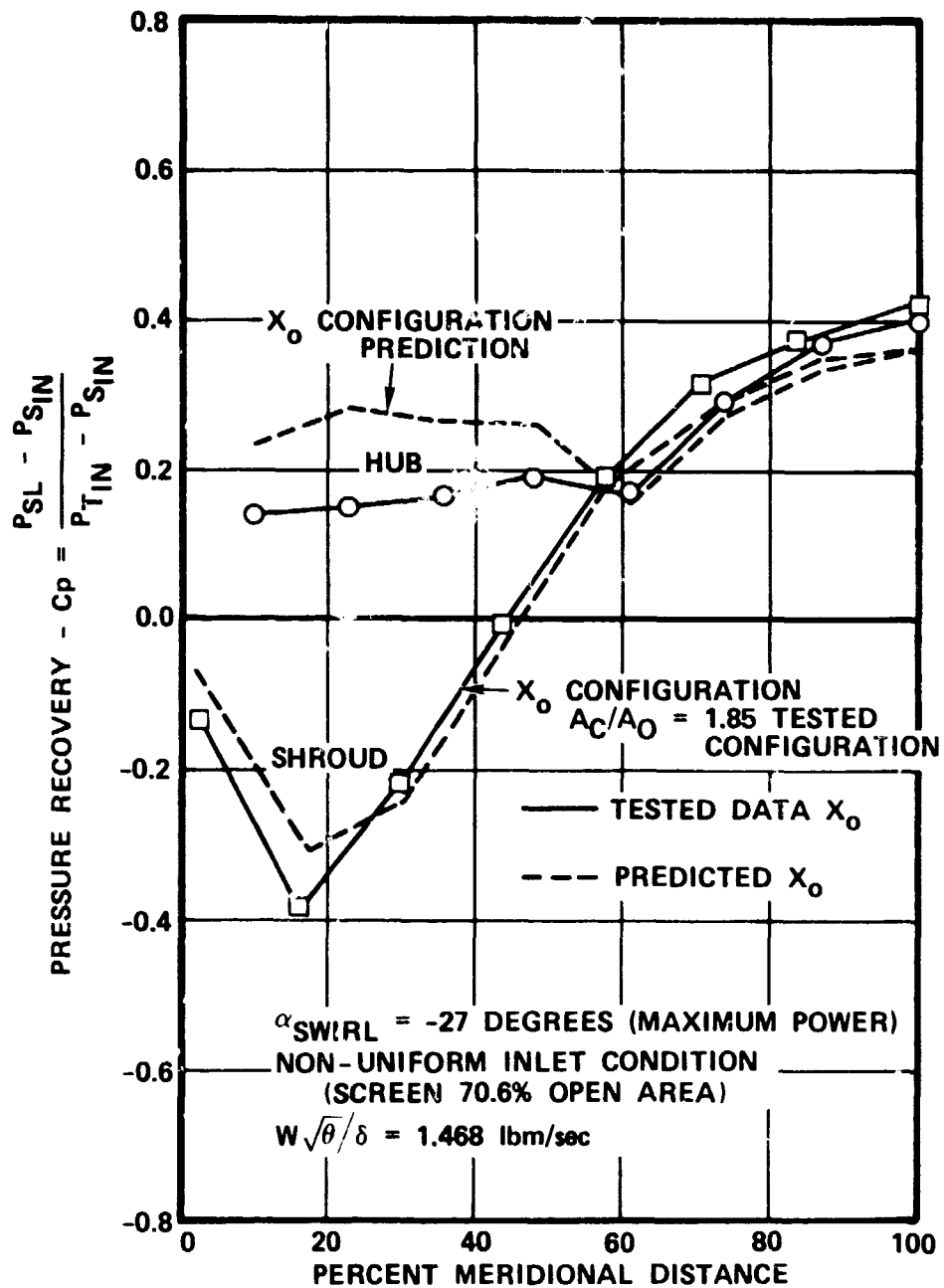


Figure 29. Comparison of Rig Test and Prediction Recovery with X_0 Diffuser at Maximum Power.

4.3 Combustion System

4.3.1 Diffusion-Flame Combustor Design

A scaled version of the Garrett GT601 diffusion flame combustor will be used in the early development of the AGT engine. Haynes 188 material will be used for fabrication, with conventional film-cooling to protect the liner surfaces. The detail design of this combustor has been completed.

Mathematical modeling of the Mod I, Build 1 diffusion flame combustion system with a 3-D elliptic (recirculating) model was completed for maximum power and idle conditions. A thermal analysis of the diffusion-flame combustor indicates liner wall temperatures to be below 1700°F for all conditions.

4.3.2 Fuel Nozzles

To date, four fuel nozzles have been received from the Delavan Corporation. The various development stages for each nozzle are as follows:

- o Pilot Combustor Nozzle - Droplet-size tests indicate that this nozzle produces acceptable droplets throughout the operating range from 0.8 lb/hr to 2.6 lb/hr (Figure 30).
- o Diffusion-Flame Main Nozzle - Initial flow tests showed that this nozzle produced unacceptable droplets at idle and cruise conditions. The nozzle was reworked by the supplier and now operates adequately at all power levels (Figure 31).
- o VG Duplex Nozzle - The 2-inch-diameter nozzle produced a droplet size of 63 to 134 microns for DF-2. Spray photographs revealed streaking and oscillations. Corrective action is being taken by the supplier.
- o VG Simplex Nozzle - This nozzle was recently received, and initial flow tests are in preparation.

4.3.3 Combustion Test Rigs

4.3.3.1 Auto-Ignition Element Test Rig

The purpose of the auto-ignition rig is to obtain ignition-delay data at inlet temperatures and pressures similar to those expected in the AGT combustion system. Testing was initiated and a total of 24 test points were completed. Testing included temperature ranges from 1400 to 1900°F and pressure levels from 30 to 75 psia.

ORIGINAL PAGE IS
OF POOR QUALITY

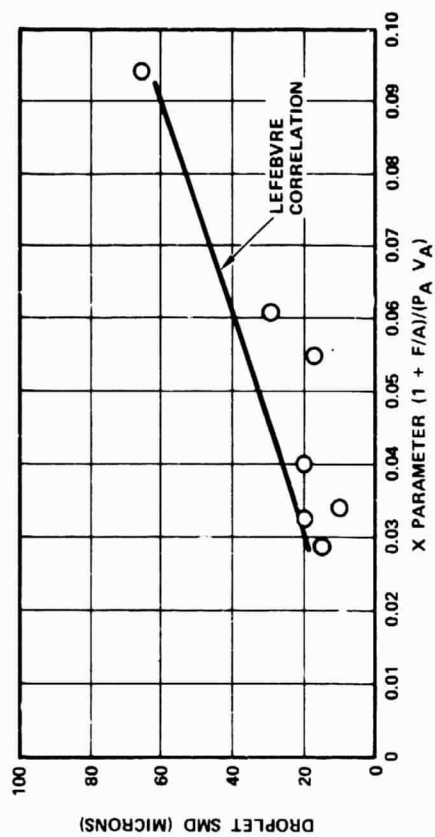
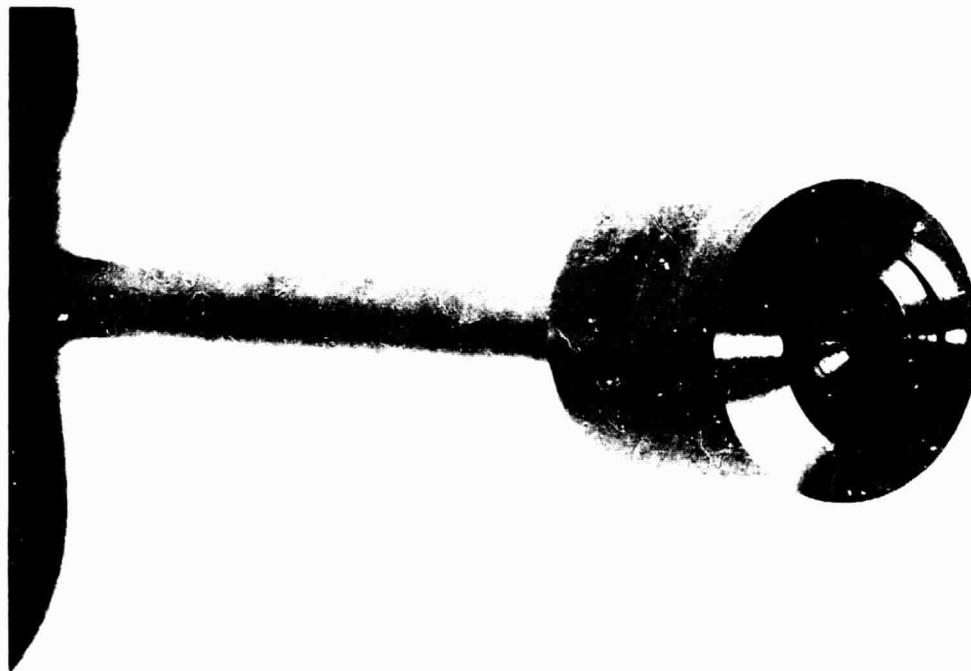


Figure 30. Pilot Combustor Nozzle,
Droplet SMD Versus X Parameter.



MP-78910

MEASURED AND PREDICTED DROPLET SMD
AS A FUNCTION OF THE X PARAMETER -
REWORKED DIFFUSION FLAME COMBUSTOR
NOZZLE

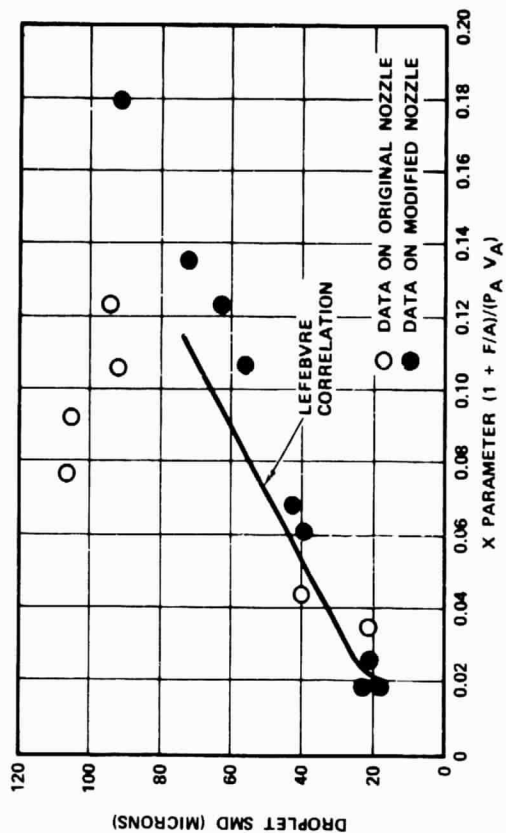


Figure 31. Diffusion-Flame Combustor Nozzle,
Droplet SMD Versus X Parameter.

Results of these tests, shown in Figure 32 and presented at the NASA-Lewis Premixed Prevaporized Combustor Technology Forum, compare well with previously published data. The data indicates that auto-ignition will occur in approximately 0.5 millisecond at the idle condition (inlet temperature 1941°F) and approximately 1.0 milliseconds at maximum power (inlet temperature 1768°F).

The rapid autoignition times should have minimal impact on the variable geometry design, since, vaporizer airflow, cup diameter and axial nozzle position, as a function of power, were selected to minimize autoignition time problems.

ORIGINAL PAGE IS
OF POOR QUALITY

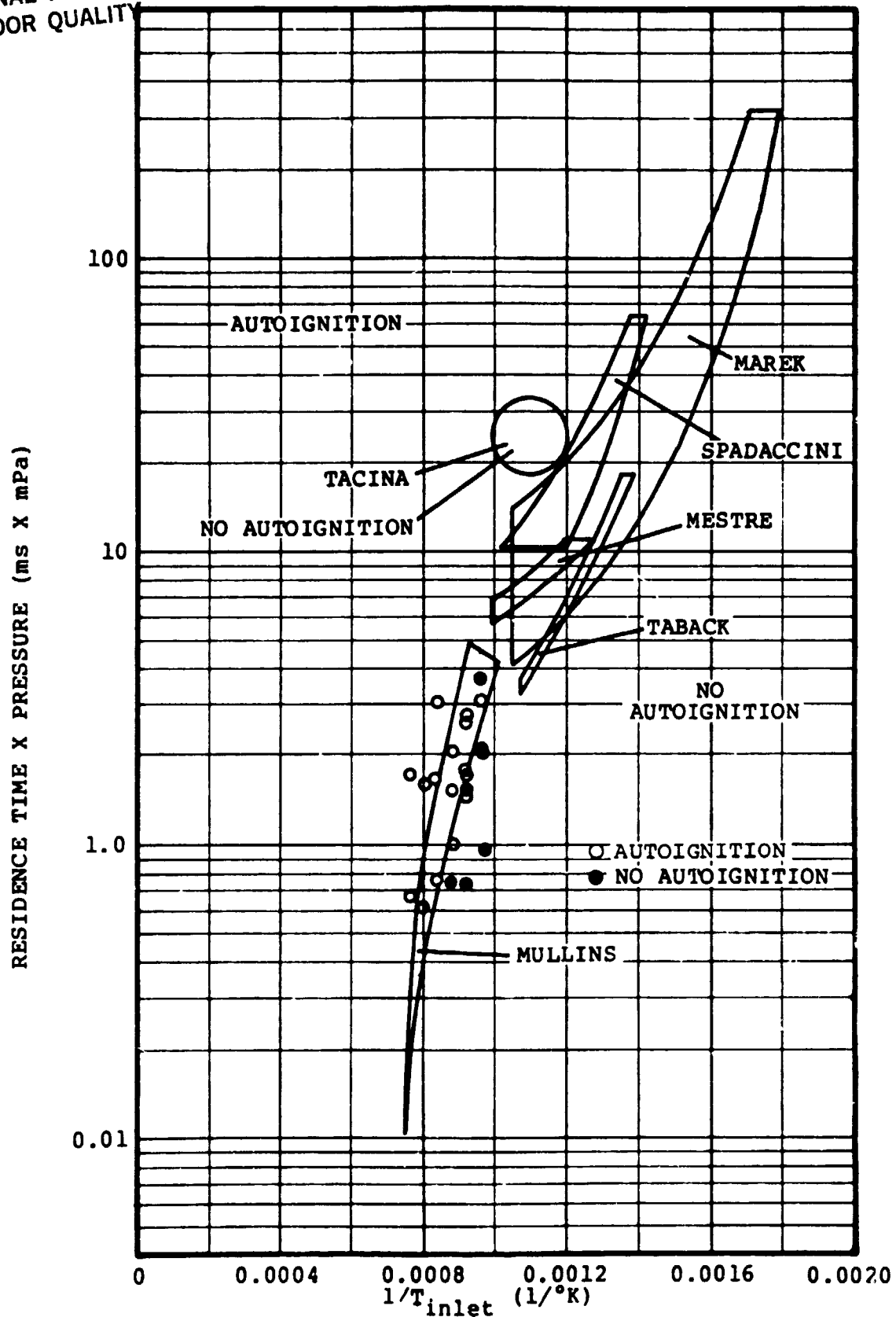


Figure 32. Autoignition Delay Data.

4.4 Regenerator

4.4.1 Ford Regenerator System

Effort during the reporting period has centered on fabrication of the regenerator components, initiation of static seal leakage tests and seal coating wear rig.

4.4.1.1 Fabrication

Five NGK cores and 3 Corning cores have been received including the core bonding fixture. The ring gears for the regenerator were received and several cores were bonded in the new fixture. These included a thick-wall LAS core, a thin-wall AS core, and a NGK segmented and extruded MAS core. In each case, the bonding process was completed without difficulty and the elastomer as well as the elastomer-gear and elastomer-matrix interfaces were visually excellent. A torque test will be conducted on the old LAS core. In this test and matrix will be clamped between a set of seal shoes and a torque will be applied to the ring gear through the pinion. It is believed that an adequate safety factor will be obtained if a torque in excess of twice the maximum operating torque can be applied without causing distress. This torque test is necessary to verify the integrity of the elastomer and interface bonds. The torque load will then be increased until a failure occurs, so that the weakest link in the core-gear elastomer bond can be determined. Material required to complete the torque test on the old LAS core will be available in January, 1981.

The inner crossarm seal, the "C" shoe seal and outer cross seal have been completely processed (coated with I-112) and are being evaluated in the various leakage and wear rigs.

4.4.1.2 Static Seal Leakage Test

The static seal leakage rig has been installed in the gas turbine lab, Figure 33. Special spacers which simulated the operating clearances of the seals in the MOD I, Build I have been added. This rig is fully instrumented and operational. The first seal system (without shoes) was assembled and tested in this rig. The leakage was slightly above the initial, state-of-the-art objective of 7.2 percent, but the test showed several locations where leakage was occurring. A second diaphragm system was fabricated and assembled with improved "secondary" diaphragms at the junction of the crossman and inner and outer peripheral diaphragms. In addition, the ends of the peripheral diaphragm were flaired in a special die rather than by hand, as was the case of the first assembly. The second assembly showed reduced leakage when evaluated in this rig, as well as locations where further leakage reductions could be made. As a result "second generation" dies were designed and released for procurement. In the mean time,

ORIGINAL PAGE IS
OF POOR QUALITY

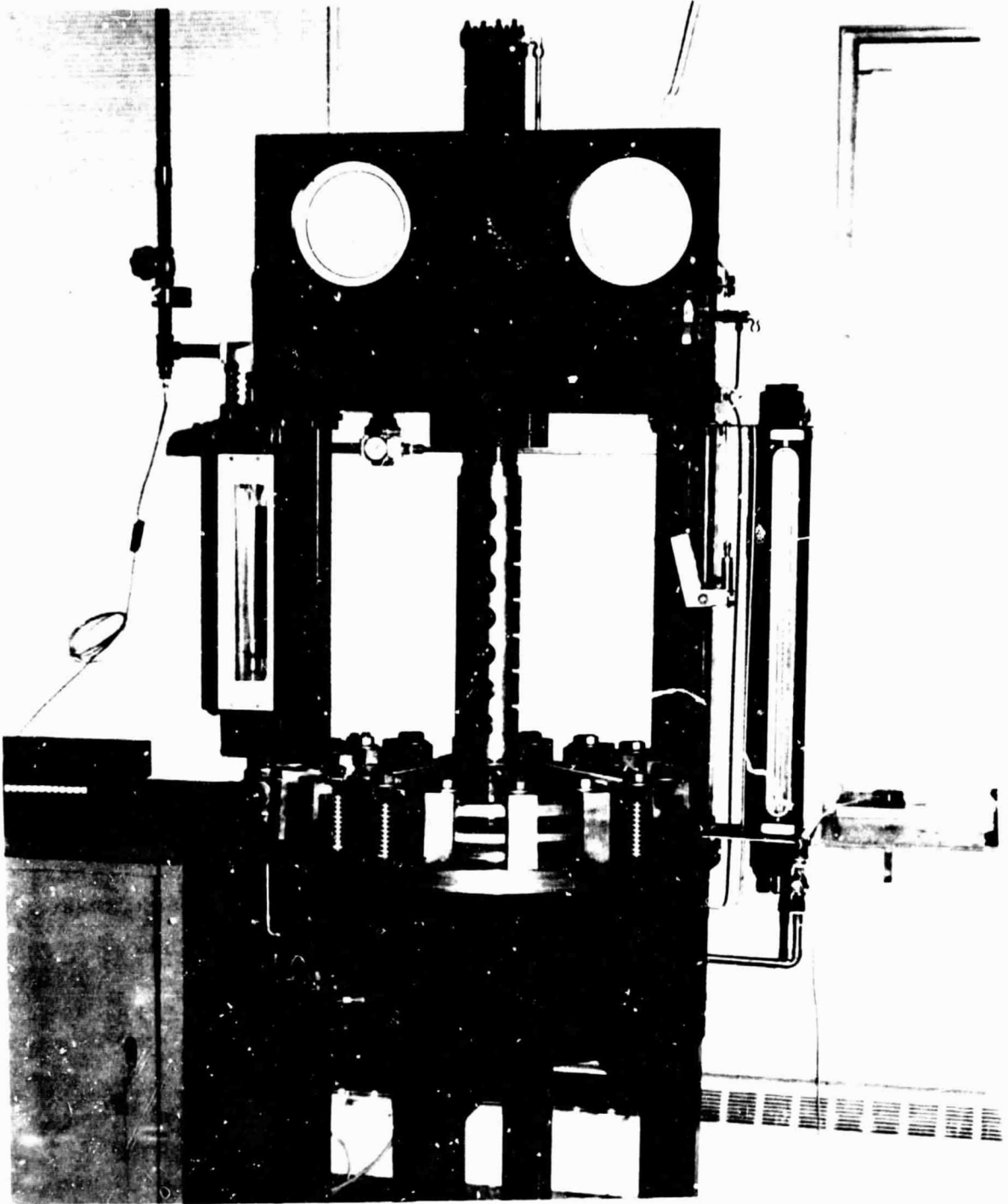


Figure 33. Static Seal Leakage Test Rig.

modified secondary diaphragm and a complete assembly of diaphragm plus hot and cold shoes were evaluated for seal leakage. The leakages appear to be fairly close to the state-of-the-art leakage rate, which was the objective for these initial seals. There are several areas where obvious leaks are occurring, but new, "second generation" diaphragm dies are required to correct this.

4.4.1.3 Seal Coating Wear Rig

The regenerator seal-coating wear rig has been fabricated and modified to accommodate the 2000°F test requirement for the hot side crossarm coating material (I-112). The test rig, Figure 34, is currently being checked out at the 1400°F condition with a previously evaluated I-112 test bar to establish a reference value for coefficient of friction and wear rate. After the test rig qualification is completed, a test bar with I-112 coating material, which was recently produced by Ferro Corporation, will be evaluated at the 1400°F condition. This step is required in order to qualify Ferro Corporation as a supplier for this coating material.

During the check-out a problem has surfaced. An instability or "chatter" condition exists at temperatures between 1000°F and 1400°F with and without load on the coated test bar. The cause of this instability is currently being investigated.

4.4.2 Garrett Regenerator Test Rigs

4.4.2.1 Regenerator Cold Rigs

As described in Reference 1, two cold flow regenerator test rigs, low pressure (LP) and high pressure (HP), were designed and fabricated in order to:

- (a) Determine circumferential and radial pressure profiles imposed by engine geometry on the regenerator core
- (b) Evaluate profile control mechanisms
- (c) Allow analytical prediction of the regenerator installed effectiveness based on the test profiles obtained in Steps (a) and/or (b).

Construction of an analytical flow and heat transfer model of the regenerator system in 3-dimensional form has been completed.

The cold rig testing programs for both the LP and HP rigs have also been completed. Sizeable amounts of data have been obtained from the cold rigs relating to flow distortion patterns, distortion treatments and combustor inlet flow control. These data are currently being reduced and are being subjected to analytical evaluation (using

ORIGINAL FILED IN
OF POOR QUALITY

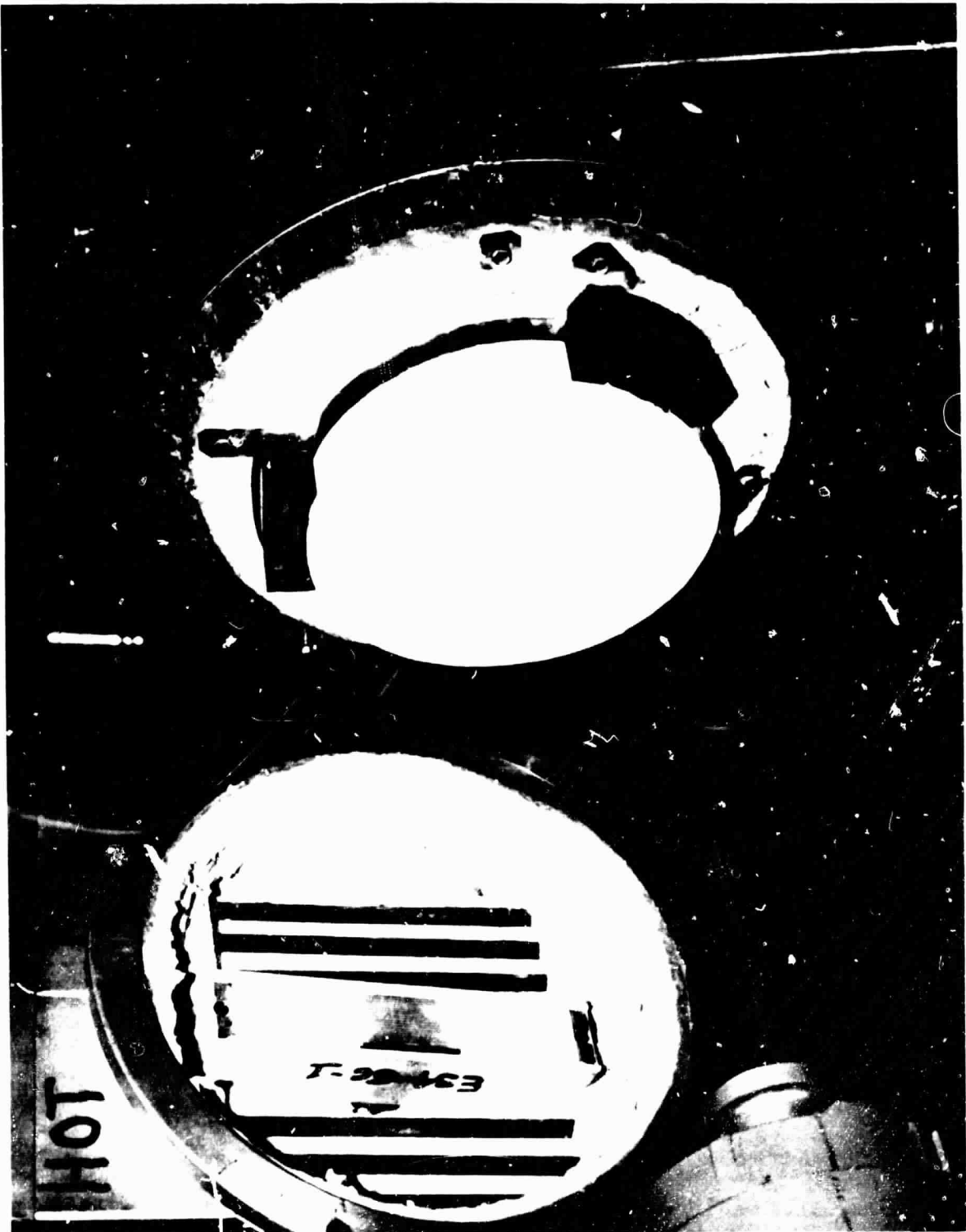


Figure 31. Regenerator Seal-Coating wear Test Rig.

the 3-dimensional analysis) to determine impact on regenerator performance.

The results obtained will be fully presented in the next reporting period.

4.4.2.2 Regenerator Hot Rig

The regenerator hot rig objectives are summarized below:

- o The hot regenerator rig is designed to measure regenerator seal leakage by the use of an inert gas (helium), seeding/detection system
- o The regenerator hot rig will be utilized to optimize flow distortion treatment geometry
- o The matrix effectiveness will be determined at optimum core rotational speeds for idle, cruise, and maximum power simulated conditions. Seal leakage will be factored into the core performance
- o Core drive torque will be determined under the following conditions:
 - o New seal breakaway torque
 - o New seal break-in interval (idle conditions for approximately 10 hours)
 - o Core drive torque during engine start sequencing
 - o Steady-state torque at idle, cruise, maximum power engine conditions.
- o Verify matrix $\Delta P/P$ (HP/LP) at idle, cruise, maximum power simulated engine conditions
- o Measure cavity pressure at core KD under idle, cruise, maximum power simulated engine conditions, and size-bleed orifice to LP discharge to limit pressure in this area

The regenerator hot rig design was completed (Figure 35). The rig was designed to minimize leakage paths (at seal locations) by eliminating all seals not required for unit assembly. Braze joints replace seal joints so that leakage from the HP side of the rig to the LP can only occur across the static side of the regenerator seal, flipper seal, and the dynamic face of the regenerator seals. The rig will operate initially with an NGK core and first-generation (Ford-designed/fabricated) seal assembly. Core performance will be evaluated at idle, cruise, and maximum power Mod I Build 1 simulated engine conditions (except swirl entering the LP cavity).

ORIGINAL PAGE IS
OF POOR QUALITY

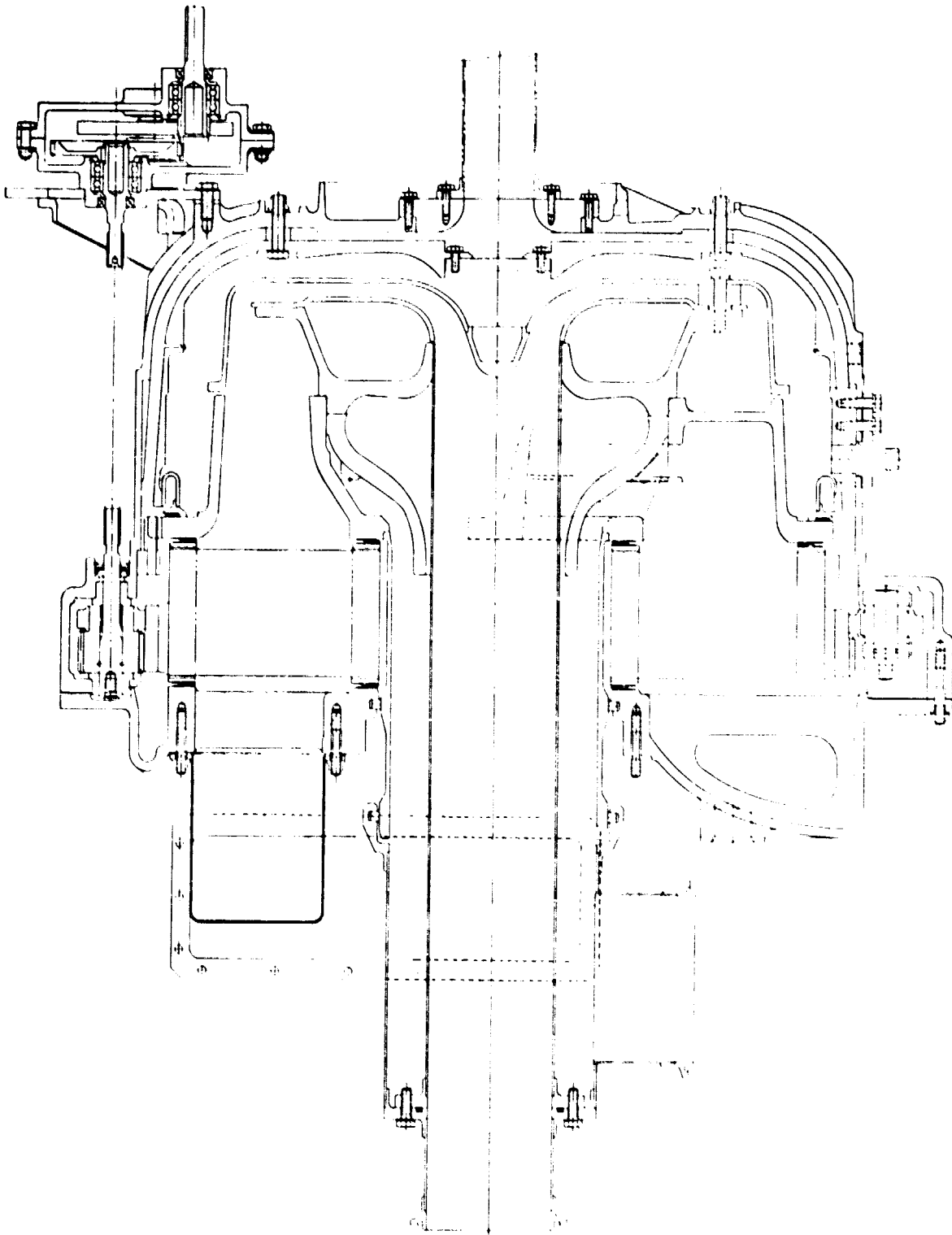


Figure 35. Hot Regenerator Rig Schematic.

4.5 Gearbox/Transmission

The detail design for the AGT101 development gearbox and variable stator torque converter (VSTC) has been completed. Gearbox detail component fabrication will be initiated in January 1981, pending receipt and analysis of price and delivery quotations currently being processed. The fabrication of two VSTCs required for initial development testing was initiated.

The design modifications required to adapt the Ford Automatic Overdrive (AOD) transmission to the AGT101 gearbox have been completed. The interface control logic between the AOD and AGT gearbox is being simplified and refined to provide optimized transmission shifts and control of the VSTC.

The need for a separate gearbox/VSTC test rig was eliminated by incorporating the planned gearbox/VSTC development testing into the drivetrain simulator test rig. Program schedule changes have provided an opportunity to consolidate the gearbox/VSTC and drive train testing within a slightly modified drive train simulator. The drive train simulator test rig detail design was completed and the quotation-procurement cycle initiated.

The regenerator drive gearbox design was completed, and development components were placed on order. The cross section of the regenerator drive gearbox is shown in Figure 36.

ORIGINAL PAGE IS
OF POOR QUALITY

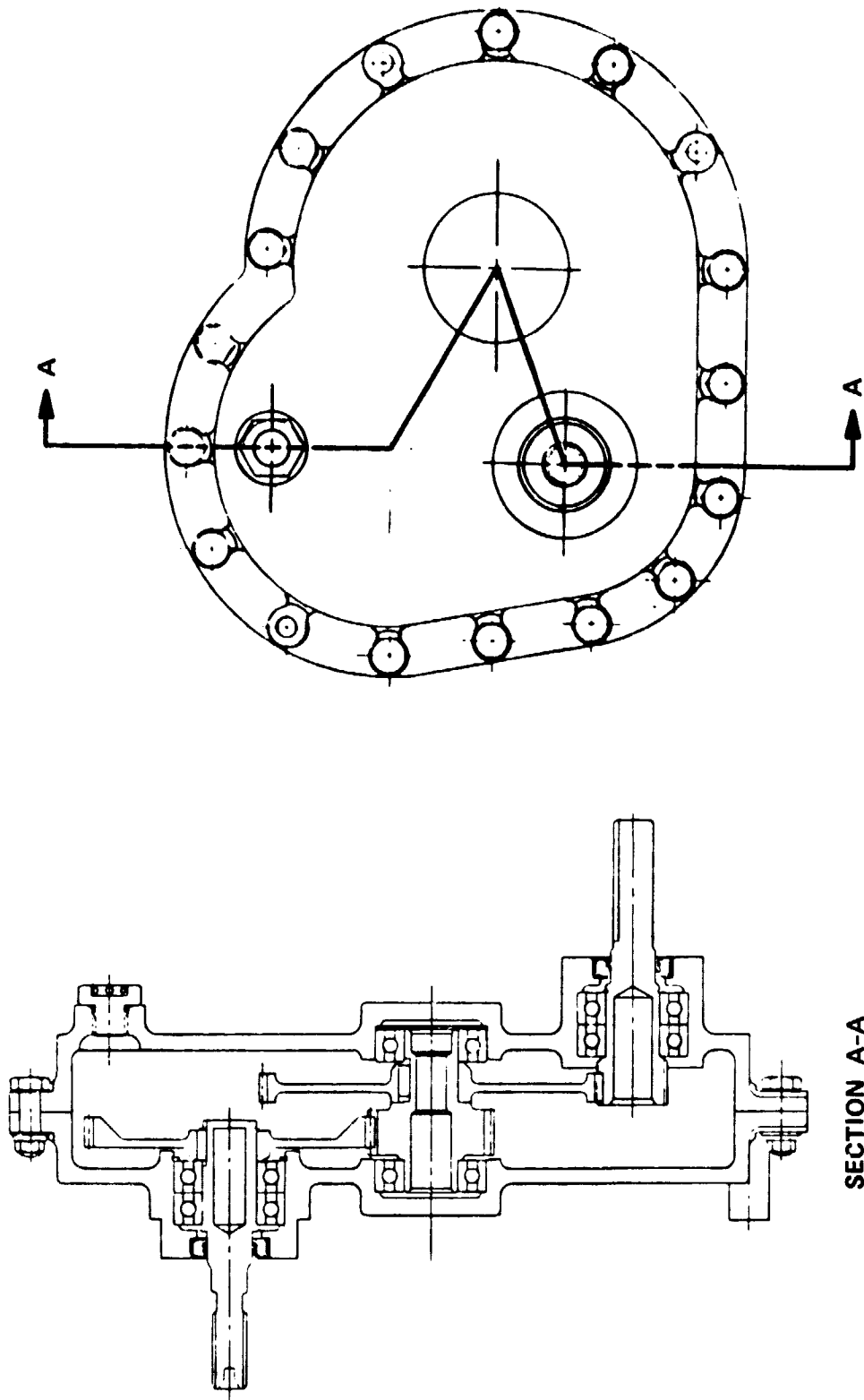


Figure 36. Regenerator Drive Gearbox.

4.6 Ceramic Structures

4.6.1 2000°F Structures Rig (Objectives)

The 2000°F structures rig (Figure 37) is being designed to subject the hot gas flowpath ceramic components (less turbine rotor and combustor) to 2000°F maximum gas temperature. The hot regenerator test rig metallic structures are replaced with ceramic structures while maintaining a common compressor housing assembly and laboratory plumbing.

Simulated engine steady-state and transient thermal gradients will be closely duplicated in this rig such that a complete ceramic static assembly can be evaluated prior to engine testing.

4.6.2 Design

The 2000°F structures rig design closely duplicates Mod II engine flowpath geometry, mechanical loading, and hot gas flow path temperature to 2000°F. A 2500°F test rig is currently planned for FY 82 that will evaluate the hot gas flowpath from the combustor to the turbine inlet.

Due to the degree of flow turning in the stator, a nonrotating ceramic wheel to deswirl the flow is planned to occupy the rotor envelope, thus preventing a potential choke problem at the higher flow levels in either the turbine shroud or radial diffuser locations.

ORIGINAL PAGE IS
OF POOR QUALITY

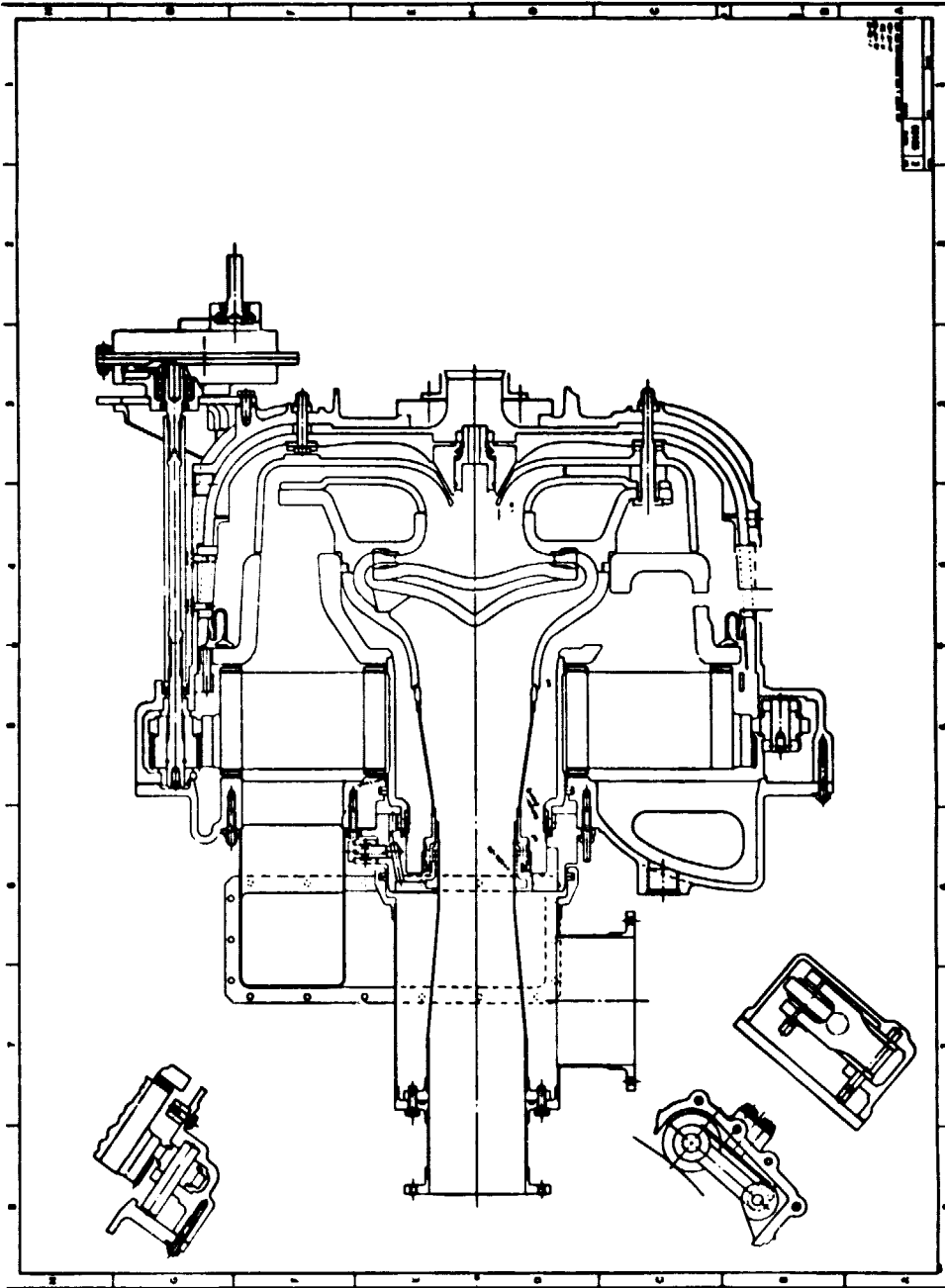


Figure 37. 2000°F Structures Rig.

4.7 Ceramic Component Development

This section discusses ceramic material and component development and evaluation at the Garrett Turbine Engine Company and at the sub-contractors during this reporting period.

4.7.1 Ceramic Material Evaluation

The baseline material evaluation plan was presented in Reference 1, followed by a summary of the results during the first 9 months of the program. The following paragraphs present additional data for the baseline materials, plus results of ceramic interface evaluation.

4.7.1.1 Strength Update for Carborundum SASC

Additional baseline strength tests have been completed on fine-grained cold-pressed and slip-cast sintered alpha silicon carbide (SASC).

Table 6 summarizes the Weibull parameters obtained on fine-grained cold-pressed SASC. This material has slightly higher strength than that with exaggerated grain growth (Cold-Pressed I) reported previously⁽¹⁾. The electrolytically etched microstructure of these two materials is shown in Figure 38. The strength is not degraded significantly by the presence of the large grains.

The characteristic strength of SASC flexural test bars is decreased to 32 ksi when transverse rather than longitudinal grinding is used. However, the baseline strength can be restored by an oxidation treatment that has been standardized at 4 hours, 2200°F in air. The oxide layer developed during this treatment is very thin and if desired can easily be removed by HF etching. However, there are indications (Table 6) that a decrease in strength results. Vacuum annealing at 2200°F for 4 hours also restores the strength of transverse machined test bars to longitudinal machined levels.

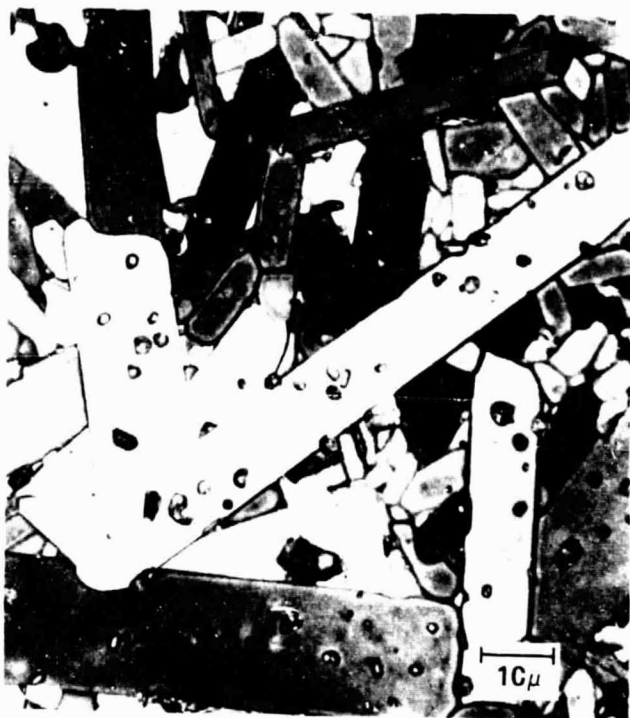
All the slip-cast components will be fabricated from a bimodal casting mix in which coarse silicon carbide (SiC) powder is added to submicron powder to improve casting rates. Shrinkage is reduced, which aids in dimensional control, but the added porosity generally results in a strength decrease. The initial set of as-received bars resulted in a baseline characteristic strength of 49.4 ksi. Under the Common Effort, Carborundum obtained similar results (Table 7). Prior to testing, the second group of test bars were given the 2200°F/4-hour annealing in air planned for use on components. The resulting Weibull parameters are also given in Table 7. Although the Weibull modulus is similar to previous values, the characteristic strength is significantly higher. The densities of Groups I and II were similar--2.84 versus 2.89 g/cm³. The microstructures, shown in Figure 38, differed slightly, Group II having a larger grain size. Since SASC generally

TABLE 6. WEIBULL PARAMETERS OBTAINED FROM FLEXURAL TESTS
ON COLD-PRESSED SASC

Material (population)	Temperature (°F)	Characteristic Strength (ksi)	m-Value
Cold-Pressed II (30)	72	58.5	8.6
Cold-Pressed II (10)	2200	58.0	8.8
Cold-Pressed II (30)	2500	57.9	12.9
Cold-Pressed II (10)*	72	51.2	8.0
Cold-Pressed II (10)**	72	61.4	8.8

*Transverse machined, 2200°F/4-hours air annealed, 50 percent HF etch

**Transverse machined, 2200°F/4-hours vacuum annealed



COLD-PRESS I (S/N 7125)



COLD-PRESS II (S/N 8297)



SLIP-CAST I (S/N 8631)



SLIP-CAST II (S/N 9001)

Figure 38. Etched Microstructure of Cold-Pressed and Bimodal Slip-Cast SASC.

**TABLE 7. WEIBULL PARAMETERS OBTAINED FROM FLEXURAL TESTS
ON BIMODAL SLIP-CAST SASC**

Material (population)	Temperature (°F)	Characteristic Strength (ksi)	m-Value
Slip Cast I (30)	72	49.4	5.8
Slip-Cast I (9)	2500	41.4	6.7
CBO Data (30)	72	46.5	4.7
CBO Data (30)	2192	45.3	8.3
Garrett/CBO Data (60)	72	47.9	5.3
Slip-Cast II (30)*	72	58.1	6.6

*Oxidized, 2200°F/4-hours/air

fails from volume flaws, the oxidation treatment is not expected to affect significantly the strength. Therefore, the baseline strength level of bimodal slip-cast material and the effect of oxidation heat treatment will be closely monitored in future experiments.

4.7.1.2 Stress Rupture Testing

Stress rupture screening evaluations have been performed on several AGT candidate materials to verify their suitability for AGT development. Two types of testing were performed--static furnace exposures on AiResearch Casting Company (ACC) SNN522 and gas-fired furnace exposures on ACC RBN104 and Carborundum cold-pressed SASC.

Static furnace exposure stress rupture testing was performed on ACC SNN522 sintered Si_3N_4 to evaluate material characteristics under critical rotor conditions. Test conditions included temperatures of 2000 and 2100°F with stresses from 31.5 to 49.1 ksi. Test bars 0.214-inch wide by 0.108-inch thick were loaded in quarter-point bending with an outer span of 1.5 inches. Loading durations were limited to approximately 330 hours. Test bars surviving stress rupture loading were subsequently fractured at 2000°F in quarter-point loading with a cross-head speed of 0.02 in/min. A summary of results is presented in Table 8.

As noted in Table 8, all but one of the SNN522 test bars survived loading to a maximum duration of 338 hours. All test bars exhibited 2000°F post-exposure flexure strengths above the baseline 2000°F characteristic strength of 66.1 ksi. Additionally, all test bars surviving stress-rupture testing at 2000°F had flexure strength values exceeding all but one value obtained on the 30 as-sintered test bars during 2000°F baseline evaluations. These results indicate that a strengthening effect occurred during stress rupture exposures.

The nature of this strengthening effect has not been specifically studied for SNN522. However, studies on other Si_3N_4 materials suggest the following potential mechanisms; (1) crystallization of partial crystallization of glass at the grain boundaries, and (2) impurity desegregation from grain boundaries into the lattice structure into the specimen surface.

Results in Table 8 also indicate that test bars loaded to 49.1 ksi at 2000°F and to 39.7 ksi at 2100°F exhibited creep deflection when measured from the inner-span load points. Fracture surface examination of all test bars exhibiting creep revealed no evidence of slow crack growth. Conditions under which creep was observed exceeded the anticipated peak stress and temperature for the AGT rotor. Thus, the stress rupture and flexure strength results confirm the suitability of SNN 522 for rotor development.

TABLE 8. SUMMARY OF STATIC FURNACE STRESS RUPTURE RESULTS FOR ACC SNN 522

Specimen S/N	Static Furnace Temperature, °F	Stress, ksi	Time, hr:min	Stress Rupture Results*	2000°F Fracture Stress*, ksi
7949	2000	31.5	325:00	No failure.	84.7
8233	2000	39.7	336:00	No failure.	80.7
8012	2000	49.1	00:4	Fractured at large inclusion.	
8112	2000	49.1	336:00	No failure. Creep of 0.003- inch deflection	82.5
8072	2000	49.1	333:00	No failure. Creep of 0.005- inch deflection	86.5
8133	2100	39.7	338:00	No failure. Creep of 0.009- inch deflection	74.8
8173	2100	39.7	331:00	No failure. Creep of 0.008- inch deflection	74.4

*All testing performed using quarter-point loading. Outer span = 1.5 inches. Fracture testing performed at 0.02 in/min cross-head speed.

**Baseline flexure strength values ranged from 48.2 to 80.7 ksi with a characteristic value of 66.1.

Stress rupture evaluations in a gas-fired furnace atmosphere were performed on eight test bars each of ACC RBN104 and Carborundum cold-pressed SASC. RBN104 specimens were tested after an oxidizing treatment of 2 hours at 1350°C. Sintered SiC bars were tested in the as-machined condition. All tests were performed at 2500°F in a gas-fired furnace to evaluate material potential for static structure applications. Test bars of 0.125 x 0.250 inch cross sections were used. Test bar loading was accomplished using quarter-point SiC bend test fixtures with a 1.5-inch outer span. Testing was performed to 300 hours at two stress levels. The initial 150 hours of testing were performed at a stress level corresponding to a fast fracture cumulative probability of failure (CPF) of 10^{-5} , and the remaining 150 hours were performed on survivors at a stress level corresponding to a CPF of 10^{-4} . Stress levels were obtained from previously determined elevated temperature, baseline Weibull characteristic strength and modulus values of 50 ksi and 10 for RBN104, and 55 ksi and 13 for SASC.

RBN104 test bars were initially exposed to 2500°F at a stress level of 16 ksi. At 150 hours, all test bars had survived, and the load was increased to 20 ksi for the remaining 150 hours. All specimens survived without fracture. The eight test bars were separated into two groups of four and were flexure-tested at room temperature and 2500°F. Results are tabulated in Table 9 and illustrate that no degradation in the flexure strength of RBN104 occurred during stress rupture exposure. Analysis indicated that the fracture typically initiated from the tensile surface of each test bar. An average weight change of -0.05 percent was measured for all test bars exposed to the 2500°F gas furnace environment for 300 hours.

SASC test bars were initially exposed to 2500°F at a stress level of 23 ksi. At 150 hours, all test bars had survived, and the load was increased to 27 ksi for the remaining 150 hours. One specimen failed at 27 ksi after 6.7 hours. The remaining bars were separated into two groups and were flexure tested at room temperature and 2500°F. Results are tabulated in Table 9 and indicate that no general degradation in strength occurred during the stress rupture tests. The bar that failed after 6.7 hours at 27 ksi fractured from the processing related subsurface flaw shown in Figure 39. This type of origin is typical of SASC, and no slow crack-growth is evident.

Thus, the survival of, and the strength retention of, both RBN104 and SASC exposed to the 2500°F gas-fired stress rupture testing is supportive of their selection as structural component materials for AGT development.

4.7.1.3 Ford Reaction Bonded Si_3N_4

Ford injection-molded reaction-bonded silicon nitride test bars were received and inspected. Thirty-nine test bars were broken at room temperature in four-point flexure. The mean room temperature

TABLE 9. STRESS RUPTURE SUMMARY

Material	Gas-Fired Furnace Temperature, °F	Stress, ksi/Time, hr	Results	Residual Strength, ksi/m
ACC RBN104	2500	16/150 + 20/150	No failures	53.5/29 at 80°F (4 specimens)
Carborundum Cold-pressed Sintered -SiC	2500	23/150 + 27/150	No failures One failure after 6.7 hour	53.0/12 at 2500°F (4 specimens) 64.7/1.8 at 80°F (4 specimens) 53.1/8.1 at 2500°F (4 specimens)

NOTE: All testing performed in four-point bending. Outer span = 1.5 in. Inner span = 0.75 in.

ORIGINAL PAGE
BLACK AND WHITE PHOTOGRAPH

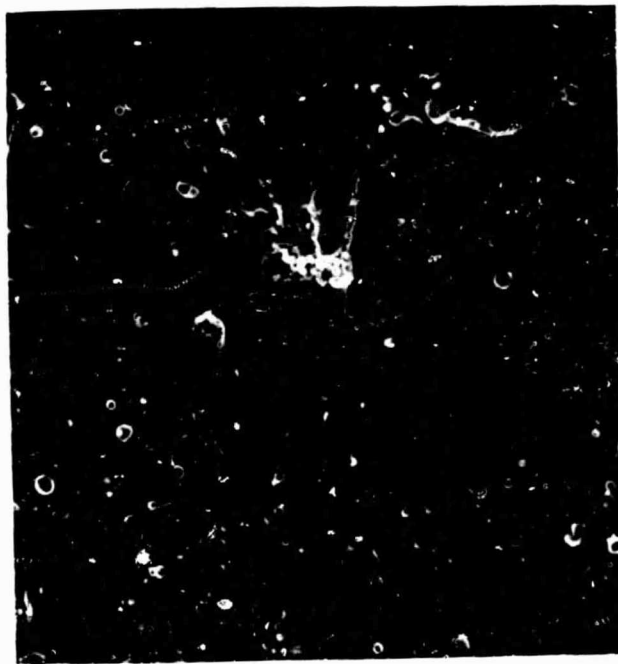


Figure 39. Failure Origin for Cold-Pressed SiC Stress-Rupture Bar Which Failed After 150 hours at 23 KSI and 6.7 Hours at 47 KSI.

modulus of rupture (MOR) was 40.9 ksi, with a standard deviation of 5.33 ksi. Ten test bars were broken at 2200°F. The MOR at 2200°F was 43.0 ksi, and the standard deviation was 6.6 ksi. Also, ten test bars were broken at 2500°F. The flexure strength at 2500°F was 44.3 ksi, and the standard deviation was 4.6 ksi. Figure 40 shows the Weibull curves for the Ford RBSN at room temperature, 2200°F, and 2500°F. Figure 41 shows the characteristic strength of the Ford RBSN compared with other candidate materials over the temperature range of 70 to 2500°F. The Ford material maintains flexure strength over the entire temperature range and appears to be a suitable candidate for static structure components.

4.7.1.4 Ceramic Interface Evaluation

The contact test rig and test procedure were described previously^(1,2,3,4). Figure 42 shows a schematic of the interface test apparatus.

Initial tests on RBN104 and SASC were conducted with point contact (1/4-inch crown against 1/4-inch crown) at loads ranging from 10 to 57.3 pounds normal force (F_N) and at temperatures ranging from room temperature to 2000°F. For the elevated temperature tests, the specimens were held at temperature for 30 minutes prior to application of the tangential force (F_T). A relative movement of 0.04 inch was applied at a rate of 0.02 in/min to allow calculation of the static and dynamic coefficients of friction.

Each test was repeated six times to check the test rig reproducibility and to provide a good data base for the RBN104 and SASC. Figure 43 shows the degree of data scatter for the static coefficient of friction versus the normal load at room temperature. The scatter is not excessive. The most important observations are that the SASC has a substantially lower room temperature static coefficient of friction than does the RBN104, and the static coefficient of friction does not vary significantly over the load range evaluated for the point-contact condition.

Further information is available by comparing the actual F_T versus contact traverse distance curves for each material at each temperature. These curves for RBN104 and SASC under 25 pounds point-contact are shown in Figure 44 with coefficient of friction values. These curves were reproducible from specimen to specimen; the following observations were noted:

- (a) At room temperature, the curves for both materials were continuous with no abrupt change between static and dynamic coefficients of friction. The curve for RBSN gradually increased and then decreased. Examination of the contact surface suggested that surface damage had occurred and that particulate debris was being pushed ahead of the contact

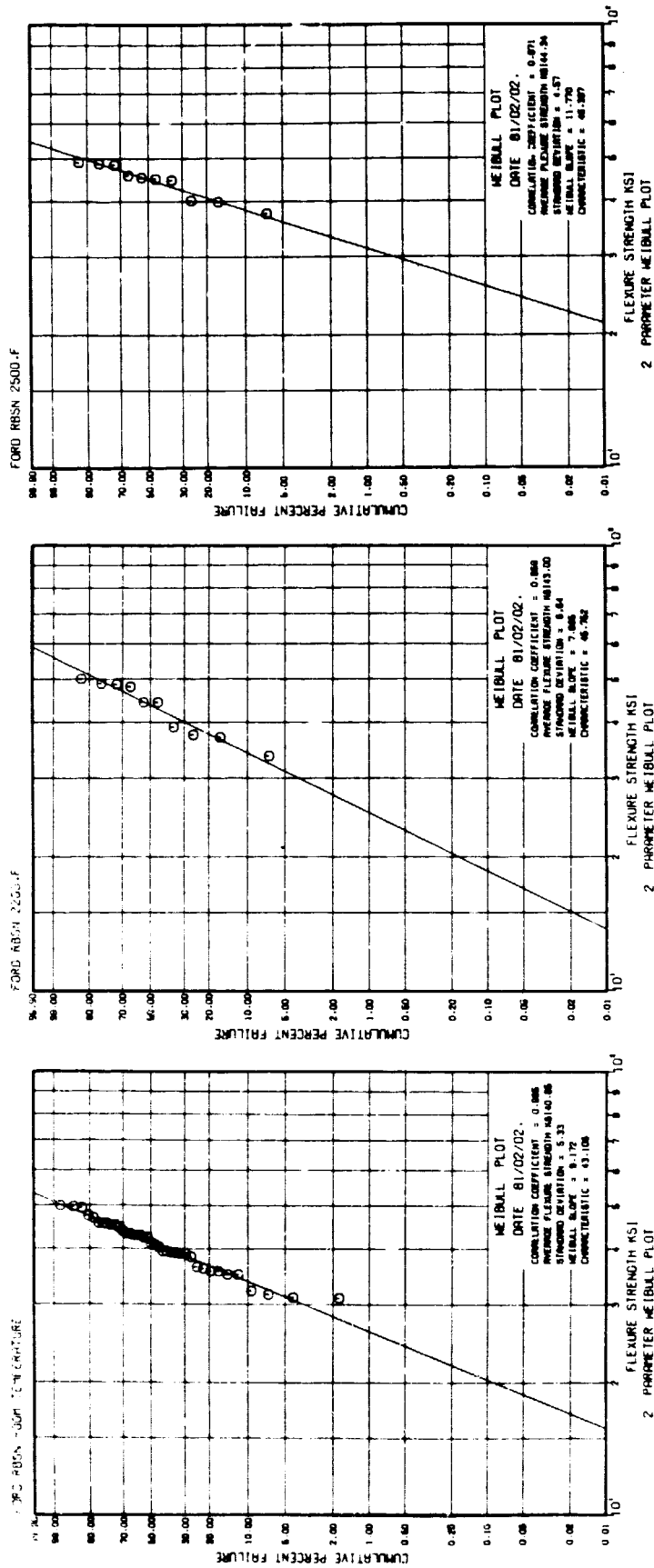


Figure 40. Weibull Plots For Ford RBSN at Room Temperature, 2200°F, and 2500°F.

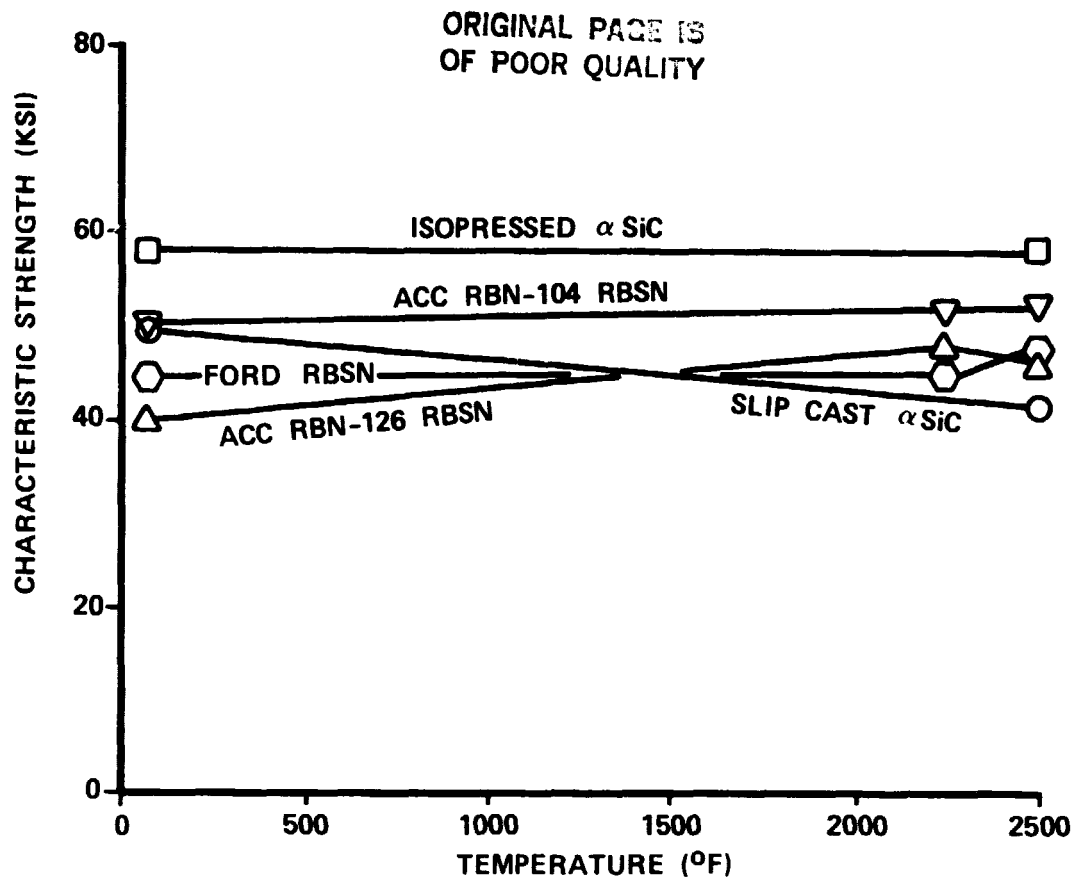


Figure 41. AGT101 Candidate Structure Materials, 1980 Test Bar Data.

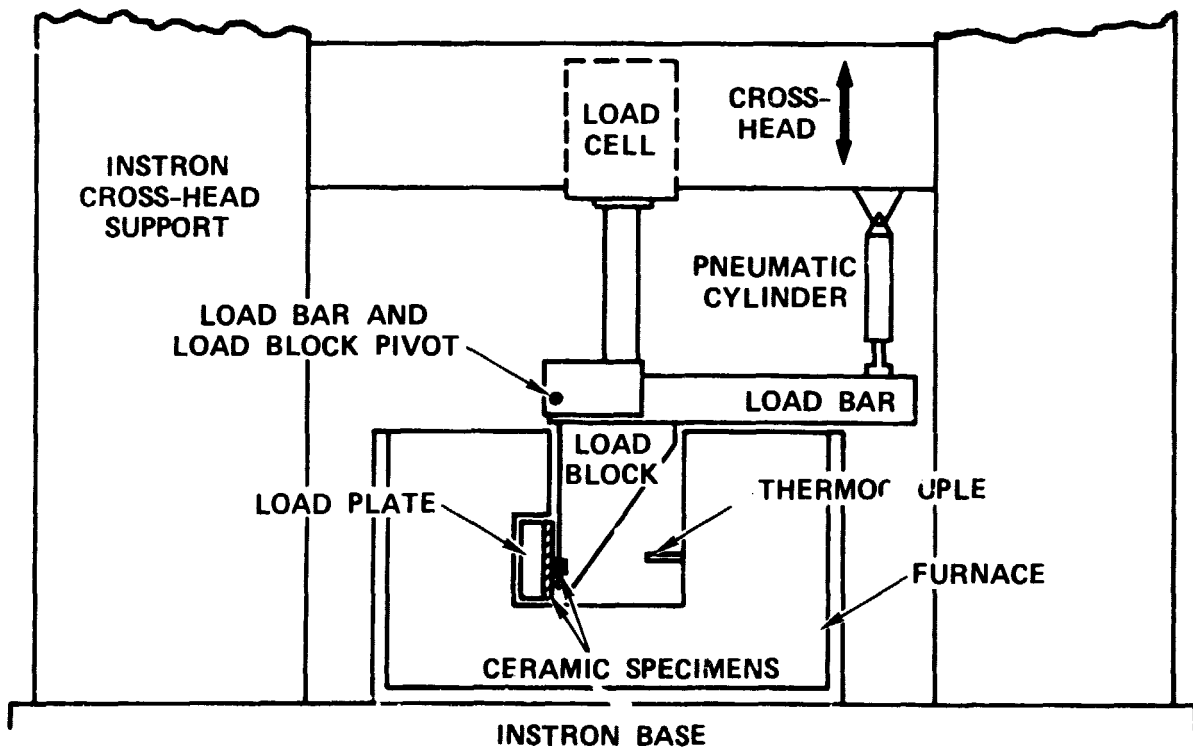


Figure 42. Interface Test Apparatus.

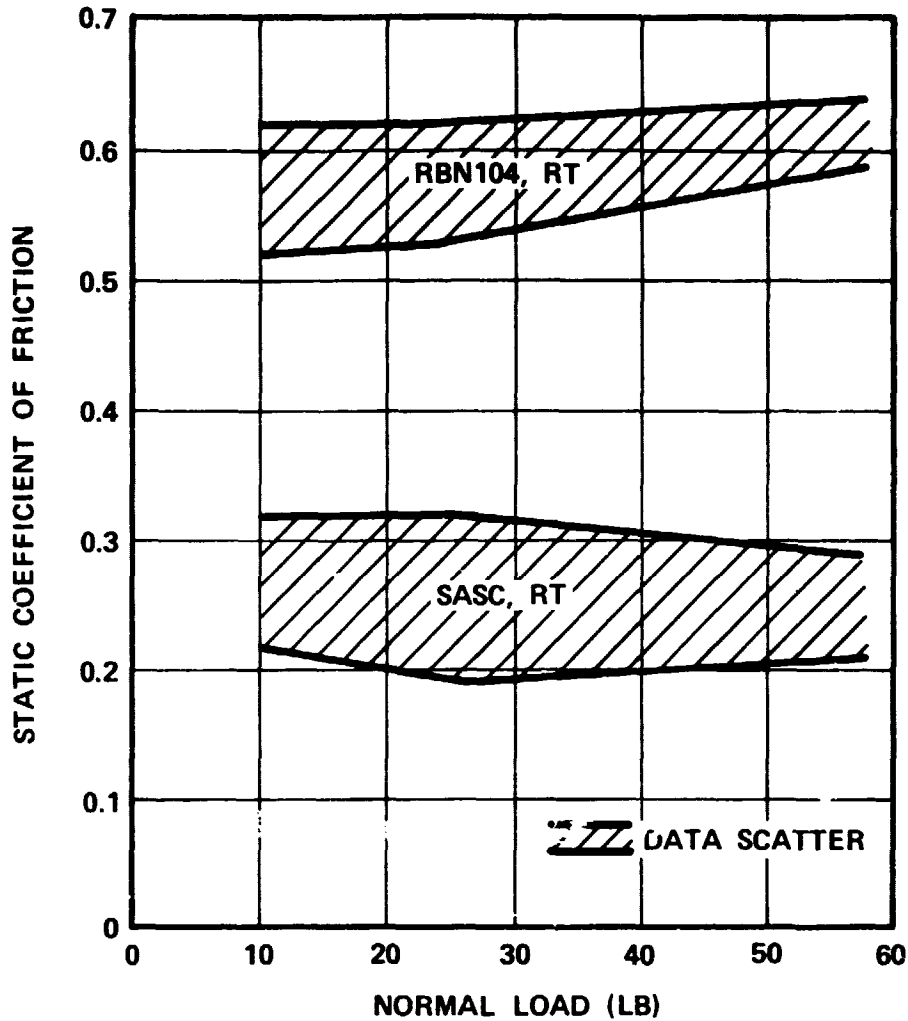


Figure 43. Static Coefficient of Friction Versus Normal Load for RBN104 RBSN and Sintered Alpha SiC (SASC) at Room Temperature.

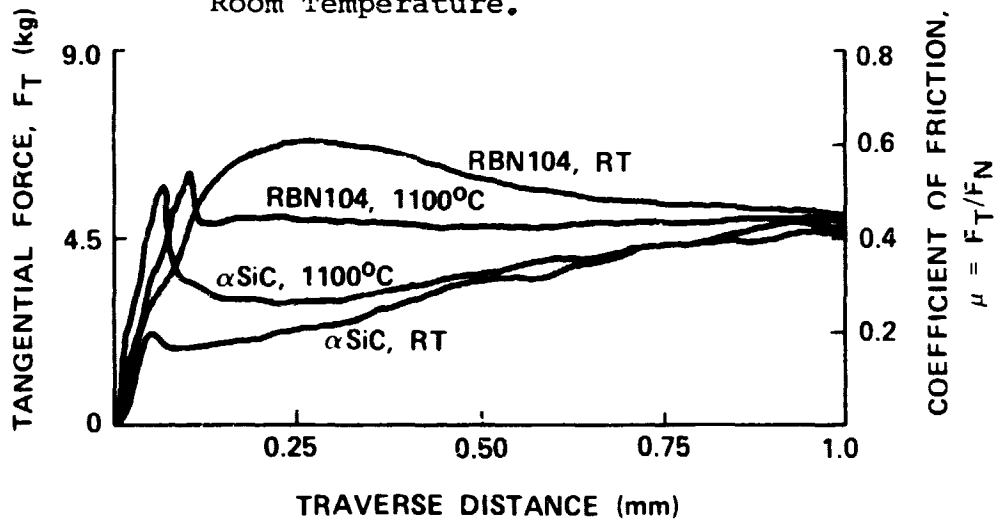


Figure 44. Friction Versus Relative Motion for Bare SASC and RBN104 Under the Point Contact Condition With a Normal Load of 25 Pounds.

interface, which could explain the steady increase in friction. Once a sufficient amount of debris was present, it could begin acting as a dry lubricant, which could explain the later decrease in friction. Very little surface damage was visible on the SASC stationary specimen, but a roughening had occurred on the moving specimen. The accumulation of surface damage on the moving specimen could account for the continuous increase in friction.

- (b) At elevated temperatures, the curves for both materials had a discontinuity between the static and dynamic friction, representative of a breakaway condition. The mechanism has not been fully identified but is suspected to be associated with sticking, due to surface oxidation. Contact surface examination suggests that oxidation is enhanced in the contact region and that, once breakaway occurs, the oxide acts as a viscous lubricant.
- (c) The dynamic coefficient of friction for RBN104 is lower at 2000°F than at room temperature and is approximately constant at 0.45 for normal loads of 10 to 57.3 pounds. The dynamic coefficient of friction for SASC increases with traverse distance at 2000°F and room temperature to the 0.45 range. Friction also appears to increase with normal load at 2000°F.

Most engine components will be pre-oxidized prior to rig and engine testing. Figures 45 and 46 summarize contact data for pre-oxidized RBN104 and SASC. The RBN104 and SASC were pre-oxidized for 2 hours at 2400°F. Pre-oxidation appeared to decrease the room temperature coefficient of friction but had little affect for elevated temperatures.

The point-contact tests at 25 pounds are considered more severe than the static structure components will be exposed to in the AGT101 engine. Current estimates are that the load will not exceed 3.5 pounds over a comparable point-contact area. The purpose of the exaggerated contact loads was to identify the mechanisms of contact damage and to determine the sensitivities of the candidate ceramic materials to surface damage.

Additional tests were conducted at 25 pounds or less with line contact. Initial tests suggest that the data scatter is larger for line-contact than for point-contact. The high-temperature friction data are almost identical for both RBN104 and SASC contact conditions. The room temperature coefficient of friction appears to be substantially lower for the line-contact condition for both materials. The line contact friction data for RBN104 and SASC for the 25-pound normal load are shown in Figure 47.

ORIGINAL PAGE IS
OF POOR QUALITY

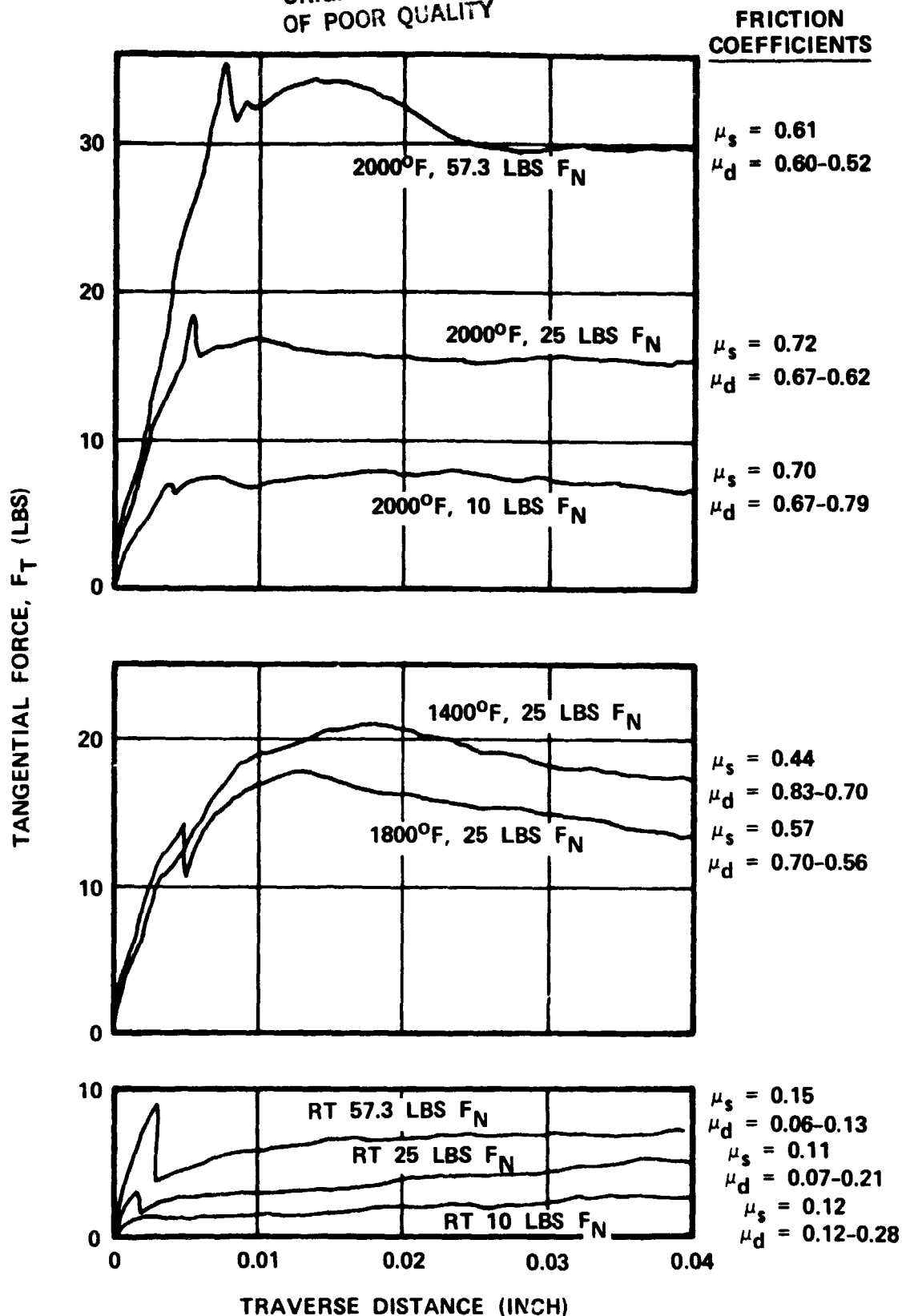


Figure 45. AGT 5072 Oxidized RBN104 Point Contact.

ORIGINAL PAGE IS
OF POOR QUALITY

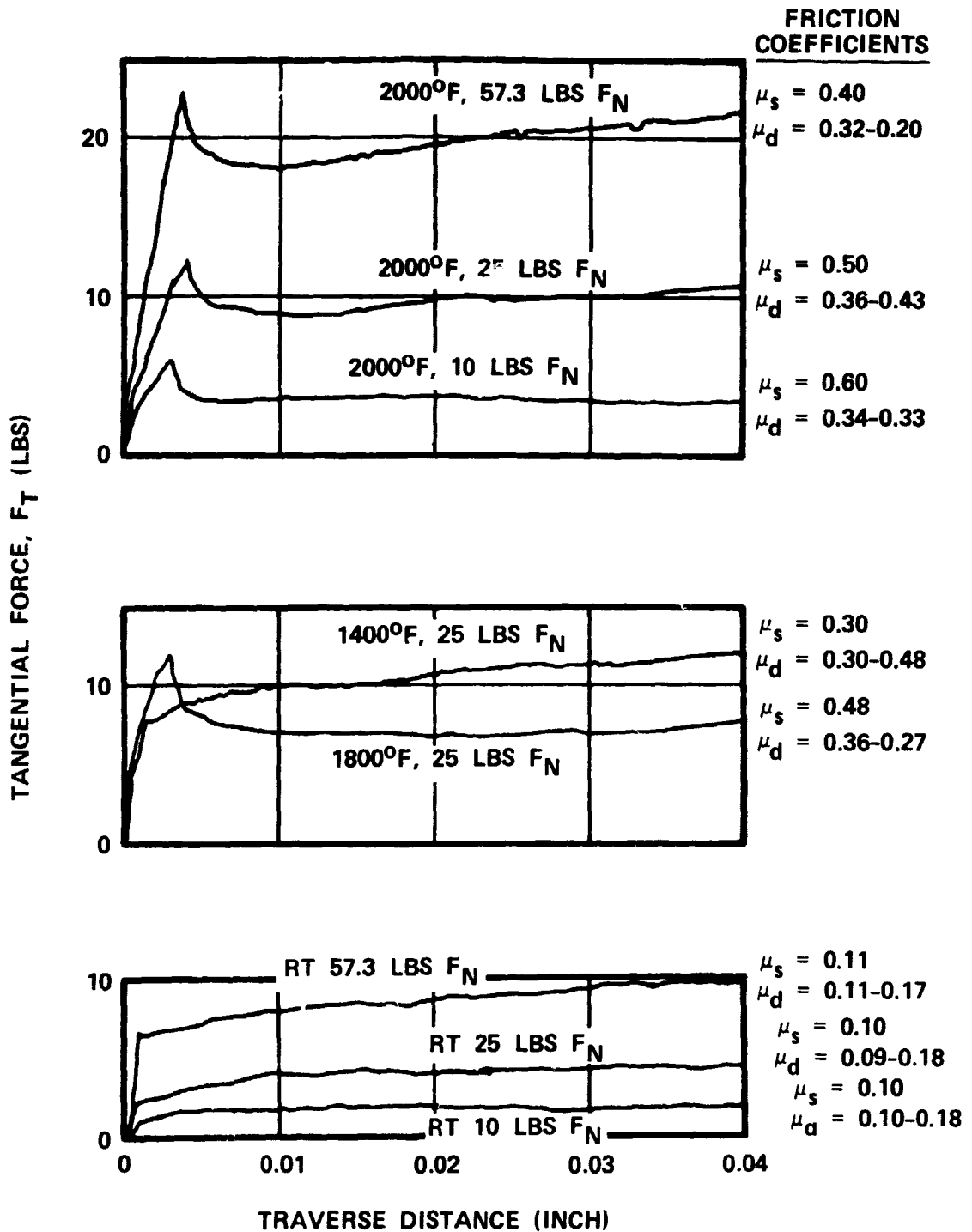


Figure 46. AGT5071 Oxidized SASC Point Contact.

ORIGINAL PAGE IS
OF POOR QUALITY

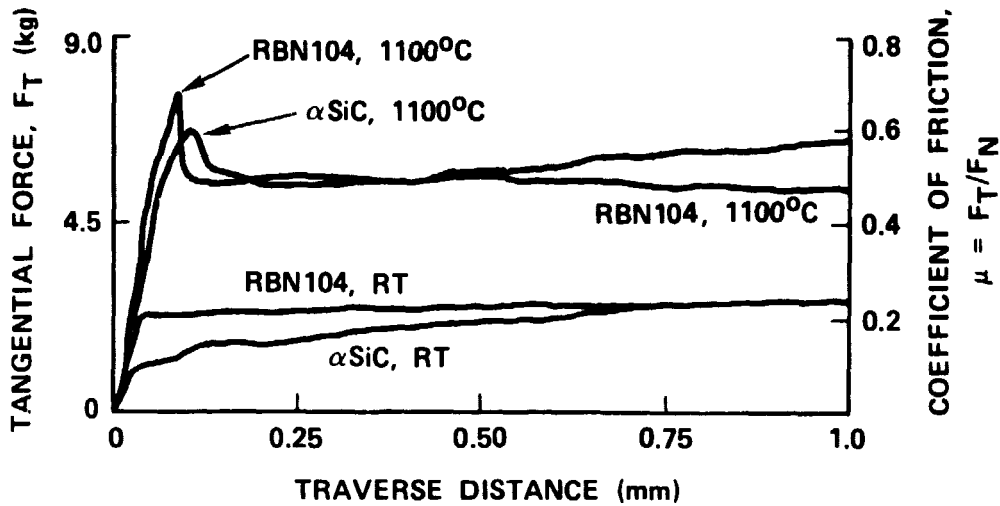
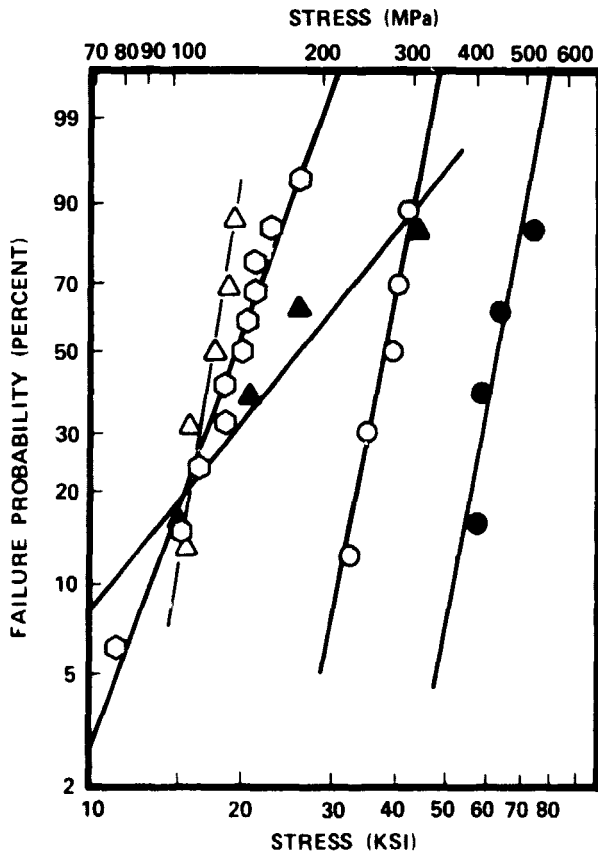


Figure 47. Friction Versus Relative Motion for Bare SASC and RBN104 Under the Line Contact Condition With a Normal Load of 25 Pounds.



LEGEND

MATERIAL	CONTACT	CONTACT TEST TEMPERATURE	AVERAGE 4 POINT MOR (MPa)
△ RBN104	POINT	1100°C	121
▲ RBN104	LINE	1100°C	186
○ NC 350	POINT	RT AND 1100°C	132
○ SASC	POINT	1100°C	258
● SASC	LINE	1100°C	433

Figure 48. Room Temperature Strength of RBN104, NC-350 and SASC After Line and Point Contact Tests.

After contact testing, each specimen was fractured in four-point bending. The strength data are plotted in Figure 48 for point-and line-contact conditions. Obviously, the RBSN materials have lower residual strength than SASC, and the point-contact results in lower strength than line-contact. More specifically, the RBN104 and NC-350, exposed to point-contact biaxial loading, have residual strengths of 17.5 and 19.1 ksi (121 and 132 MPa) respectively. Strengths of these materials prior to contact exposure typically range from 40 to 55 ksi (275 to 380 MPa). Strength degradation in the range of 60 percent has occurred.

The line-contact strength curve in Figure 48 for RBN104 intersects the point-contact curve, although most of the individual line contact data points are higher. Examination of the line-contact surfaces shows that contact (and the resulting damage) only occurred at high points and varied from specimen to specimen. Specimens having a low residual strength typically had contact only along a small segment of the line. As the degree of contact along the line increased, the residual strength increased, suggesting that load distribution and load sharing are important in minimizing contact damage in RBSN. This also explains the spread in the data for RBN104 in "line" contact.

Figure 48 shows that SASC has higher residual strength than RBSN. Specifically the average strength of SASC after point-biaxial contact is 37.4 ksi (258 MPa). The average strength prior to contact exposure for the configuration tested is approximately 65 ksi (450 MPa). The resulting strength degradation for the SASC, therefore, is approximately 43 percent for point-contact and 4 percent for line-contact.

To estimate the actual tensile stresses applied at the ceramic surfaces during biaxial contact loading, the contact apparatus data for RBN104 and SASC were run through a contact stress analysis computer program developed under an Office of Naval Research Program⁽⁵⁾. The results for room temperature and 1100°C point- and line-conditions are summarized in Table 10. The 1100°C results are plotted in Figure 49 and compared with baseline four-point flexural strength data for the line-contact configuration.*

The predicted stresses for the point-contact condition considerably exceed the baseline strengths of both RBN104 and SASC and would be expected to produce the degree of surface damage that would yield the severe strength degradation measured. Peak stresses for line contact are substantially reduced, only exceeding the baseline strengths of RBN104 and SASC at normal loads above 15.4 pounds (for the configuration studied).

*Specimen-oriented in the four-point test fixture with the flat surface in tension and the 0.63-cm radius surface in compression.

ORIGINAL PAGE IS
OF POOR QUALITY

TABLE 10. PREDICTED CONTACT TENSILE STRESSES FOR POINT-
AND LINE-CONTACT CONDITIONS

Material	Normal Load, lb	Contact Test Temperature, °C	Point-Contact		Line-Contact	
			μ_s^*	$\sigma_p',^{**}$ ksi	μ_s^*	$\sigma_p',^{**}$ ksi
RBN104 RBSN	10	Room	0.62	148	0.18	10
	25		0.62	219	0.22	20
	57.3		0.64	293	0.22	31
	10	1100	0.64	152	0.54	32
	25		0.60	212	0.68	64
	57.3		0.52	236	0.53	75
Sintered α -SiC	10	Room	0.25	67	0.25	20
	25		0.19	77	0.09	11
	57.3		0.26	154	0.15	28
	10	1100	0.66	170	0.62	5
	25		0.51	200	0.61	75
	57.3		0.51	290	0.70	131

* μ_s = static coefficient of friction

** σ_p = calculated peak tensile stress

ORIGINAL PAGE IS
OF POOR QUALITY

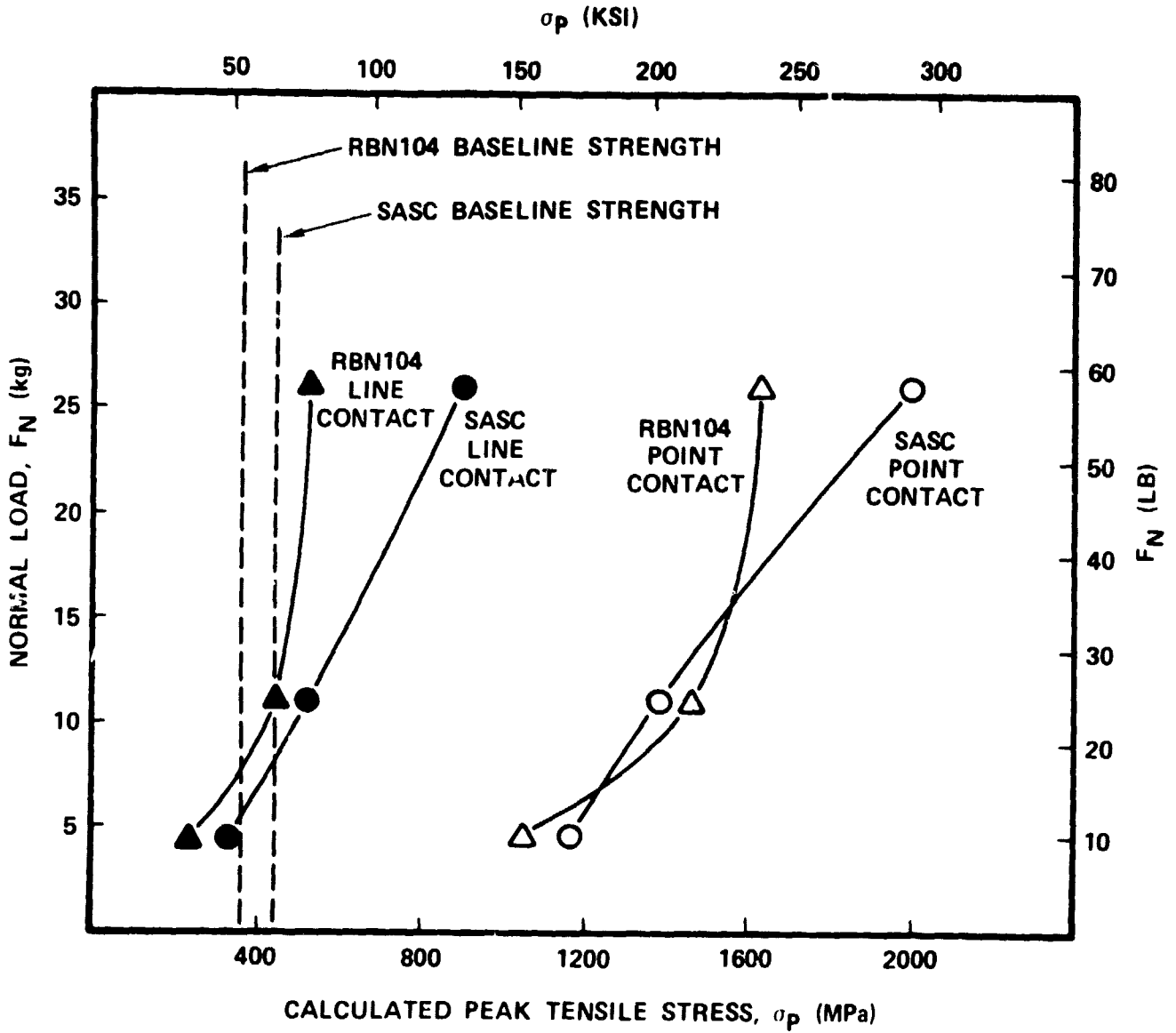


Figure 49. Calculated Peak Tensile Stresses for 1100°C Contact Tests of RBN104 and SASC.

Correlation between analytically estimated peak stresses (see Figure 49) and retained strength are not as good for SASC in line-contact. Estimated contact stresses substantially exceeded the baseline strength of the material, yet very little strength degradation occurred.

The high calculated stress is due primarily to the high static coefficient of friction value used in the calculation. The analysis assumed elastic conditions and that the complete tangential force defined in the static coefficient of friction was producing tensile stress in the ceramic. Examination of the contact surface (Figure 50) shows that a glass layer was present, and examination of the friction curves (Figures 44 and 47) shows that sticking occurred at high temperature. With a viscous glass layer at the contact surface, a portion of the tangential force would be consumed in initiating and sustaining motion in the glass, thus reducing the stress on the ceramic. To understand the contact stress conditions for a ceramic component in an engine, the analysis approach must be modified to include viscoelastic as well as elastic effects. Experiments to provide the appropriate data are in progress.

4.7.1.5 Coating Development

Effort has continued to develop plasma-deposited ceramic coatings for component interfaces that will reduce contact stresses by reducing friction, reducing sticking, and distributing loads. Plasma-sprayed coatings evaluated so far are ZrO_2 , Al_2O_3 , Cr_2O_3 , mullite ($Al_6Si_2O_{13}$) and Ford Ill2. Some friction and retained-strength data were presented in Reference 1; additional data and an assessment follow.

Three specimens did not survive the 2000°F cycling. The ZrO_2 coating on the SASC test bar spalled, due to a poor bond between the specimen and the coating. Both the glassy finish and dull finish Ford Ill2 coatings on SiC spalled during the 2000°F cycling, due to poor bond strength between the coating and the SiC specimen. The remaining five specimens survived both the 2000 and 2250°F thermal shock test with no apparent damage or reaction between the coating and test bar. Two of the five specimens survived the 2600°F test with the coating intact, although some damage was noted on one of the two. The mullite-coated SASC specimen showed no sign of damage after the 2600°F exposure. The ZrO_2 -coated RBN104 specimen remained intact, although the coating had a small crack. Both SASC and RBN104 specimens with the combination mullite/ ZrO_2 coating and the RBN104 specimen with mullite coating showed melting in the coating. Figures 51 and 52 show the specimens before and after the thermal shock test. There appears to be a reaction between the test specimen and the coating on the three specimens that showed melting.

In summary, ceramic coatings have been successfully applied to RBSN and SASC by plasma spray techniques. To date, of the coatings

ORIGINAL PAGE IS
OF POOR QUALITY

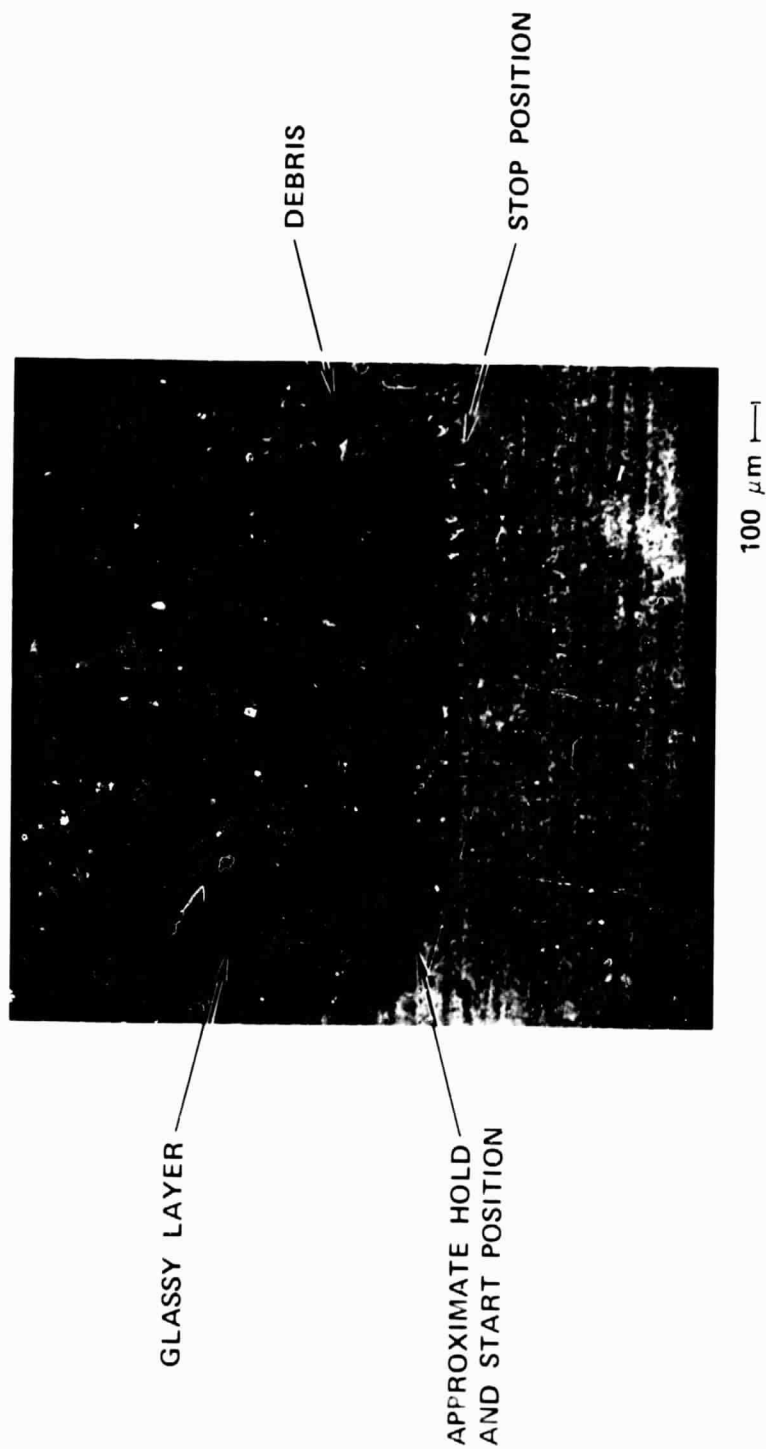


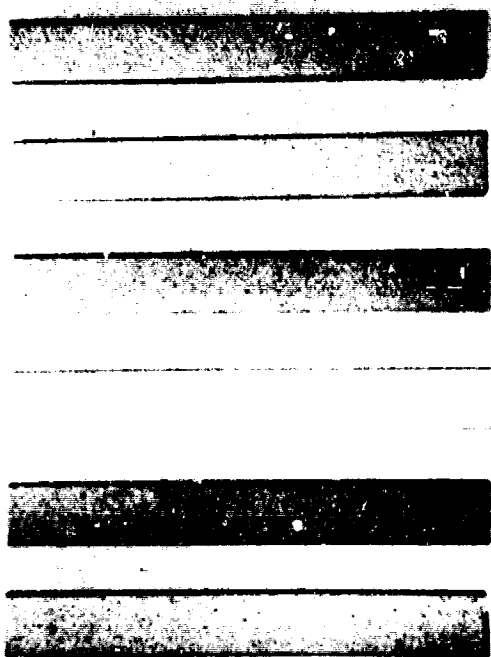
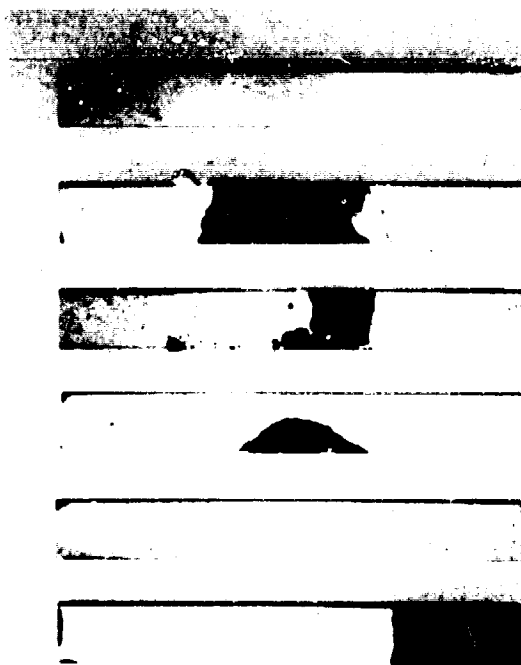
Figure 50. Scanning Electron Photomicrograph Showing the Contact Surface Features for SASC Tested at 1100°C With a Normal Load of 25 Pounds.

ORIGINAL PAGE
BLACK AND WHITE PHOTOGRAPH

MP-25547

RBN104

α SiC



2600
SURVIVED
COATING
CRACKED

2600
MELTING

2600
MELTING

2600
MELTING

2600
SURVIVED

2000
SPALLING

ZrO₂

ZrO₂ +
MULLITE

MULLITE

ZrO₂ +
MULLITE

MULLITE

ZrO₂

POST THERMAL SHOCK

AS PLASMA SPRAYED

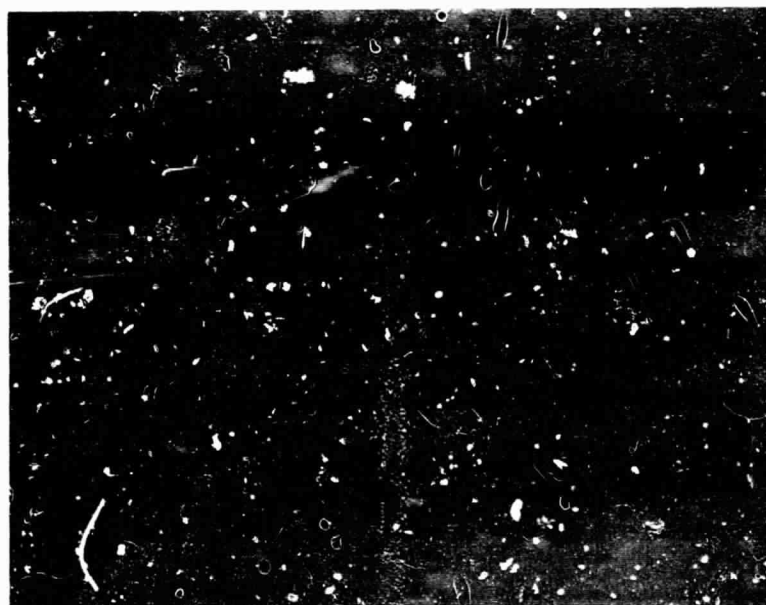
Figure 51. Thermal Shock Results for Plasma Coatings.

ORIGINAL PAGE
BLACK AND WHITE PHOTOGRAPH



GLASSY I112 DULL I112

AFTER 5 CYCLES TO 2000°F
2X



GLASSY I112 DULL I112 UNCOATED SPECIMEN

AS-COATED SPECIMENS
2X

Figure 52. α SiC with Ford I112 Plasma-Sprayed Coatings.

evaluated, mullite has the best adherence and temperature capability. Mullite does not reduce the high-temperature friction, but does appear to provide compliancy (because of the low as-deposited elastic modulus) which helps distribute the applied load and reduces surface damage in RBSN or SASC.

Coating development and evaluation is continuing, but at a low level of effort. Effort will be directed to preparation of fluxed coatings.

4.7.2 Ceramic Component Interface Rigs

4.7.2.1 Bolted Interface Rig

The AGT101 Mod I complete and Mod II engines replace the metallic structures of Mod I, Build 1, with high-strength ceramic components. Interface tests discussed in Section 4.7.1.4 revealed high coefficients of friction between pairs of ceramic surfaces at elevated temperatures. These results, however, do not include the combined interaction of layered ceramic components with ceramic-to-ceramic and ceramic-to-metal interfaces bolted together in a common stack. The large differences in thermal expansion, with the variation of surface microstructures between these components in severe thermal gradients, give rise to the need for a simulation of the bolted interface prior to engine operation.

A bolted interface rig can be seen in Figure 53 in which two identical stacks of ceramic and metal plates and washers simulate the static components of the actual engine. Objectively, this rig must duplicate the thermal gradients, relative expansion characteristics, and tolerances of the engine but will not duplicate the displaced loads at the interfaces caused by dynamic (pressure) loading of the engine components. The contact stress levels, due to the relative motion between these parts and the corrosion factor at elevated temperature, will have priority in this test rig.

- o Rig Design - The rig has been designed such that two bolted interface stack assemblies are bolted to the top of a rotating (approximately 120 rpm) pedestal and secured with varying bolt-clamping loads. Then, the assemblies are subjected to a directed-flame front, while being rotated so that heating to 2000°F can be achieved uniformly in the assemblies. The assemblies are initially thermocoupled, and the flame calibrated to a focused pyrometer prior to testing.

Cooling air is supplied to the inner cavity of the rotating pedestal to provide the proper thermal gradient between the ceramic-to-metal interfaces.

- o Test Evaluation - Configuration evaluation will be achieved by visually inspecting the interfaces at 40X magnification

ORIGINAL PAGE IS
OF POOR QUALITY

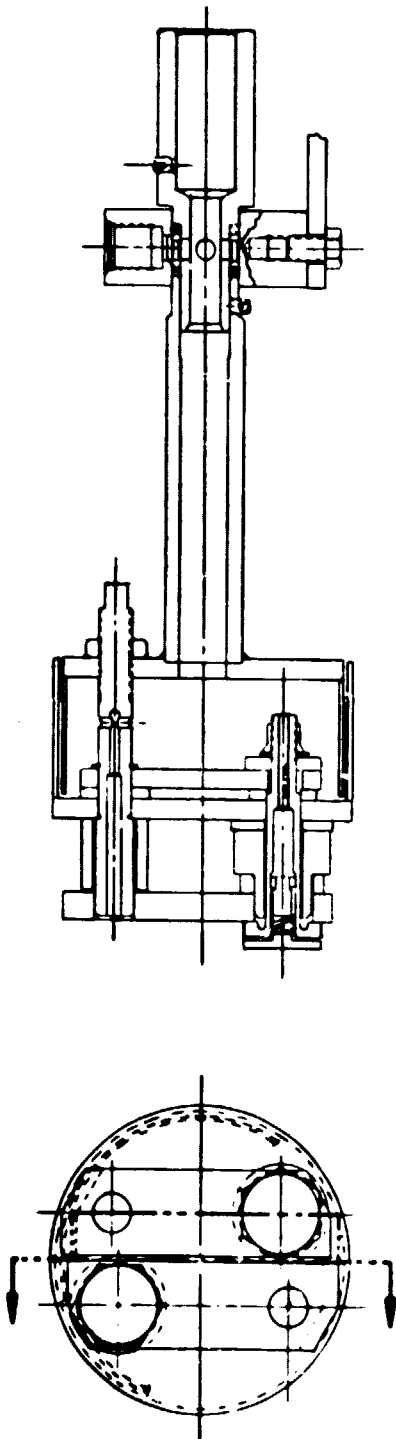


Figure 53. Bolted Interface Rig.

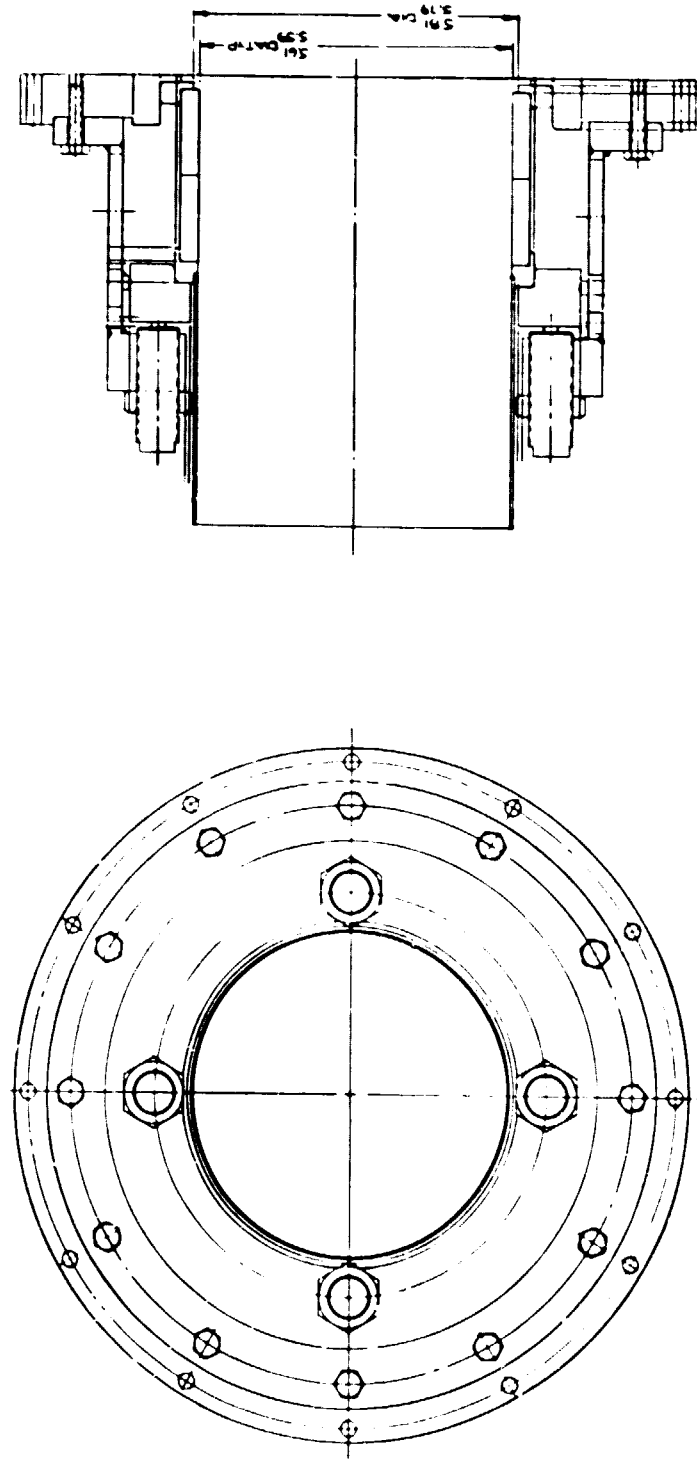


Figure 54. Ring Type Interface.

(minimum) to determine if mechanical or chemical interaction of the interface surfaces exists.

Coatings will be evaluated (as required) in like manner so that contact stress levels can be controlled to acceptable levels.

4.7.2.2 Ring Type Interface Rig

The difficulty with current contact stress evaluations lies in the inability to duplicate the complex interactions of stress between surfaces of cylindrical geometry. The AGT101 has several such interface locations, i.e., regenerator shield to flow separator housing, combustor liner to transition duct, combustor baffle to turbine backshroud, etc.

Displaced loads and temperatures vary in each of these locations and will be closely duplicated in this rig. As in the bolted interface rig ceramic-to-ceramic and ceramic-to-metal (combustor liner to transition duct), interface must be duplicated. Further, a well-defined interface geometry (area, radius, interrupted, etc.) is necessary that will meet engine duty cycle requirements.

- o Rig Design - The rig design is comprised of two cylindrical rings which affect the interface. The rig can accommodate similar materials, dissimilar ceramics or ceramic and metal.

Figure 54 shows the test specimens located within the rig, and the four hydraulic cylinders that supply a combined load up to 1000 pounds. The loading cylinders are connected to electrically actuated solenoids that receive their respective input signals from a programmable control box. This provides for uniform or non-uniform loading of the ceramic interfaces, as required for completeness in testing.

The heat source (not shown in this view) is composed of a circular torch head mounted to a pneumatic cylinder under the rig mount, which provides axial motion of the flame-front past the interface parting line. As in the hydraulic loading, this heat source is programmable for cyclic axial movement at a predetermined rate based upon the rate of specimen heating.

- o Test Evaluation - This test will be evaluated based on visual inspection of the respective interfaces by 40X magnification (minimum) to determine again if interface surface degradation exists. Testing will proceed until a suitable combination of interface geometry, surface finish, and/or coating has been achieved.

4.7.3 Simulated Rotor Spin Testing

An SASC simulated rotor, fabricated by Carborundum, achieved a room temperature burst speed of 72,400 rpm. This rotor consisted of a sintered core formed from isopressed material hot-press-bonded to a sintered shell formed by injection molding. A plastic SiC mix, applied to the interface prior to hot-pressing, served as the bond material. Radiographic inspection prior to testing indicated several small cracks in the bond region but only in low-stress regions.

The rotor shaft was machined to provide a interference fit with a 4340 Stainless Steel spin test arbor. The arbor was heated to 500°F prior to assembly to provide a shrink-fit. The rotor/arbor assembly was then balanced and attached to the spin-pit output shaft, which was powered by an air turbine motor. The spin-pit facility was fully instrumented to measure rotor speed and shaft excursion. The rotor was uniformly accelerated to burst, which occurred at 72,400 rpm. No significant rotor shaft excursions occurred prior to 68,000 rpm, at which point 2 mils of radial excursion occurred until burst speed was reached. Stacks of computer cards were placed inside the spin-pit circumference to catch the burst rotor pieces and to minimize secondary fractures.

The rotor fragments, with the arbor attachment, are shown in Figure 55. The larger fragments were from the shell. An examination of these fragments indicated that some de-bonding occurred, primarily at the core/plastic mix interface. However, the absence of imbalance prior to burst, with a fairly uniform distribution of fragments around the spin-pit circumference, indicated that fracture initiated in the core rather than by de-bonding. The maximum principal stresses in the rotor at burst are shown in Figure 56. The maximum core stress was 16.3 ksi. The radial stress along the bond line was 8 to 9 ksi.

A second rotor, identical to the spin-test rotor, was sectioned to determine the strength of the isopressed core material. The results are shown in Figure 57 and indicate a much lower characteristic strength than obtained in baseline material testing. This is evidently due to the low density achieved in the isopressed core of both the sectioned and spin-test rotor. With the measured Weibull parameters used for the core material (36.1 ksi, $m = 7.5$), a probability of failure of 97 percent was obtained for the simulated rotor at 72,400 rpm. These results suggest that the analytical prediction of rotor failure is conservative.

4.7.4 Rotor Development Status

4.7.4.1 Rotor Materials

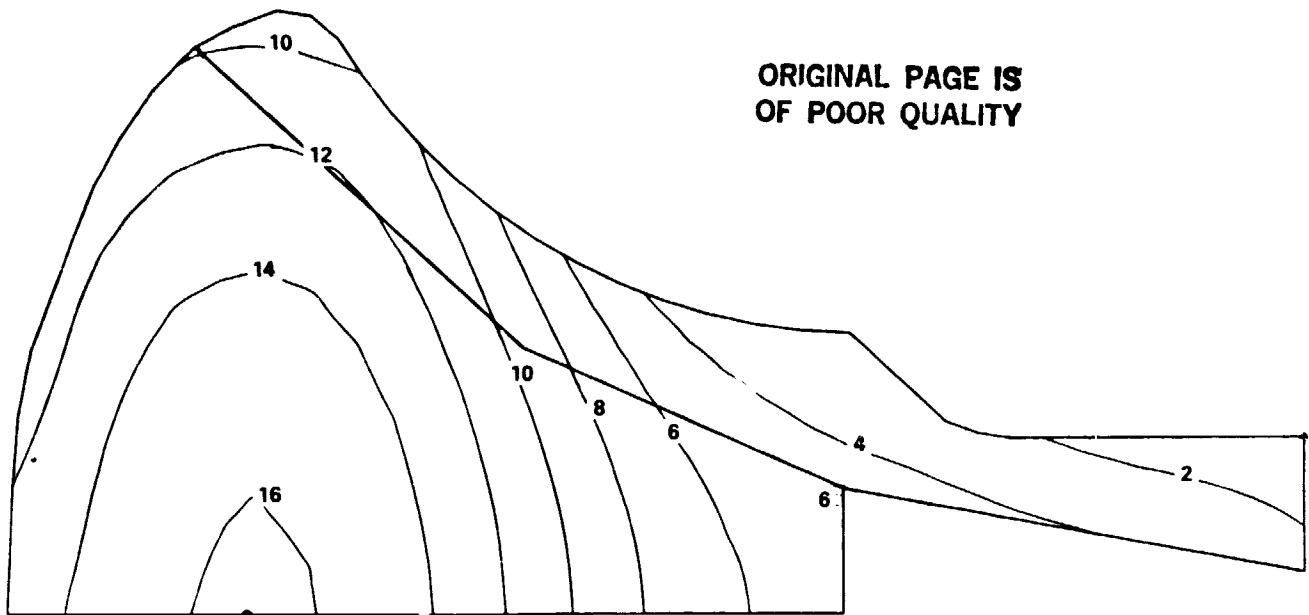
Rotor material evaluations indicate that the majority of candidate rotor materials meet, or nearly meet, the first-year material

ORIGINAL PAGE
BLACK AND WHITE PHOTOGRAPH



Figure 55. Simulated Ceramic Rotor Particles
following Sping Test.

ORIGINAL PAGE IS
OF POOR QUALITY



SIGMA PMX

0.001 IN. INTERVAL

Figure 56. SASC Simulated Rotor - 72,400 RPM.

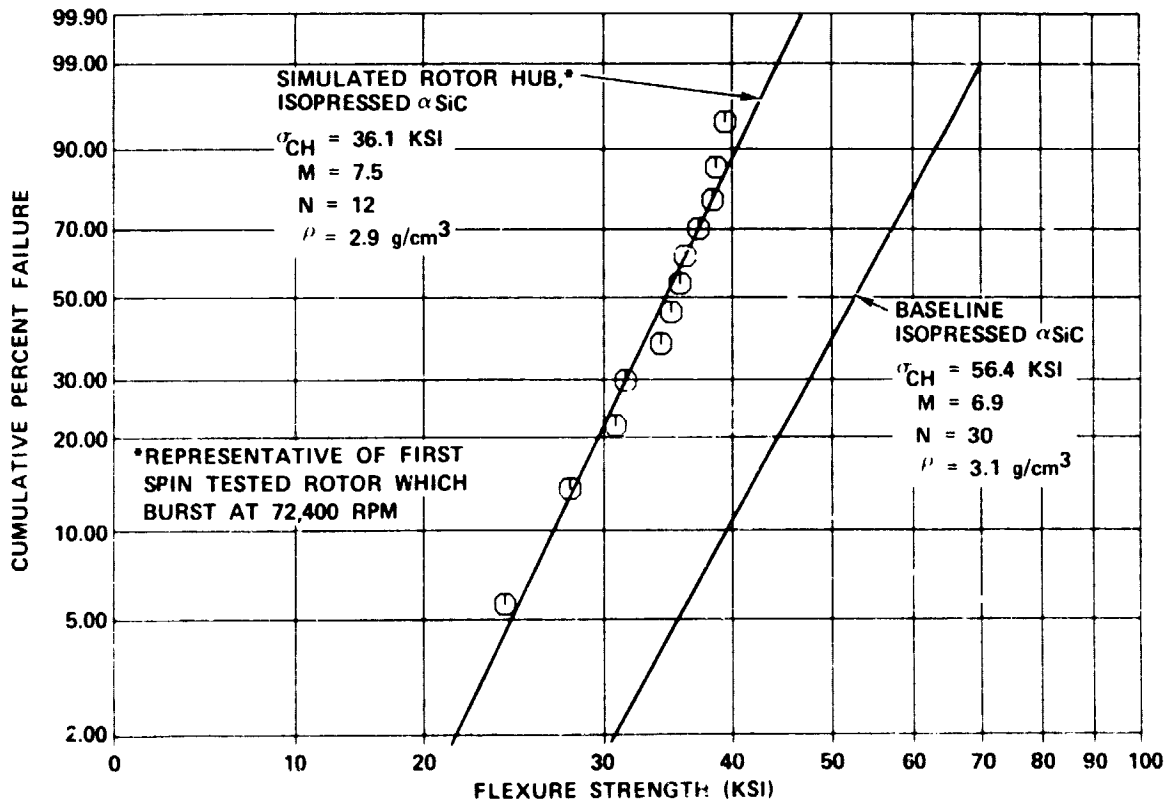


Figure 57. Strength of Low Density Carborundum α SiC Cut From Simulated Rotor Hub.

strength goals. Nominally, these goals are a Weibull characteristic strength of 68 ksi and a Weibull modulus of 12 at 2000°F and are based on a rotor stress distribution that peaks at approximately 30 ksi within the rotor hub.

Material characterization results indicate that the strengths of both Ford sintered RBSN and ACC SNN522 sintered Si_3N_4 fall off with increasing temperature; however, the Ford material strength exceeds the goals at both room and elevated temperatures. The decrease in strength with temperature of the ACC SNN522 results in strength values just below the first-year goals at 2000°F. However, the results of SNN522 material evaluated in stress rupture at 2000°F (reported in Section 4.7.1.2) confirm the suitability of this material for rotor development applications.

Although no Pure Carbon REFEL reaction-sintered SiC material has been tested under the AGT program, results reported by Garrett under the "3500-Hour Durability Testing of the Commercial Ceramic Materials" Program on extruded REFEL material procured in 1979 indicated a characteristic strength of 73.2 ksi and a Weibull modulus of 10 at 2000°F. These results indicate that the REFEL material is suitable for rotor development. The properties of the isopressed REFEL rotor material, on order from Pure Carbon, are expected to meet or exceed these values.

Although Carborundum's SASC is still below first year strength goals. Carborundum has demonstrated characteristic strengths of 120 ksi in a hot-pressed α -SiC material that may be suitable for rotor core application using a two-piece rotor fabrication approach. Optimization of the hot-pressing composition and bonding procedure for the core insert is in progress.

In summary, suitable rotor candidate material properties have been demonstrated for first-year rotor development for three materials.

4.7.4.2 Rotor Fabrication

All rotor suppliers have made significant advancements in rotor fabrication development, however, simulated rotor fabrication remains a challenging problem. Difficulties are primarily a result of the large volume and thick cross section of the simulated rotor. ACC is approaching the challenge with two development techniques--slip-casting and injection-molding of SNN522 sintered Si_3N_4 . Both approaches have produced the desired shape and surface appearance requirements in the green ware, but cracking during drying and sintering of slip-cast parts and during binder removal and sintering of injection molded parts, continues to occur. Similarly at Ford, rotor shape capability has been demonstrated with a slip-cast sintered RBSN approach, but cracking during drying remains a problem area.

Carborundum has produced the only "spin quality" SASC rotor, i.e., free of X-ray indications and significant visual defects. This rotor was fabricated with an isopressed and sintered core and an injection-molded and sintered shell, which were assembled during a hot-press bonding operation. The delivered rotor was spin-tested by Garrett and provided good correlation between analysis and material properties, as reported in Section 4.7.3. However, since the current SASC does not meet first year strength goals, this fabrication approach is unsuitable. As an alternative, Carborundum has demonstrated the required material strength capabilities with a hot-pressed α -SiC, and is currently developing techniques to fabricate rotor cores by this method. Scale-up and shape capabilities of the hot-pressed core approach remain to be demonstrated.

Pure Carbon Co., in conjunction with British Nuclear Fuels, Ltd (BNFL), is fabricating simulated rotors from reaction sintered SiC. Initially, the ability to obtain full reaction of the thick cross-section rotor during SiC/carbon conversion was questioned. Based upon this doubt, BNFL chose to produce the simulated rotor by isopressing and machining the "green" rotor, prior to conversion. One such rotor has been formed successfully, reacted, and inspected and has been delivered to Garrett. Follow-up evaluation by Garrett, including cut-up and spin testing, is contingent on the Pure Carbon/BNFL ability to demonstrate the reproducibility of the fabrication process. Currently, Pure Carbon is fabricating additional simulated rotors.

In summary, although advancements in rotor fabrication are being made by all suppliers, only minimal rotor deliveries have been made to Garrett. Continued effort is required by all suppliers to achieve rotor fabrication success.

4.7.5 Subcontractor Ceramic Development

The following sections describe progress in component fabrication development by the subcontractors.

4.7.5.1 Ford Motor Company

The Ford report is included as Appendix I.

4.7.5.2 AiResearch Casting Company

The ACC report is included as Appendix II.

4.7.5.3 Carborundum Company

The Carborundum reports for common and unique tasks are included as Appendixes III and IV, respectively.

4.7.5.4 Pure Carbon Company

The Pure Carbon report is included as Appendix V.

4.8 Foil Gas Bearing

Seven foil bearing configurations were characterized and developed on the single bearing test rig shown in Figure 58. All seven of the configurations exhibit acceptable stability, load capacity, and low power-loss characteristics advantageous for use in the AGT Mod I and Mod II Engines. The foil bearing configurations cover a range of spring rates and power-loss characteristics that will provide flexibility to optimize the bearing to the specific requirements of the Mod I and Mod II rotating groups. Three of the seven configurations were fabricated for evaluation on the rotor dynamics test rig. The power-loss characteristics of the three bearings selected are shown in Figure 59. A typical foil bearing configuration is shown in Figure 60.

The AGT engines will incorporate foil bearings with high temperature coatings compatible with the predicted environment. However, to expedite bearing and rotor dynamic development, all foil bearings currently in test have been coated with Teflon-S material with a practical temperature limitation of approximately 600°F. These coatings are acceptable for use in the lower temperature Mod I Engine and all preliminary development on the rotor dynamics test rig. Higher temperature coatings, suitable for the predicted environment of the Mod II engine, are under development in separate R&D programs and will be introduced into the AGT program at a later date.

BLACK AND WHITE PHOTOGRAPH

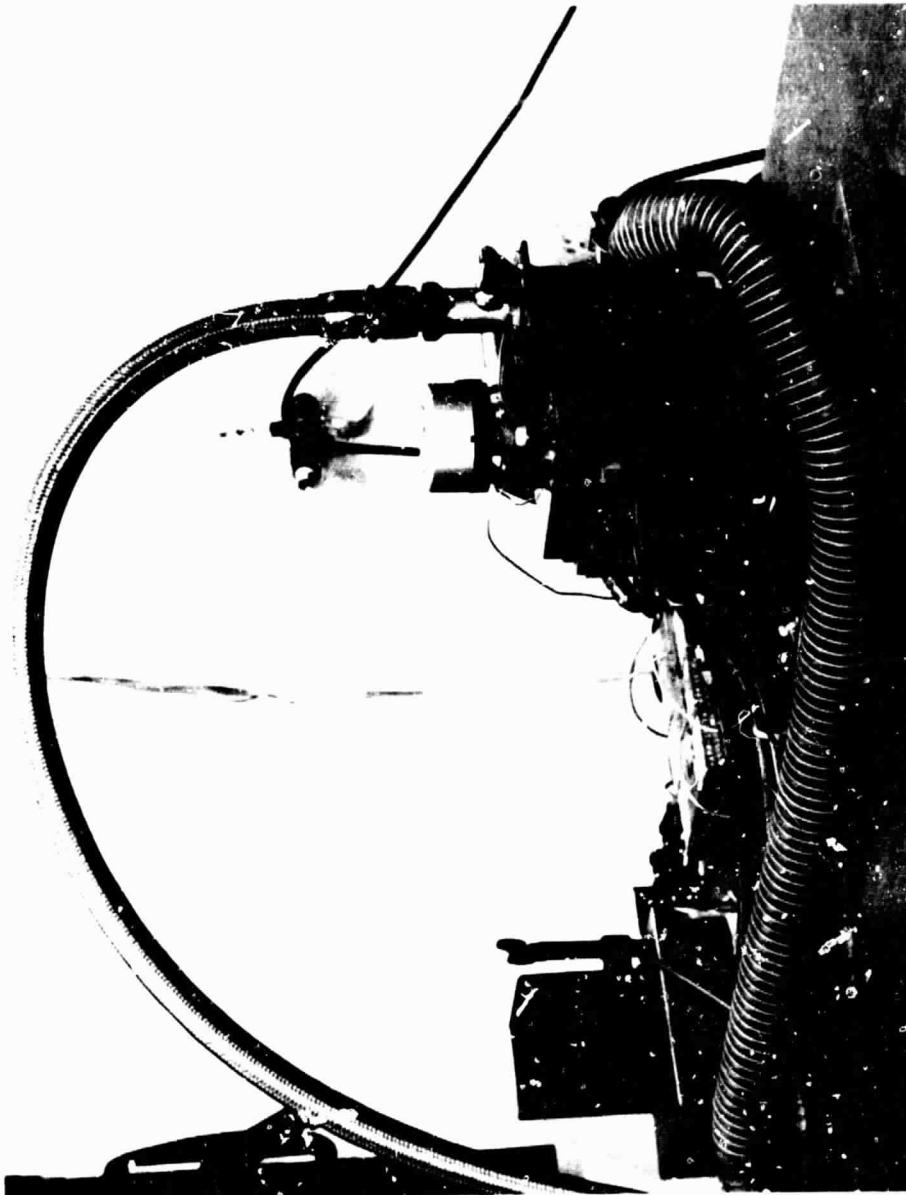


Figure 58. Single Bearing Test Rig.

ORIGINAL PAGE IS
OF POOR QUALITY

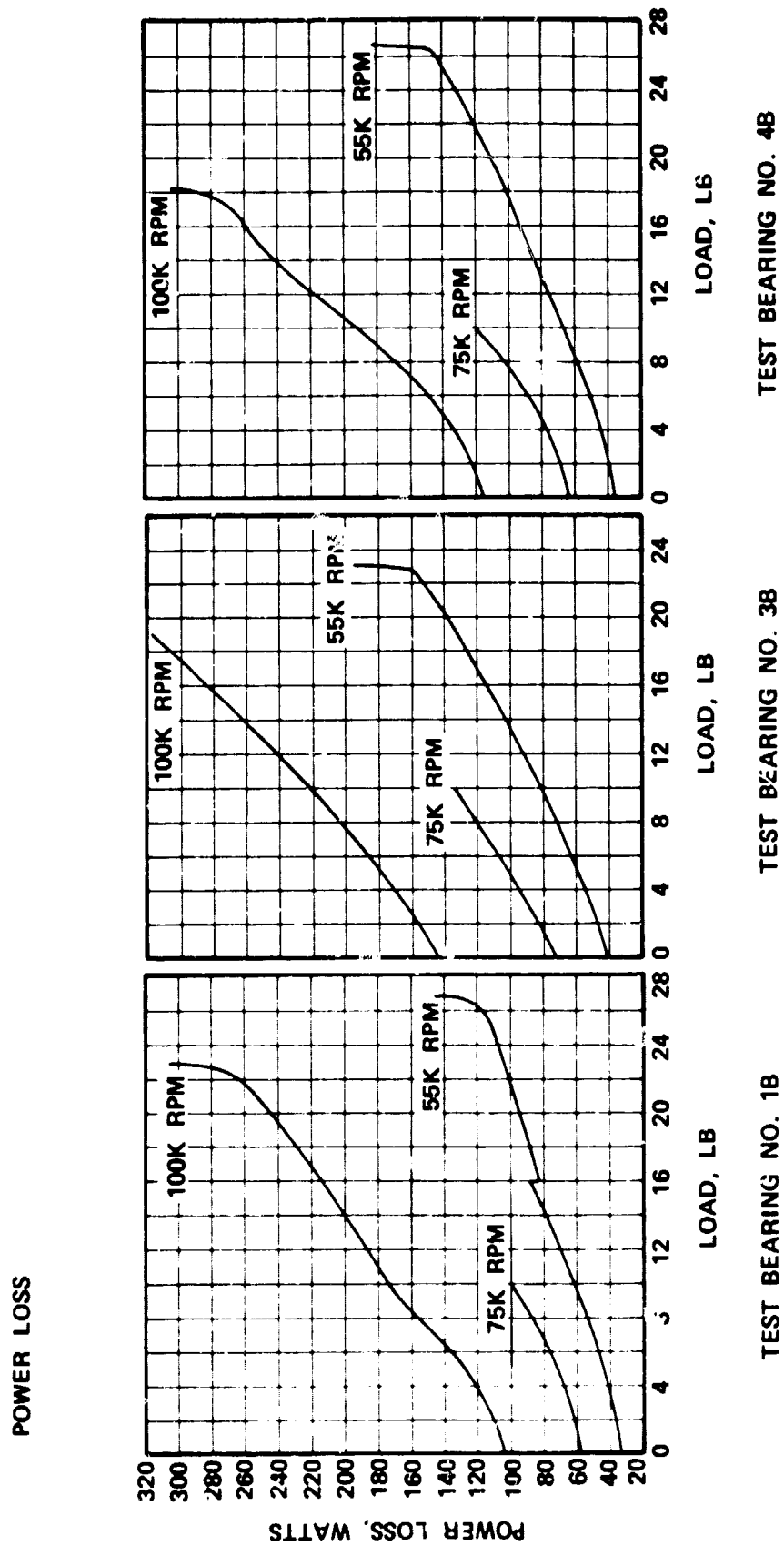


Figure 59. Foil Bearing Development.

ORIGINAL PAGE IS
OF POOR QUALITY

FOIL BEARING



Figure 60. Typical foil Bearing Configuration.

4.9 Bearings and Seals

Quantities of the high-speed pinion bearing and shaft ring seals were delivered for rig use and evaluation. The pinion bearing is shown in Figure 61.

The ring seal assembly for the Mod II design is shown in Figure 62. The ring seals will be developed and evaluated in a seal test rig and rotor dynamic test rig prior to engine test.

Bearings for the AGT gearbox were placed on order for delivery by July 1981.

C-2

ORIGINAL PAGE
BLACK AND WHITE PHOTOGRAPH

PINION BEARING

AGT101

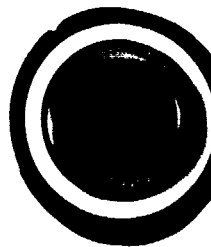
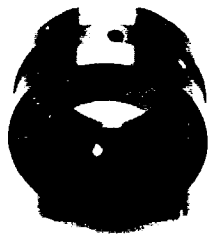


Figure 61. Pinion Bearing from FAG Bearing, Inc.

ORIGINAL PAGE
BLACK AND WHITE PHOTOGRAPH



RING SEAL ASSEMBLY



Figure 62. Ring Seal Assembly.

4.10 Rotor Dynamics Development

Fabrication of the rotor dynamics test rig was nearly complete. The test facility, with the rig drive and the rig main housings in place for alignment, is shown in Figure 63.

4.10.1 Drivetrain Simulator

The drivetrain simulator, shown in Figures 64 through 66 will be designed and fabricated to meet the following objectives:

- o Verify gearbox function and performance
- o Verify VSTC function
- o Verify integration of gearbox/AOD transmission
- o Verify control logic
- o Verify integration and function of engine accessories
- o Verify function and integration of power section, gearbox, AOD transmission and controls.

ORIGINAL PAGE
BLACK AND WHITE PHOTOGRAPH

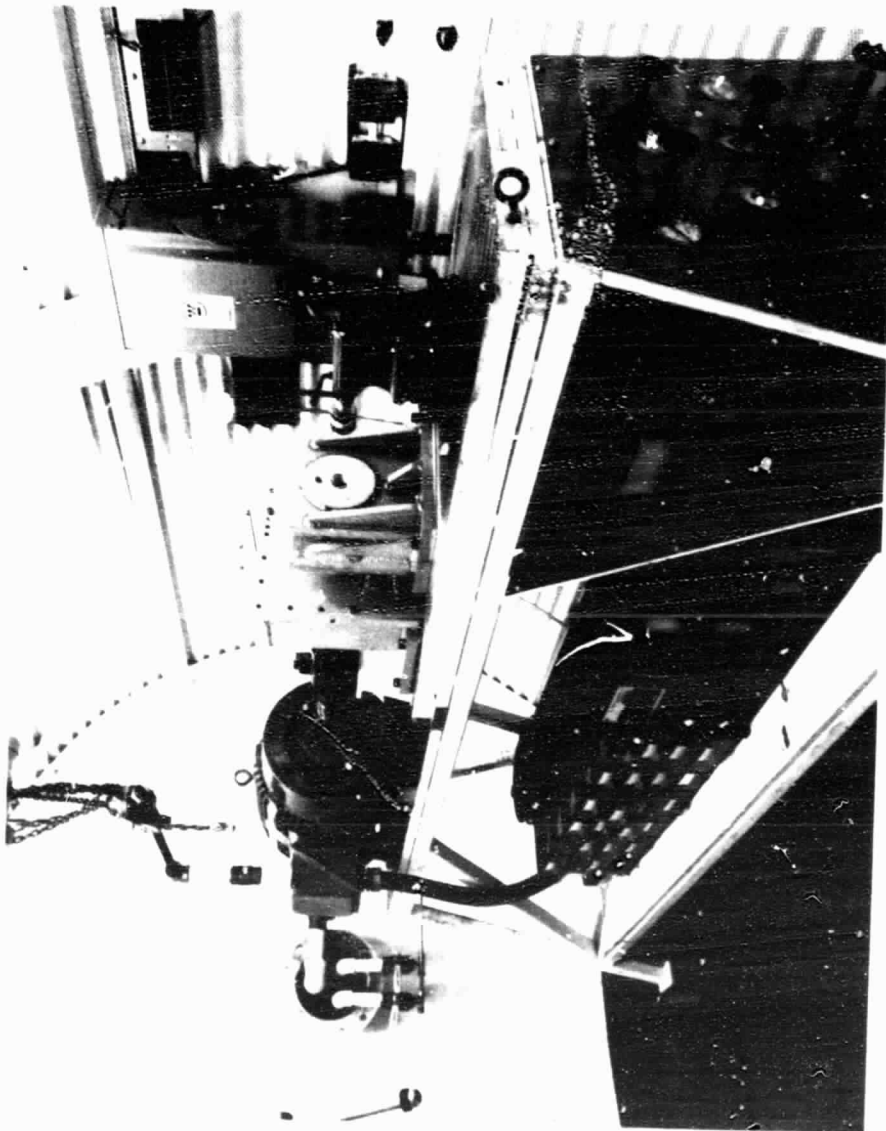


Figure 63. Rotor Dynamic Test Rig Facility.

ORIGINAL PAGE IS
OF POOR QUALITY

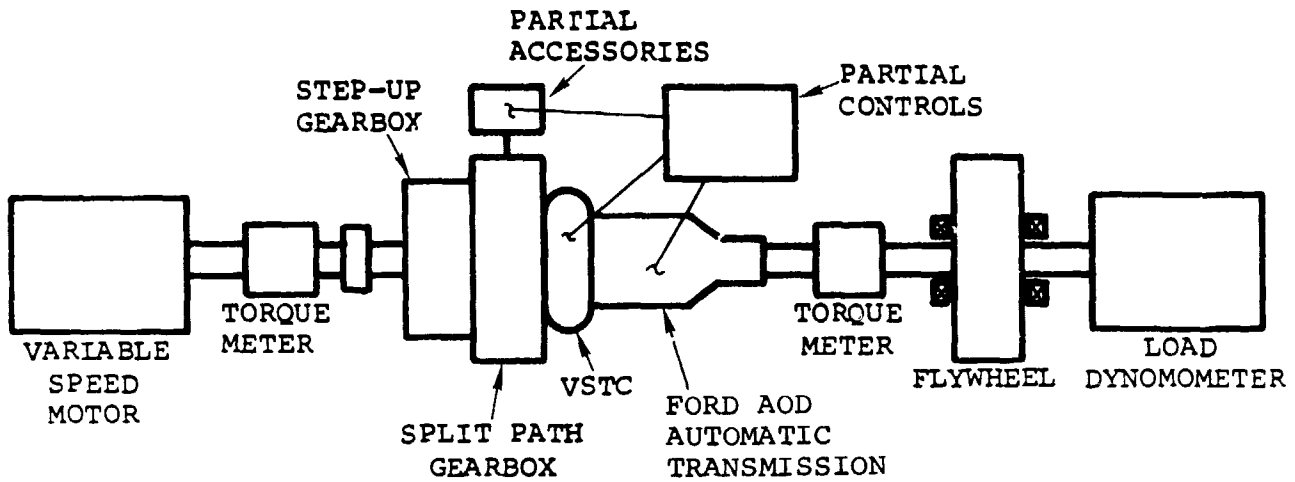


Figure 64. Drivetrain Simulator Basic Configuration.

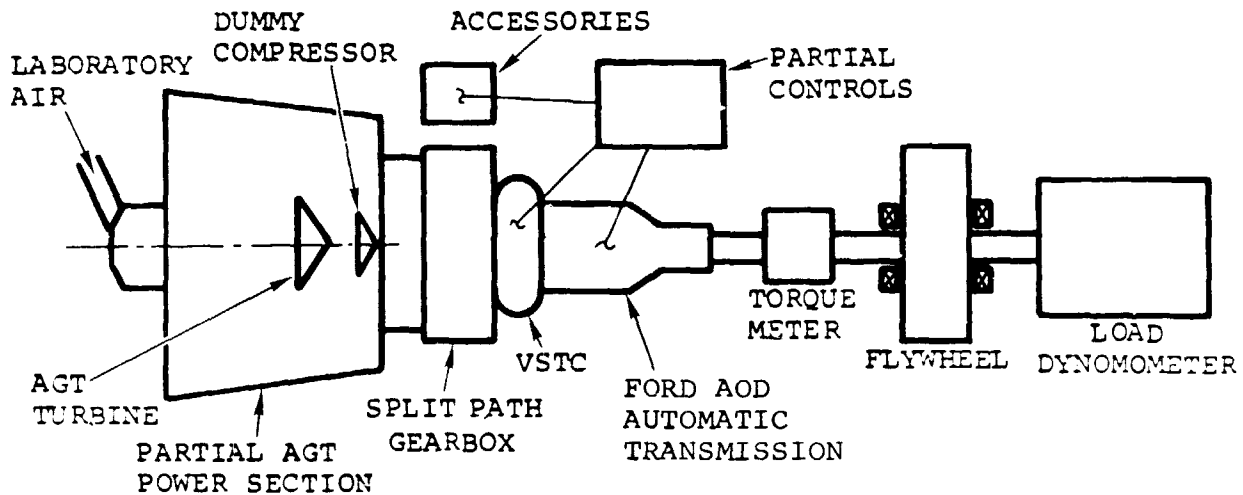


Figure 65. Drivetrain Simulator with Partial Power Section Turbine Drive.

ORIGINAL PAGE IS
OF POOR QUALITY

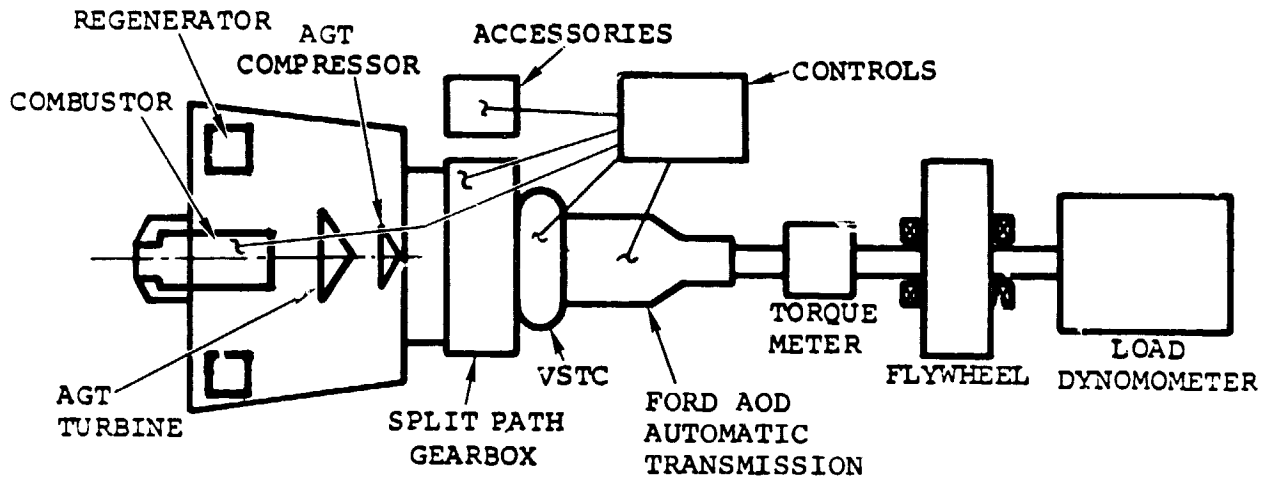


Figure 66. Drivetrain Simulator Full AGT Power Section Drive.

4.11 Controls and Accessories

4.11.1 Fuel System

The major effort during the period has centered on development testing of an interim fuel delivery system for the first AGT engines. This component combines the elements of pumping and metering in a single unit which is based on the Fluid Power Design (FPD) piston pump. Several metering approaches were evaluated in conjunction with the FPD pump.

The original concept, previously tested, involved an integral inlet metering valve positioned by an electro-mechanical actuator. A second approach involved the use of a standard production version automotive fuel injector as the metering device to the pump. The injector was tested and its performance documented as a separate component prior to integration with the FPD pump.

The two components were then combined into a prototype assembly in which the automotive injector metered low pressure flow into the FPD piston pump inlet. Testing of this assembly demonstrated that the low frequency pulsations of the injector were eliminated during the pumping operation, and that good flow control was obtained at fuel flow rates down to 1 LB/HR. Subsequent testing, accomplished with hot and cold diesel fuel and gasoline, pointed up the problem of flow sensitivity of the design to fuel vapor pressure, fuel density, and viscosity.

As a result of the limitation uncovered during testing, a design layout incorporating a spill-back metering concept was initiated. Additional research of this concept uncovered a spill-back diesel pump design which bore some resemblance to the new design. As a result, a problem statement was prepared and submitted to sixteen fuel control vendors in an effort to benefit from any existing expertise in this field which might be applicable to the AGT requirements. Layout and design of the spill-back concept will be completed. A review of the proposals and quotes will result in a make-or-buy decision.

A third metering pump assembly was evaluated which was based on a torque motor metering valve in combination with the FPD pump. Additional hot and cold fuel and other functional and performance tests were accomplished on this unit. Consistent repeatable performance of this combination under normal laboratory conditions makes this system a good candidate for test cell operation of the first engines, until the final configuration fuel control, more suited to vehicle operation, is available. System response testing of the prototype assembly has been initiated.

Layout and design of the pilot combustor pump control has also started as shown in Figure 67. Work on the flow divider and air pump

ORIGINAL PAGE IS
OF POOR QUALITY

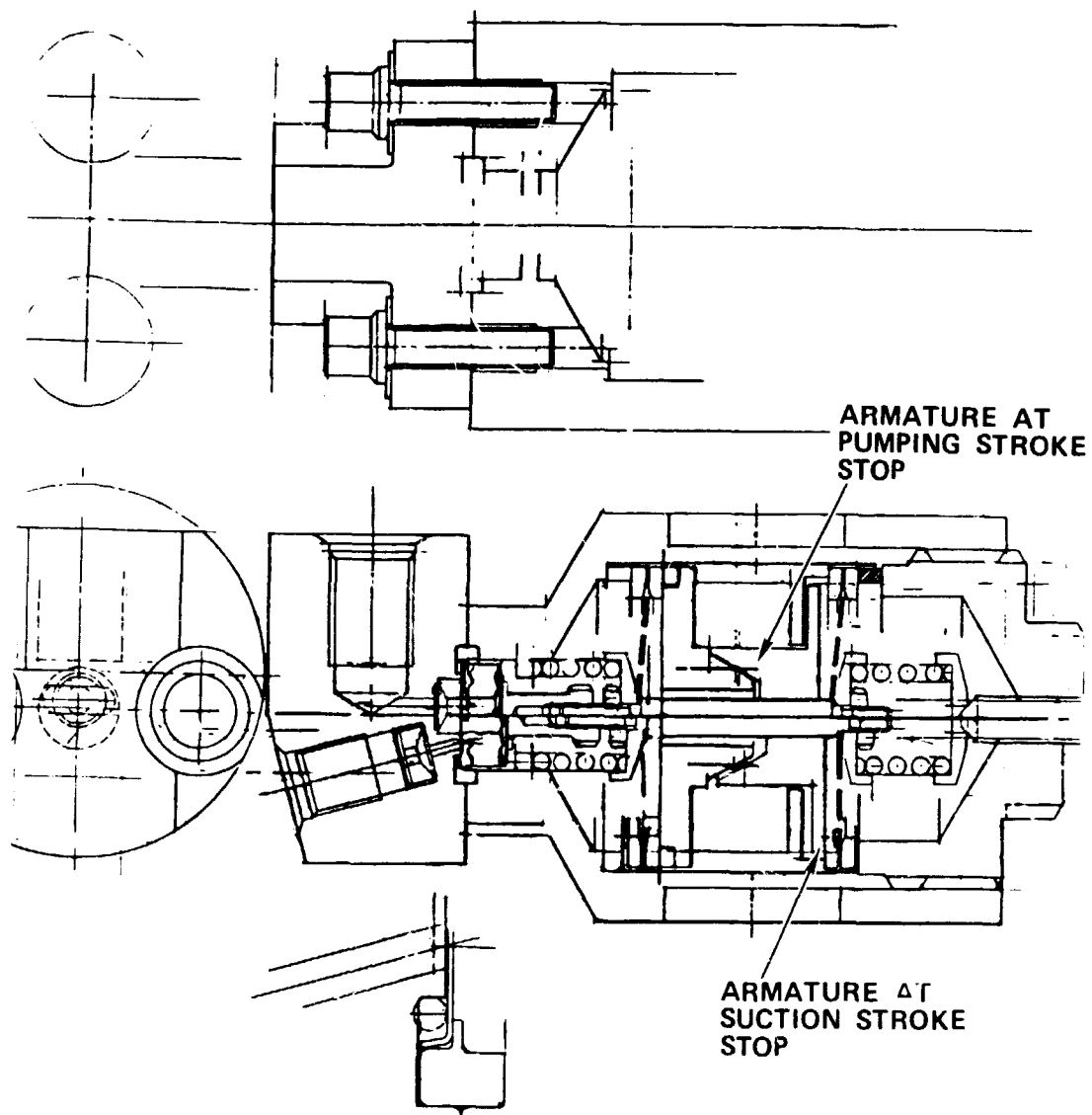


Figure 67. Pilot Combustor Pump Control.

has been deferred until fiscal year 1982 because the first engine has a simplex atomizer (which does not require a flow divider), and shop air can be used for air assist atomization purposes in lab testing of the first engines.

4.11.2 System Analysis

4.11.2.1 Shift Logic

The transmission shift points will be controlled through electrically actuated shift solenoids. This provides maximum acceleration as well as maximum fuel economy during steady-state operation. Present shift logic calls for upshifting when the variable stator torque converter (VSTC) vanes reach an open position (approximately 12 degrees) and downshifting when the vanes reach the closed position (84 degrees). Analysis indicates that it is not necessary to adjust VSTC vanes coincident with a shift, based on consideration given to gearbox stress as well as turbine inlet/turbine exhaust gas temperature transients occurring as a result of the gear ratio change. However, it may be desirable to reposition the VSTC vanes during shifting in order to provide smoother shifts.

4.11.2.2 Idle/Low Speed Operation

An underspeed governor was added to the control logic to keep engine speed from dropping significantly below the idle speed. This was accomplished by opening inlet guide vane (IGV) in proportion to the speed droop.

The vehicle creep velocity (zero throttle, brake off) is approximately 16 mph. To travel at velocities less than the creep speed requires applying the brake, as for the conventional automobile. However, as the brake is applied, torque converter drag on the engine is increased, requiring increased engine power levels to avoid stalling the engine. This is provided by the underspeed governor control logic.

In order to minimize the time delay before the vehicle begins to move, the clutch engagement is delayed to 65-percent engine speed by fully depressing the throttle. This delayed clutch engagement feature also provides improved maximum performance accelerations, and further, computer modeling indicates that the vehicle is capable of starting on and climbing a 30-percent (16.7 degree) grade.

4.11.2.3 T₄ Loop Dynamics

Turbine inlet temperature (T_4) on Mod I final build and subsequent engines is obtained by calculation (rather than direct measurement) as a function of compressor discharge pressure, turbine exhaust gas temperature, ambient pressure, and engine speed. In order to

stabilize the T_4 -VSTC control loop and meet the stringent temperature requirements, the following control features have been specified and incorporated into the system requirements:

- (a) Variable 40:1 lead-lag compensation on measured T_5 (lead-lag varies with engine speed)
- (b) 0.25-second time constant on VSTC actuator

4.11.3 Electronic Control

The digital portion of the electronic control will be packaged on three circuit boards consisting of the memory/CPU, input, and output. Preliminary evaluation and testing was accomplished on prototype circuits and fabrication of the first set of boards was completed.

To aid in development and checkout of these boards, several test programs have also been written. These will be used in conjunction with the microprocessor development system in the functional "debugging" of the input and output boards.

The control software effort also continued with the design and programming of four control modules. Power-up, input, output, and turbine inlet temperature (T_4) calculations are 90-percent complete.

4.11.4 Electrical Accessories

As a result of revisions to the response requirements for the high temperature thermocouples, the combustor inlet ($T_{3.5}$), turbine inlet (T_4), and turbine exhaust gas (T_6) temperature sensors were redesigned from the previous shielded version to a higher response, open bead design.

All engine and accessory connectors have been defined, including component and electronic control pin assignments. This in turn allowed the engine electrical harness drawings to be finalized and released for fabrication; four sets are on order.

4.11.5 Mechanical Accessories

Standard automotive accessories were used as the basis of preliminary mounting location layouts, and to determine power consumption for the transient computer model performance analysis. Any additional packaging/layout work will probably be deferred until a mockup of the engine/vehicle installation is available.

The system lube pump was tested to insure adequate performance throughout the speed operating range. The pump down-sizing will be accomplished upon completion and testing of the drivetrain simulator. Pump down-sizing is intended to increase fuel economy; however, the

final size will also be influenced not only by the powertrain lubrication flow requirements, but also by transient response requirements of the various actuators in the system.

The research torque converter was run dynamically to determine actuator flows and slow rates. The VSTC servo valve was sized and ordered, and the components have been received in-house.

Design of the lube module is nearing completion. This module contains the regulator valves, check valves, bypass valves, oil pressure and oil temperature sensors, solenoid valves and the various actuator supply circuits.

APPENDIX I

FORD MOTOR COMPANY

ADVANCED GAS TURBINE (AGT) POWERTRAIN PROGRAM
SECOND AGT SEMI-ANNUAL TECHNICAL
PROGRESS REPORT

Task 2.3 Ceramic Rotor

Introduction

In Reference⁽¹⁾, the Ford concept for the fabrication of the AGT101 ceramic turbine rotor was presented. The primary approach being developed is a monolithic rotor made by a sintered reaction bonded Si_3N_4 (SRBSN) process. The initial results were encouraging. Strengths exceeding 700 MPa were measured for the SRBSN material and the fabrication of the simulated rotors was proceeding.

A back-up approach to rotor development was the conventional sintering of Si_3N_4 powder, again processed to yield monolithic rotors. Development work indicated that low as-formed and sintered densities posed formidable problems; consequently, this effort was abandoned in favor of the more promising SRBSN primary approach.

This report will update the material development and characterization of the SRBSN materials and the progress on the fabrication of the simulated rotors.

Material Development and Characterization

Composition

Previous sintering experiments were performed solely in the 8 percent Y_2O_3 - SRBSN system. Experiments were performed during this reporting period to optimize the Y_2O_3 concentration. Figure 68 shows sintered density as a function of Y_2O_3 concentration for various sintering runs. This data shows a plateau between 8 and 12 percent Y_2O_3 which results in densities of over 3.25 g/cc. Yttria concentrations of less than 8 percent and greater than 12 percent result in lower density bodies. To further optimize the desired Y_2O_3 concentration, the high temperature strength was studied as a function of the Y_2O_3 concentration (Figure 69). The strength retention at 1200°C was found to decrease with increasing Y_2O_3 . The 8 percent Y_2O_3 material is expected to retain about 85 percent of its strength while the 12 percent Y_2O_3 will retain only about 55 percent. Based on the information contained in Figures 68 and 69, the 8 percent Y_2O_3 concentration was selected as optimum.

Sintering

Previously reported sintering results⁽¹⁾ were obtained using maximum temperatures between 1800 and 2000°C and nitrogen overpressures of 20 atmospheres. An observed relationship of sintered density to the nitrided density led to the conclusion that densities exceeding 98 percent could not be achieved in a rotor configuration. This density problem was resolved with the development of the two stage sintering cycle. This cycle was derived from the work of Hardtl⁽⁷⁾ and

ORIGINAL PAGE IS
OF POOR QUALITY

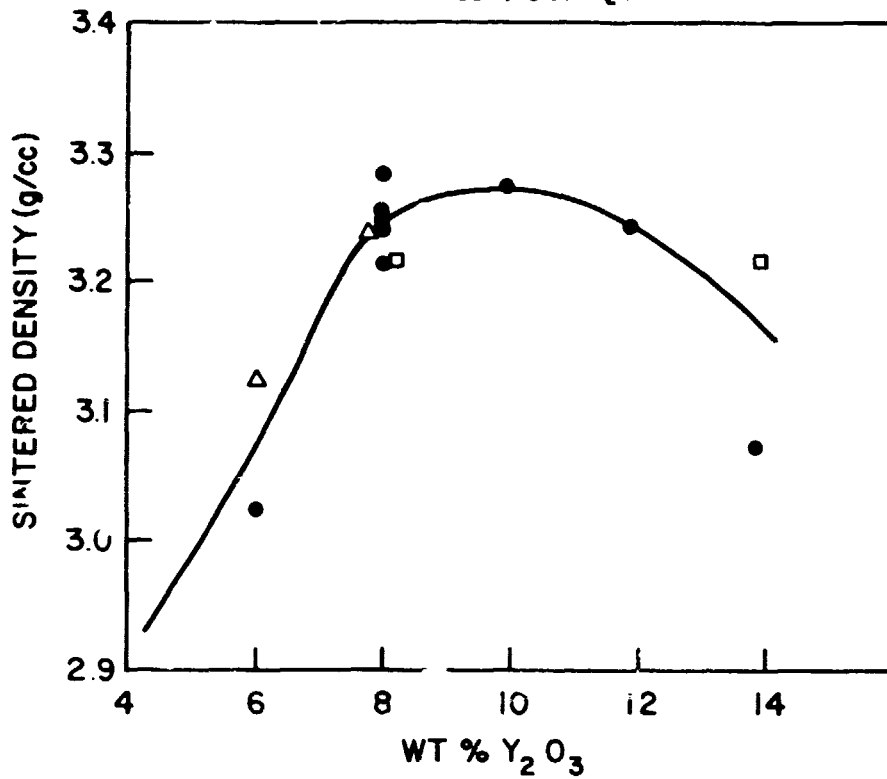


Figure 68. Sintered Density of SRBSN as a Function of Y₂O₃ Content.

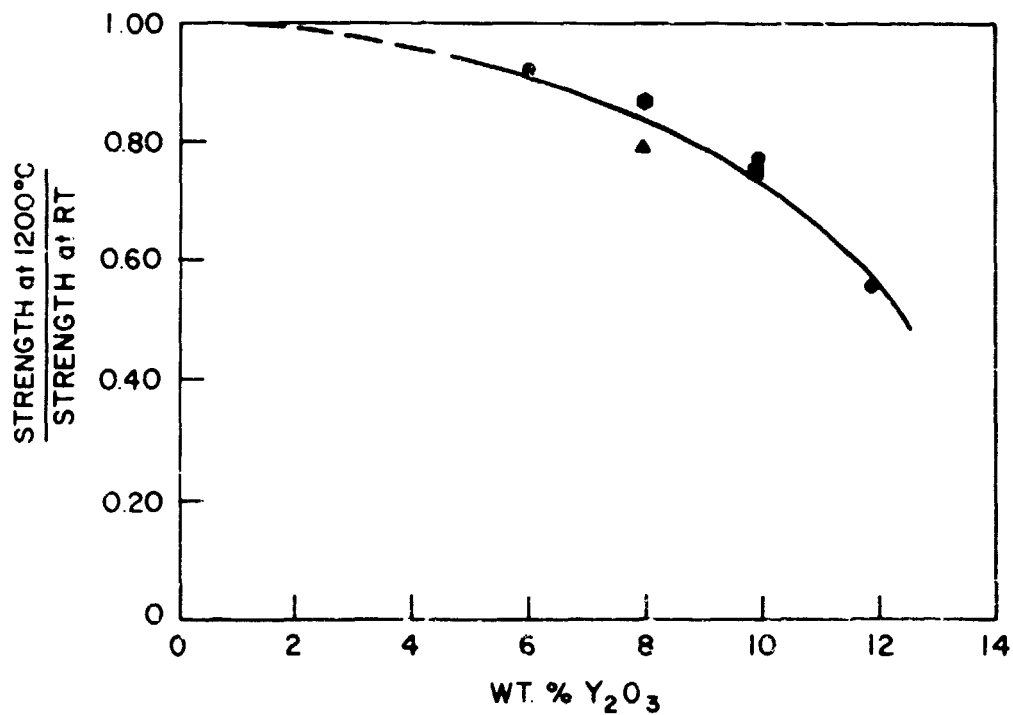


Figure 69. Strength Retention of SRBSN at 1200°C as a Function of Y₂O₃ Content.

Greskovich and Palm⁽⁸⁾. Under various combinations of temperature and pressures, densities as high as 3.31 g/cc (99 percent) have been obtained on 1 cm³ test coupons.

However run-to-run reproducibility of this cycle has not yet been fully achieved. As shown in Table 11, the densities of test coupons ranged from 3.05 g/cc to 3.31 g/cc, for the same cycle, resulting in a wide variation of strength values (453 to 741 MPa). This strength-density relation is plotted in Figure 70. The data points fit a line generated by Larsen⁽⁹⁾ to describe the strength behavior of all type of silicon nitrides.

Because of the wide density variations observed with this sintering cycle, further characterization was performed only on samples having densities greater than 3.2 g/cc. These materials were given the designation RM-1 which stands for the first generation of material to be used in rotor fabrication.

Material Characterization

The strength properties of the RM-1 material are presented in Table 12 and Figure 71, and are taken from a combination of test bars machined from three different 25 mm x 25 mm x 75 mm billets, processed in two different sintering runs.

The oxidation behavior of the RM-1 material was studied at 1000°C in a static air environment for exposure times up to 300 hours, with the results summarized in Table 13.

The observed color change, from black to gray/black mottled appearance, seems related to the phase composition of the test bar. Even though all the test bars were machined from the same billet, non-uniformities in phase composition were observed.

X-ray diffraction analysis of the surfaces of the oxidized bars revealed different oxidation products for the light and dark regions. The light regions contained secondary phases of Y₂Si₂O₇ and SiO₂ in the form of α cristobalite. The dark regions contained secondary phases of Y₂SiO₅ and SiO₂, also as α cristobalite. The light areas contained about twice the amount of SiO₂.

The oxidation kinetics follow the model suggested by Smith and Quackenbush⁽¹⁰⁾, that is, linear kinetics are observed after an initial incubation period of about 50 hours. This behavior suggests a continued reaction with the unoxidized surface; no diffusional barrier to oxidation is formed.

The rate constant for this 1000°C oxidation test, 3×10^{-11} (kg/m²) sec⁻¹, was obtained from the 300 hour data point by assuming parabolic oxidation behavior.

ORIGINAL PAGE IS
OF POOR QUALITY

TABLE 11. PROPERTIES OF 8 PERCENT Y_2O_3 - SRBSN USING
TWO STAGE SINTERING CYCLE

Run No.	Density (g/cc)	Characteristic MOR (MPa)	Weibull Slope	No. of Samples	Test Temperature (°C)
E48	3.24	741	17.8	12	RT
	3.24	583	21.1	6	1200
E49	3.05	497	13.9	10	RT
E50	3.28	625	7.5	6	RT
	3.28	540	11.3	6	1200
	3.31	645	11.6	6	RT
E54	3.14	557.4	13.0	6	RT
	3.09	453	10.3	7	RT

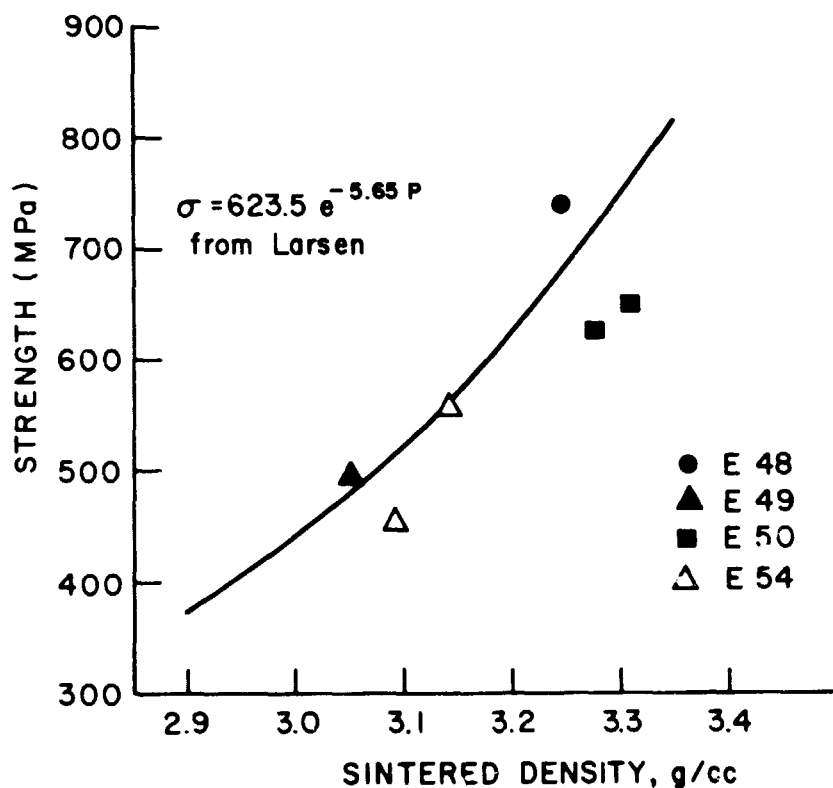


Figure 70. Strength-Density Relationship Obtained by
Two Stage Sintering.

ORIGINAL PAGE IS
OF POOR QUALITY

TABLE 12. STRENGTH PROPERTIES OF FORD RM-1 SRBSN

Density	3.26 g/cc	
Test Temperature	RT	1200°C
Strength	699 MPa	565 MPa
Weibull Slope	10.1	14.9
No. of Samples	24	12
Sinter Run Nos.	E48,E50	E48,E50
Sample Size	2.2 x 6.3 x 25 mm	2.2 x 6.3 x 25 mm
Fixture Dimensions	9.5 x 19.0 mm	9.5 x 19.0 mm
Loading Rate	0.5 mm/min	0.5 mm/min

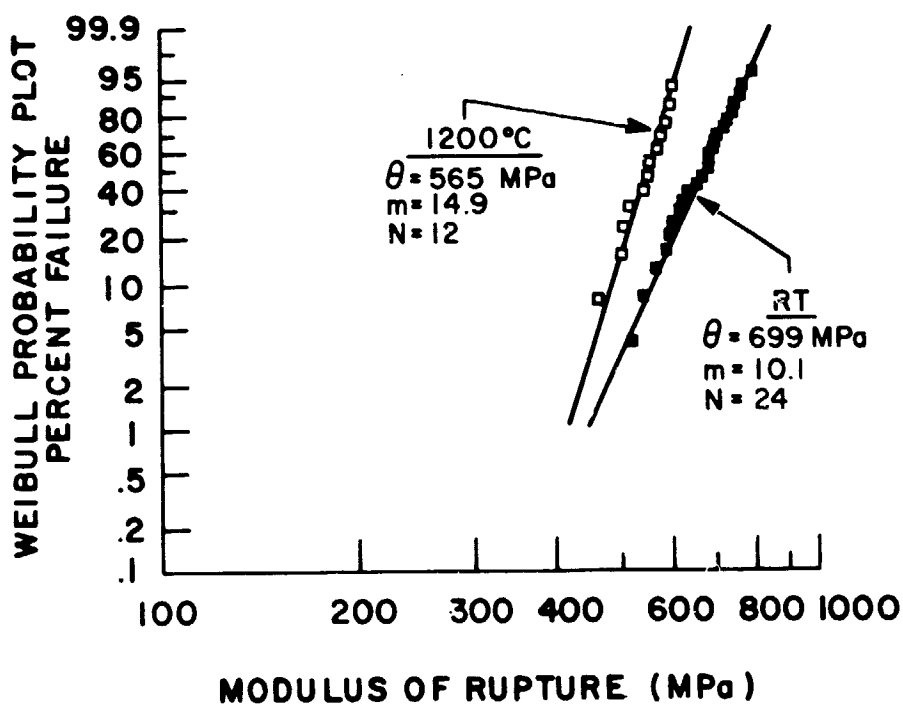


Figure 71. Distributions of Room Temperature and 1200°C Strength of RM-1 SRBSN.

The RT strength (MOR) was measured after the 300 hour oxidation exposure, and compared to virgin material (Table 13). A 4.3 percent strength loss was observed, with no appreciable change in Weibull slope. There was no significant correlation between strength and appearance or weight gain of individual test bars.

Simulated Rotor Development

Fabrication

The slip casting fabrication concept and process description for the simulated rotor was presented in Reference(1). During the last reporting period, simulated rotors had been cast and nitrided. However, a cracking problem had been experienced in the "green" state. This problem was addressed by controlling the slip properties, with the result that castings could be produced with no observable cracks prior to nitriding. However, internal cracks were still found after nitriding, constituting a major problem area which has been the focus of fabrication development effort during this reporting period.

The cracks can generally be characterized as tight radial cracks, occurring primarily in the lower half of the rotor [Figure 72(A)]. However, in extreme cases these cracks can extend over the entire rotor as shown in Figure 72(B). Cracks also typically occur on the bottom surface of rotors and are characterized usually as a "spider web" type network. All cracks extend into the interior of the component as shown in a machined half-rotor in Figure 73. These cracks range in severity from 2 cracks running radially, parallel to the dome contour [Figure 73-6(A)] to a network of cracks running both radially and axially (Figure 73-6(B))!

A nitrided rotor (No. 44) and a sintered rotor (No. 36) were sectioned according to the cutting plan shown in Figure 74. The density of each segment was measured (Table 14). A density gradient from top to bottom of the rotor was found, with the minimum density occurring in Segment 5.

It was suspected that these density gradients were the cause of the observed cracking problem. A number of steps were taken in an attempt to minimize these density gradients. The viscosity of the casting slips was increased to 100 cps and the specific gravity was increased to 1.76 g/cc. These changes were made to produce slips with less settling tendencies. The size of the plaster mold was increased by a factor of 2, providing faster water absorption and more absorption volume. These three steps combined resulted in faster casting times, thereby reducing density gradients due to particle settling. The particle size of the silicon powder was also reduced to 100 percent minus 10 microns (3 microns average) to reduce settling and allow better control of slip properties.

TABLE 13. OXIDATION BEHAVIOR OF FORD RM-1 SRBSN

Conditions:	Static Air Atm; 1000°C; 300 hr
Physical Appearance:	Color Change - Gray/Black mottled texture, no cracking.
Phase Composition:	No cracking
Initial:	$\text{Si}_3\text{N}_4 + \text{Y SiO}_2\text{N} + \text{Y}_4 \text{Si}_2\text{O}_7\text{N}_2$
After 340 hr:	$\text{Si}_3\text{N}_4 + \text{Y}_2 \text{Si}_2\text{O}_7 + \text{SiO}_2$ (light areas) $\text{Si}_3\text{N}_4 + \text{Y}_2 \text{SiO}_5 + \text{SiO}_2$ (dark areas)
Kinetics:	Linear (after a 48-hr incubation period) Wt. Gain after 300 hr: $6 \pm 4 \text{ g/m}^2$ Rate Constant: $3 \times 10^{-11} (\text{kg/m})^2 \text{ sec}^{-1}$
Strength:	RT

	<u>Sintering Run No.</u>	<u>Strength θ</u>	<u>Weibull Modulus m</u>	<u>Samples N</u>
Initial:	E50	624 MPa	7.5	6
After 300 hr:	E50	597 MPa	7.9	6

Strength (300 hr): -4.3%

ORIGINAL PAGE
BLACK AND WHITE PHOTOGRAPH

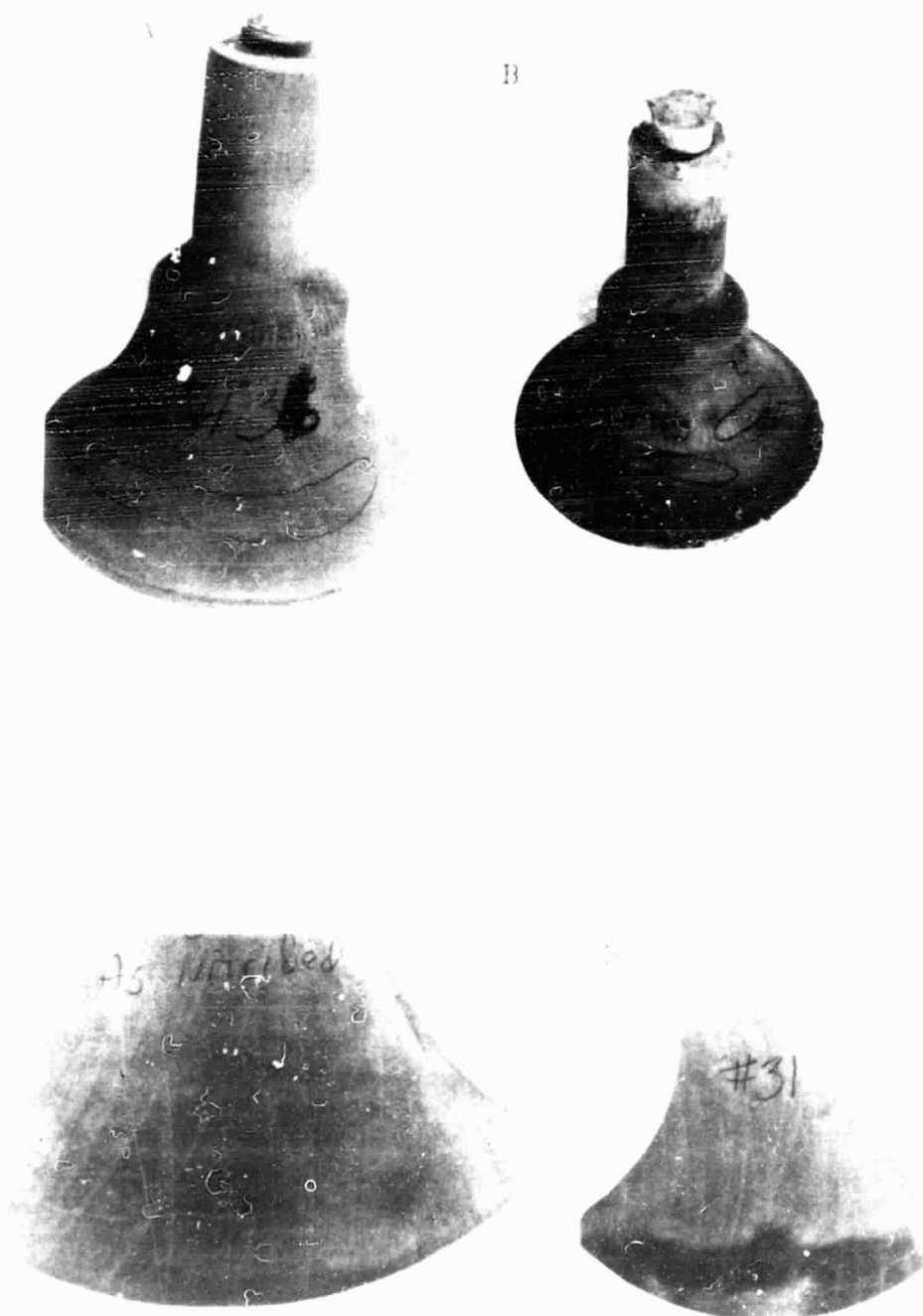


Figure 72. Slip-Cast Rotor.

ORIGINAL PAGE
BLACK AND WHITE PHOTOGRAPH

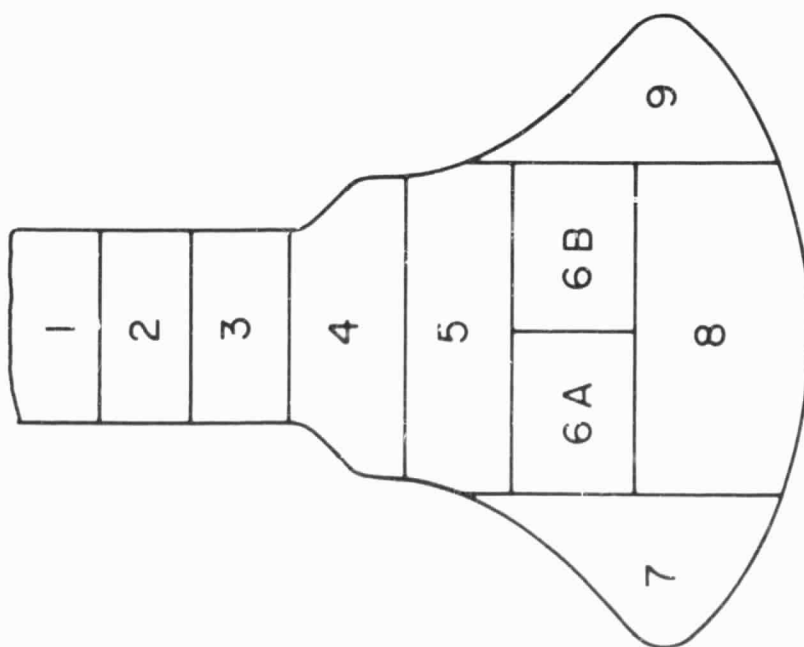


Figure 73. Section Locating Diagram and Machined Half-Rotor.

TABLE 14. DENSITY GRADIENTS IN SIMULATED ROTORS

Rotor No.	44	36	78	80
<u>Bulk</u>	2.16 g/cc	2.94 g/cc	2.27 g/cc	2.24 g/cc
Seg 1	2.12 g/cc	3.02 g/cc	2.12 g/cc	2.20 g/cc
Seg 2	2.10 g/cc	2.92 g/cc	2.10 g/cc	2.13 g/cc
Seg 3	2.11 g/cc	2.91 g/cc	2.10 g/cc	2.12 g/cc
Seg 4	2.09 g/cc	2.90 g/cc	2.09 g/cc	2.09 g/cc
Seg 5	2.08 g/cc	2.88 g/cc	2.12 g/cc	2.33 g/cc
Seg 6A	2.19 g/cc	2.95 g/cc	2.32 g/cc	2.33 g/cc
Seg 6B	2.19 g/cc	2.96 g/cc	2.35 g/cc	2.30 g/cc
Seg 7	2.25 g/cc	3.06 g/cc	2.46 g/cc	2.44 g/cc
Seg 8	2.28 g/cc	3.02 g/cc	2.40 g/cc	2.42 g/cc
Seg 9	2.28 g/cc	3.03 g/cc	2.43 g/cc	2.40 g/cc

In addition, the drying cycle for the parts was lengthened to include a 66°C forced air drying which extended for at least 72 hours prior to nitriding. The nitriding cycle also was altered so that the maximum ramp rates in any portion of the cycle were reduced to no more than 27°C/hr.

The results of all of these experiments are incomplete at this time. Visual inspection of the rotor surfaces after nitriding indicates that the quality has significantly improved. Nine of these rotors have an average of 3 flaw indications per part, while four rotors have only one indication. These indications were much smaller in size than previous cracks and were usually located closer to the shaft/neck region of the rotor. Sectioning of these parts, however, indicated little improvement in internal part quality. The only difference was that the cracks did not extend to the surface. Rotors No. 78 (one flaw indication) and No. 80 (six flaw indications) were examined for density gradients. The results, also shown in Table 14, show no improvement in the magnitude of the gradient over previous castings. However, the minimum density region in these rotors was Segment 4 rather than Segment 5, which shows that the casting behavior has changed slightly.

Sintering

Six simulated rotors and three half rotors were sintered using the two stage sintering cycle mentioned earlier. The results (Table 15) show a large variation in sintered density, similar to the variation noted for test coupons shown in Table 11. Except for rotors 34 and 35, all rotors were severely cracked. These cracks were related to cracks which were documented prior to sintering. In all cases, these existing cracks were enlarged during sintering. Figure 75 shows rotor 33 after sintering; this should be compared to Figure 73(A), which shows rotor 33 prior to sintering. One sintered rotor (36) was sectioned to determine the magnitude of the density gradient. Table 14 shows that the gradient is similar in profile to the as-nitrided rotor, however, the magnitude of the gradient was reduced.

Mechanical Testing

Two low quality simulated rotors were bonded to metal spin arbors utilizing techniques already developed(1). Visual and dimensional inspection showed that good bonds were achieved. The assemblies were balanced and cold spun to failure. Failure speeds were low as expected, but did verify the bonding method since, in both cases, the metal to ceramic bond remained intact. A procedure was developed for disassembling the ceramic stub from the metal spin arbor so that the arbor could be reused. A supply of metal spin arbors were fabricated to assure that mechanical testing could proceed without delay.



GARRETT TURBINE ENGINE COMPANY
A DIVISION OF THE GARRETT CORPORATION
PHOENIX, ARIZONA

TABLE 15. SIMULATED ROTOR SINTERING RESULTS

Rotor No.	Sintering Run No.	Density Type (g/cc)	Nitrided Density (g/cc)	Sintered Density (g/cc)	Percent Linear Shrinkage	Quality
27	50	half	2.34	3.11	10.2	Several cracks
29	51	whole	2.27	2.97	9.1	Many minor cracks
26	51	half	2.35	2.99	9.0	Severely cracked
33	54	half	2.33	3.15	11.2	Severely cracked
22	56	whole	2.44	3.26	9.5	Minor cracks
34	57	whole	2.40	3.00	9.0	1 minor crack
35	58	whole	2.34	2.99	8.7	1 minor crack
36	59	whole	2.33	2.94	9.1	Severely cracked
41	61	whole	2.27	3.00	--	Severely cracked

Task 2.7 Stator

Molding Process Development

Precise and rapid control of injection molding temperatures, pressures and sequencing times are required to produce high quality injection molded ceramic components repeatedly. The automated injection molding system that is being developed to mold monolithic AGT stators incorporates an Intel 8080 microprocessor which will control a 160 ton Tempcraft vertical injection molding machine.

Table 16 shows the sequence of events, options and set times which represent the current goal for the system. The last step in the sequence will result in a data sheet printout similar to that shown in Figure 76.

The present Intel 8080 microprocessor system is programmed in assembly language which makes programming time-consuming and difficult. During this reporting period, additional software was ordered so that control programs can also be written in Intel Basic or Intel Fortran. A simulator was designed which will take the place of the molding machine during the development of the control program. Portions of the control program can be written, checked out with the simulator and de-bugged completely, thereby freeing up the molding machine for parallel process development. Once changes to the program have been successfully checked out on the simulator, they then can be transferred to the molding machine.

Monolithic Stator Tool

The analytical study at Cornell University of the one-piece monolithic stator design did not indicate any molding problems with regard to knit lines in the vanes. Thus the design of the tooling was initiated. The design layout was reviewed and several modifications were made to incorporate more flexibility into the tool and increase the amount of instrumentation for temperature and pressure measurements. Fabrication of the molding tool is currently in progress.

TABLE 16. SEQUENCE OF EVENTS, OPTIONS AND SET TIMES FOR
INJECTION MOLDING AGT STATORS

EVENT	OPTIONS	SET VALUES
Airblast 1	On/off	Time T_1
Mold Release	On/off	Time T_2
Airblast 2	Same as Airblast 1	Time T_3
Close Die 1 (Vane inserts)		
Close Platen		
Barrel Forward		
Vacuum	On/off	
Plunger Forward		
Delay/Injection Hold Time	---	Time T_4
Plunger Pressure Relaxed	---	---
Barrel Pressure Relaxed	---	---
Delay/Platen Hold Time		Time T_6
Open Platen		
Delay/Die 1 Hold Time		Time T_7
Open Die 1		
Pull Barrel Back		
Pull Plunger Back		
Print Report	On/off	

ORIGINAL PRODUCTION
OF POOR QUALITY

FORD MOTOR COMPANY
ENGINEERING AND RESEARCH STAFF
CERAMIC MATERIALS DEPARTMENT R9130

INJECTION MOLDED CERAMIC COMPONENT REPORT

DATE: 9-22-80 OPERATOR: STILES
TIME: 03:53:05 PROCESS: SILICON NITRIDE, 1.7 G/CC
PART: ROTOR MATERIAL BATCH NUMBER: 1184
PART NUMBER: 05 BATCH CREATION DATE: 7-8-80
EXPERIMENT: MONO. ROTOR

PROCESS CONTROL SETTINGS

RUN OPTIONS

1. HUNKAR FLOW CONTROL...OFF
2. AIRBLAST.....OFF
3. MOLD RELEASE.....OFF
4. VACUUM.....ON
5. DIE 2 HOLD.....TIME
6. PLATEN HOLD.....TIME
7. DIE 1 HOLD.....TIME

TIMERS (SECONDS)

9. AIRBLAST 1.....002.0
10. MOLD RELEASE.....002.0
11. AIRBLAST 2.....002.0
12. INJECTION HOLD TIME..030.0
13. DIE 2 HOLD TIME.....000.5
14. PLATEN HOLD TIME.....000.5
15. DIE 1 HOLD TIME.....000.5

TEMPERATURES

NOZZLE.....SET.....ACTUAL..... FORWARD BARREL..SET.....ACTUAL.....
STAT. DIE.....SET.....ACTUAL..... MIDDLE BARREL..SET.....ACTUAL.....
MOV. DIE.....SET.....ACTUAL..... REAR BARREL....SET.....ACTUAL.....

FLOW CONTROL DATA

CHILL SIZE.....GRAMS INJECTION PRESSURE MAX.PSI
HOLD TIME.....SECONDS HOLDING PRESSURE MAX.PSI
CAVITY PRESSURE SET.....ACTUAL..... PSI

100.....
90.....
80.....
70.....
60.....
50.....
40.....
30.....
20.....
10.....

100.....
90.....
80.....
70.....
60.....
50.....
40.....
30.....
20.....
10.....

INJECTION PROFILE

HOLD PROFILE

PART CONDITION

GOOD

Figure 76. Computer-Printed Molding Data Sheet.

Task 2.7 Flow Separator Housing

Component Fabrication

Work during this reporting period emphasized component design iterations and initiation of tooling fabrication at Corning Glass Works. Although the initial drawings for housings were released, discussions continued relative to design changes. As a result, a number of modifications were effected to improve fabrication and machining of the component. Work was then initiated at Corning on tooling, including wood model fabrication, pattern design, pattern fabrication, and mold fabrication. These tooling items were completed by the end of the reporting period; the next task will consist of trial castings of flow separator housings.

Dimensional Stability Measurements

In Reference(1), the dimensional instability of Corning 9458 LAS was reported to be ± 100 ppm after 500 hours at 1800°F . Additional stability results were obtained during this reporting period.

The LAS material was machined into one inch cubes, and subjected to temperatures varying from 1800°F to 2200°F for 500 hours at each temperature in increments of 100°F . Dimensional measurements were made on cube faces prior to the test and at about 250 hour intervals during exposure, using an optical comparator and a series gage block. This technique resulted in measurement accuracy of ± 10 ppm. Results of this test are shown in Figure 77. It is apparent that the Corning 9458 LAS material remained within ± 100 ppm stability over 2000°F . Above 2100°F , additional contraction occurred, and the material fell below the lower limit of ± 100 ppm.

Mechanical Testing

The flow separator housing is subjected to thermal and mechanical loads in the engine. In order to provide some assurance that a housing will sustain mechanical loads in an engine and to eliminate defective housings early in processing, a test fixture was designed and fabricated to submit the housing to pressures equal to the engine static operating pressures.

The housing test fixture assembled with a flow separator housing wooden model is shown in Figure 78. The test fixture was designed to support the housing, simulating engine mounting conditions while sealing the housing to the fixture with rubber gaskets. The fixture was designed to use water to apply pressure loads within a containment vessel available at Corning. Lifting eyes are provided to assist in moving the assembly in and out of the containment vessel. The upper plate is provided with fittings for a pressure line and an air bleed valve. The flow separator housing is mounted on a silicone rubber

ORIGINAL LINE
OF POOR QUALITY

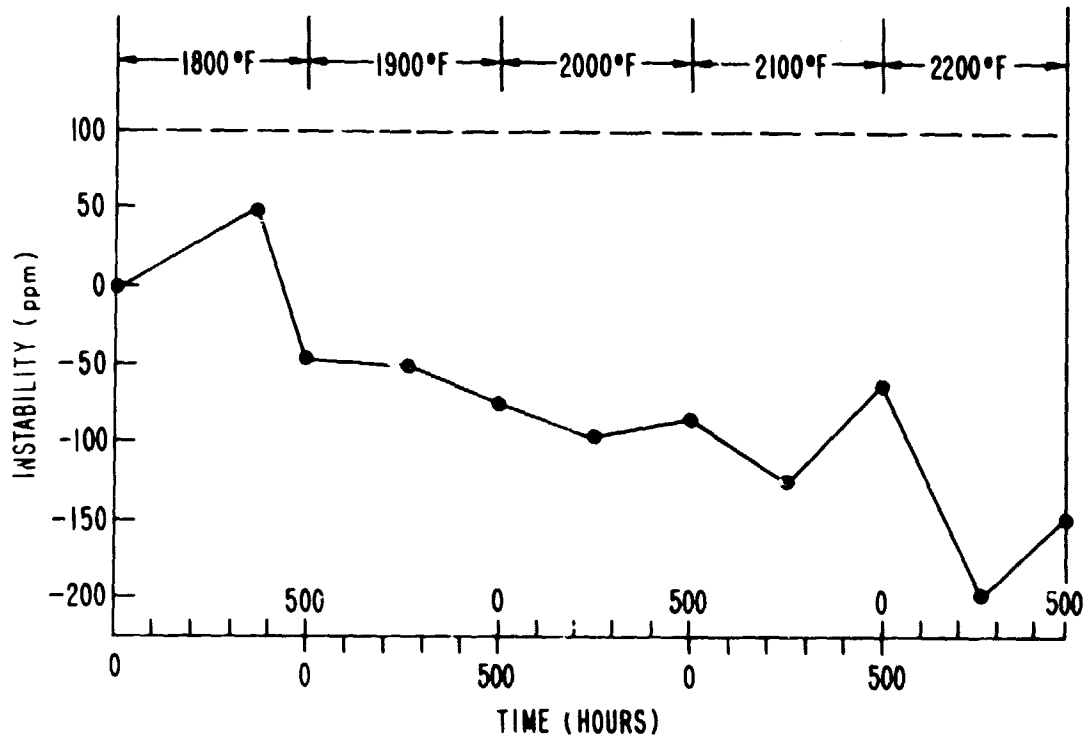


Figure 77. Dimensional Stability of Corning 9458 LAS Material at Various Times and Temperatures.

ORIGINAL PAGE
BLACK AND WHITE PHOTOGRAPH

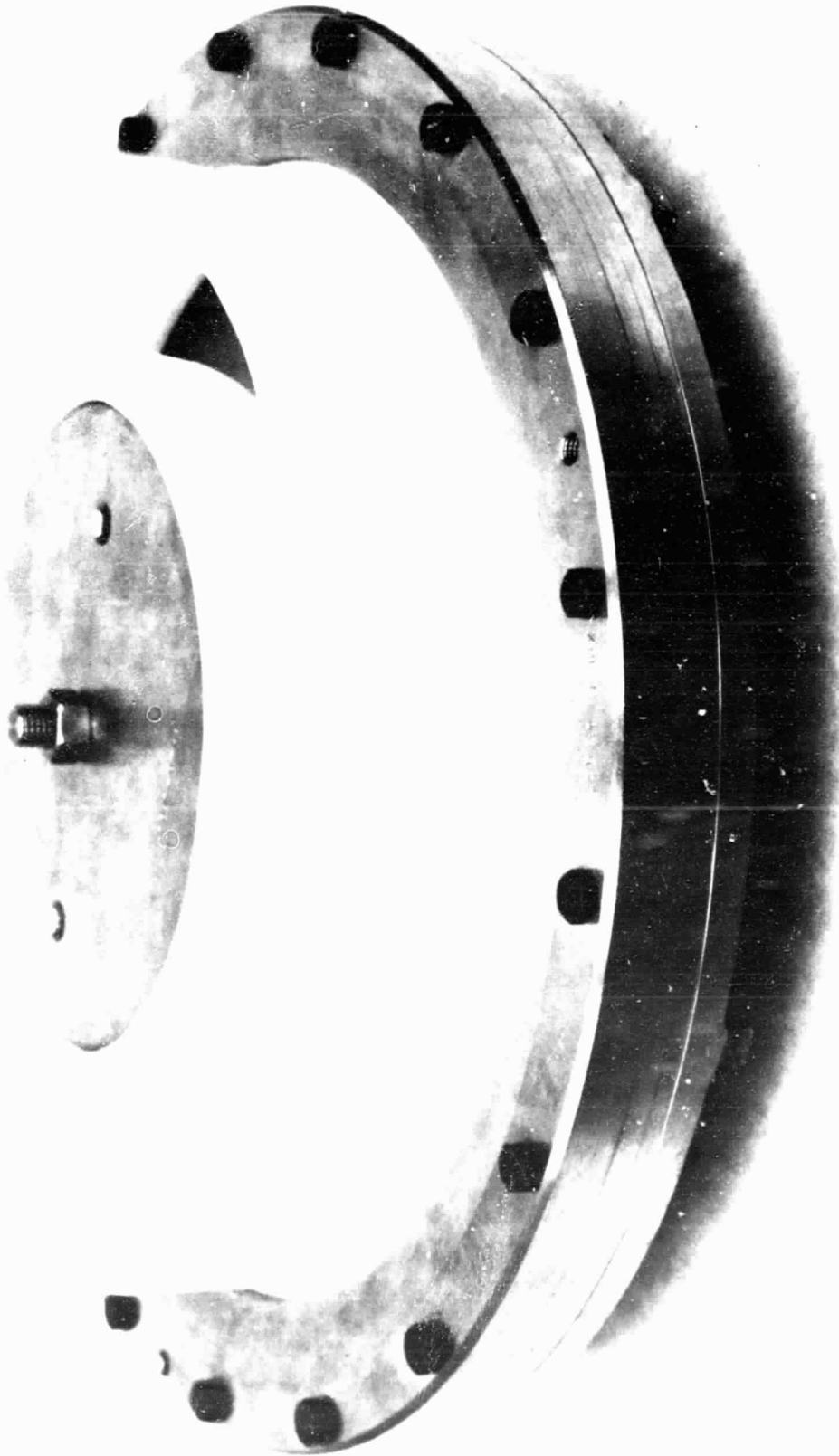


Figure 78. Flow Separator Housing Pressure Test Fixture Shown
Assembled to Wooden Model of the Housing.

gasket which has the same configuration as the regenerator cold seal assembly. The gasket is molded to the base plate. On the under side of the clamp ring is a silicone rubber gasket which functions as the engine's flow divider regenerator seal. As the clamp ring is bolted to the base plate the housing flanges are sandwiched between the two gaskets, and the gaskets are compressed to 80 percent of their free height. In the upper plate an "O" ring provides the sealing normally provided between the transition duct, the turbine shroud, and the flow separator housing in the engine. With these gaskets and "O" ring, the high pressure cavity is sealed so that pressure can be applied to simulate engine operating pressures. Each flow separator housing will be tested at engine maximum power static pressure as a proof test.



GARRETT TURBINE ENGINE COMPANY

A DIVISION OF THE GARRETT CORPORATION
PHOENIX ARIZONA

APPENDIX II

AIRESEARCH CASTING COMPANY (ACC)

**ADVANCED GAS TURBINE (AGT) POWERTRAIN PROGRAM
SECOND SEMI-ANNUAL TECHNICAL
PROGRESS REPORT**

ROTOR-MATERIALS AND FABRICATION DEVELOPMENT

In reference 1, the ACC Concept for fabrication of AGT101 ceramic turbine components was discussed. This report updates the fabrication developments for simulated rotors and static components.

Transfer Molding

The base of the original three-piece injection molding rotor tool was modified for use on the Mohr extruder modified for use as a transfer molder (Figure 79). The tool was equipped with heater bands and thermocouples for accurate temperature control. The extruder has chamber evacuation capability so that a billet of material can be compressed under vacuum, prior to extrusion into the mold.

After the first attempt to transfer-mold a simulated rotor, insufficient vacuum was being maintained and a larger quantity of material in the chamber was necessary to permit complete mold-fill. Additional O-ring seals were added to this permit the chamber to be evacuated while the material was pressed into a billet to eliminate entrapped air. After molding, a grainy appearance in the material was obvious, which looked similar to the pelletized batch prior to molding. This indicated that the hold time at temperature was insufficient to fluidize the binder within the more massive portion of the rotor. Another batch was prepared and molded and left in the mold at temperature overnight. After cooling and removing from the mold, the interior of the rotor appeared the same as the previous molding. Loss of binder resulting from repeated use of the material batch is suspected to have caused a situation whereby insufficient binder remained to completely homogenize the material. Additional work on this approach was not continued due to the more promising results obtained in the concurrent injection molding studies.

Injection Molding

Originally, the entrapped air in injection molded simulated rotors was assumed to be the major reason for the inability to produce a satisfactory rotor. In an effort to determine the actual material flowpath during injection, a clear plastic was substituted for the Si_3N_4 . The material flowed from the backface (where it entered the tool) moved along the tool wall, and on into the shaft end and sealed off the air trapped in the center.

As a result of this experiment, much of the problem encountered with voids in the injection molded rotors was traced to the fact that the rotor was not cooled sufficiently within the tool to solidify the binder before holding pressure was lost. Pressure time was thus increased from 6 minutes to 30 minutes. When the resulting rotor was split open, it was solid throughout, showing no evidence of voids. Another rotor was injected that also did not visually have any flaws as determined (30X) by X-ray radiography. The part was placed in a slow binder-extraction cycle but cracked at some point during the cycle.

ORIGINAL PAGE
BLACK AND WHITE PHOTOGRAPH

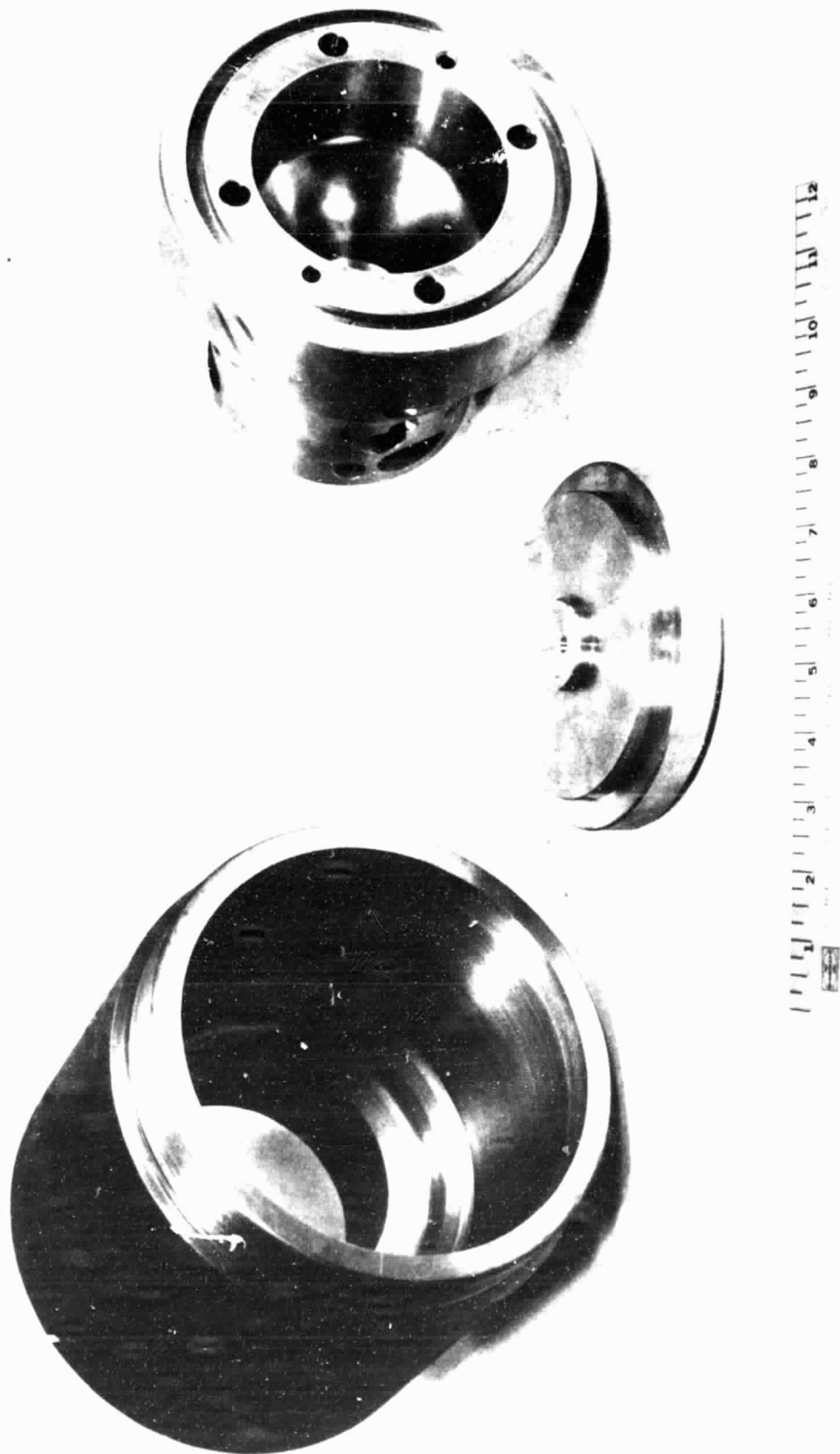


Figure 79. Three Piece Rotor Tool.

On a subsequent attempt to inject a rotor, the plunger galled within the cylinder. The galled end of the original plunger was cut off and replaced with a Teflon tip of sufficient diameter to provide a tight fit. This has eliminated the loss of material between the plunger and barrel walls.

When molding trials were resumed, it was found that the top (dome) portion of the injection mold tool appeared to cool too rapidly, which induced porosity on the surface of the backface. A flat board of phenolic insulative material (trade name, Synthane) was machined to form the sprue, and flat-domed rotors were molded with no evidence of porosity. Another Synthane mold was machined to provide the complete backface shape.

Several rotors using the Synthane backface-shape portion of the tool were fabricated, which evaluated parameters of injection speed, tool temperature, injection pressure, etc. These rotors were void- and crack-free and, except for slight porosity on the backface surface, were perfect as-formed rotors.

Binder removal evaluations were conducted to determine whether the method of surrounding the part in Si_3N_4 powder had any significant effect. Small cylinders were used where one cylinder was left completely exposed. A second cylinder was placed in a crucible on loose powder, and additional powder was poured over it. The third cylinder was placed in a crucible on top of a bed of firmly tamped powder, with additional powder poured over and tamped down. All three cylinders were placed in a 275°F oven for 1 hour and removed. Cylinder No. 1 was badly blistered and cracked; cylinder No. 2 was blistered but did not show evidence of cracking; cylinder No. 3 did not blister or crack. Experiments are continuing to more fully evaluate the affect of compacting powder around the injection molded component. Simulated rotors will be placed in a standard binder extraction run both loosely packed, as has been normal, and firmly packed.

Slip Casting

Several SNN502 simulated rotors were slip-cast. One was permitted to air-dry after removal from the mold but showed evidence of cracking shortly thereafter. Another rotor was vacuum-dried and subsequently sintered. This rotor also cracked during the sintering run, but the crack direction was different from that observed previously. The rotor split in two from backface to shaft end in almost equal halves. Each half showed no evidence of additional cracking and appeared to be homogenous. One half was given to Phoenix for evaluation. Several other slip-cast rotors were dried in a humidity oven where the humidity was high at the start of the cycle (98-percent relative), and the temperature was gradually increased to 175°F. At this temperature, the humidity was decreased. Humidity oven-dried rotors have been sintered, with several showing slight surface cracking. However, X-ray radiography has revealed the presence of internal flaws.

A simulated rotor was slip-cast and placed in the humidity chamber while still in the mold. Humidity was maintained at 75 percent overnight. The part was then removed from the mold and replaced in the chamber. Temperature (dry bulb) was increased 5°F/hour, and the humidity was held between 90- and 98-percent relative until the temperature was increased to 175°F. At this point, the humidity was decreased to 10-percent relative and the temperature maintained at 175°F overnight (16 hours). The temperature was then reduced 10°F/hour to room temperature. Despite this carefully controlled cycle, the rotor showed evidence of hairline cracks. Apparently, vacuum drying is the most effective method to date of controlled drying slip-cast SNN-series material.

Slip Improvement

In order to reduce or eliminate the reactivity of Y_2O_3 when added as a sintering aid to water-based Si_3N_4 slips, the Y_2O_3 - Al_2O_3 additives were milled together and pre-reacted at 1600°C for 6 hours in vacuum. X-ray diffraction patterns revealed complete reaction forming Y_2O_3 - Al_2O_3 garnet with no free Y_2O_3 or Al_2O_3 . Si_3N_4 powder was added to form the baseline SNN502 formulation and milled according to normal procedures. Slip was prepared, and plates were cast that will be sintered and machined into test bars.

Alternate Mold Study

One of the original slip-cast mold configurations consisted of a plaster base that contained the backface shape and an all-rubber, two-piece mold for the hub and shaft. An iteration designed to reduce the length of casting time involved changing the all rubber portion of the mold to one-half rubber and one-half plaster. Several rotors were cast in this dual-material mold, but the portion of the casting in contact with the rubber face and poor surface quality exhibited what could be classified as an out-gassing condition with extensive surface porosity. A thin wax coating was applied to the rubber face portion of the mold, which improved the condition only marginally. The casting surface in contact with the plaster was excellent.

Another mold was prepared that is entirely plaster. The shaft portion was coated to render it non-absorbent in order to prevent preliminary casting in this area inasmuch as slip is poured through the shaft end of the mold.

The total batch (Si_3N_4 plus sintering aids) was precalcined at 1200°C for 16 hours and remilled to break up agglomerates. A slip-batch was prepared, and a rotor was cast in the all-plaster mold configuration described above. The casting appeared to be free of flaws detectable visually or by X-ray radiography. This rotor will be sintered upon the availability of the sintering furnace. Test specimen plates were cast from the same slip-batch and will be sintered with the rotor for machining into test bars.

All of the controls necessary for automatic programming of the sintering furnace have been installed. A checkout program cycle was conducted, and all sequencing functions operated as designed. One minor problem became evident at 900°C when the thermocouple circuit acted erratically. The cause was traced to field feedback into the field control unit. An isolation transformer was installed that resolved the problem. Subsequently, several cycles have been conducted using the programming capability of the system. Except for minor learning-curve-type problems, the entire system is operating satisfactorily.

Shaft Attachment Studies

Fabrication of approximately 5-inch long shafts for shaft-attachment studies has continued. However, the first five shafts submitted during this report period were not satisfactory due to warpage in the sintering run. Shafts were made of sufficient length to machine two shafts of the desired length from each one. However, by the time the OD was machined to remove the warp, only one shaft could be obtained and the remaining portion was undersize. A new tool with a larger OD is being fabricated to increase the machine stock, which should allow for the 2-for-1 shaft configuration. In the meantime, other methods of supporting the shaft during sintering are being evaluated.

Another experiment was conducted to evaluate various plaster-mold coatings for improved casting uniformity and surface condition. Normal procedure has been to spray the plaster-mold casting surface with water, which was an improvement over casting into a dry mold. Several different percentage compositions of polyvinyl alcohol (PVA) and ammonium alginate were used on small cylinder molds (1 inch in diameter by 1 inch in length). The coating providing the best results, with respect to casting uniformity and surface condition, was a 0.5-percent solution of ammonium alginate. Three shafts were cast for the shaft attachment study in non-coated, all-plaster molds. X-ray revealed centerline shrinkage in all three. A fourth mold was coated prior to casting with the 0.5-percent alginate solution and no centerline shrinkage could be seen in X-ray. A rotor was slip-cast with slip prepared from precalcined powder into an alginate-treated mold. The part was removed from the mold and appears to be free of surface flaws. The rotor is presently in vacuum-drying and will be sintered as soon as the present automated control system, installed on the sintering furnace, has been fully tested.

BCD Ceramic Structures

Nitriding runs to compare the standard H_2-N_2 atmosphere baseline run with a run containing helium in addition to H_2-N_2 have been completed. Both runs contained baseline test specimens, specimens prepared from different nitriding aid chemistries and levels of nitriding

aid, and specimens prepared from slips of different particle-size classifications. The results are tabulated below.

<u>Specimen</u>	<u>H₂-N₂ MOR, ksi</u>	<u>H₂-N₂-He MOR, ksi</u>
Baseline (RBN104)	47.0	47.0
Nitriding Aid Chemistries:		
1.5% Fe ₂ O ₃	39.7	41.7
1.5% Cr ₂ O ₃	38.8	38.8
1.5% Fe ₂ O ₃ + 1.5% Cr ₂ O ₃	41.8	41.0

Also intended to be included in these runs were specimens prepared from fractions of air-classified powders; however, test specimens were not prepared in time. These will be included in future runs that will evaluate variations from the normal nitriding cycle with respect to length of cycle time.

Tooling required for mold preparation of the turbine shroud and turbine outer diffuser has been received. However, one part of the outer diffuser was returned to the supplier for rework.

A slip-cast shroud was fabricated and removed from the mold successfully. After drying, the part was pre-nitrided with no observable flaws. During the casting, the ID portion of the mold floated loose, which permitted excess fill in that portion of the part. The shroud will be nitrided and the OD will be measured to determine accuracy to print tolerances. The balance of the ceramic structure tooling has been promised in January 1981.

APPENDIX III

CARBORUNDUM COMMON WORK

ADVANCED GAS TURBINE (AGT) POWERTRAIN PROGRAM
SECOND SEMI-ANNUAL TECHNICAL
PROGRESS REPORT

PRECEDING PAGE BLANK NOT FILMED

1. INTRODUCTION

This report summarizes technical progress of the AGT common work between 1 July 1980 and 31 December 1980. The report is classified into four broad areas of activity, which include development efforts in rotor fabrication, non-destructive evaluation, mechanical properties, and physical properties.

2. SUMMARY

2.1 Rotor Fabrication

Hot pressure silicon carbide was investigated as a hub material for the AGT rotor program. Room temperature MOR (modulus of rupture) results indicated that very high strengths are possible for certain compositions. These high strengths were obtained on small hot-pressed disks. However, translating these strengths to large, thick sections needs further development. The results have indicated the potential usefulness of hot pressed SiC as a core material for the AGT rotor.

The coating of as-fired alpha SiC by four different CVD and CNTD suppliers was evaluated by room temperature strength determinations, microstructure, and failure analysis. The strength evaluation is summarized in Table 17. There was no significant strength enhancement or reduction in the variability of the original strength distribution. Microstructural examination revealed that, in general, coatings are well bonded to the substrate and with an absence of microporosity in the CVD coatings. Therefore, these coatings can accomplish a useful sealing function.

Hipping of partially sintered alpha silicon carbide is being accomplished by NASA with Carborundum participating. The results have indicated density increases by hipping of up to 98.5 percent of the theoretical value. Strength evaluation and correlation with NDE are in process.

2.2 Non-Destructive Evaluation

Significant progress was made in detection of approximately 0.004- to 0.005-inch voids in 0.1-inch thick disks. The defect detection capability level was established as 3.5 to 4.3 percent of section thickness using microfocus X-ray radiography. The results are summarized in Table 18.

The applicability of high frequency ultrasonics (35 MHz) to examine B₄C inclusions and voids in sintered alpha silicon carbide was demonstrated.

TABLE 17. STRENGTH EVALUATION OF CVD-COATED ALPHA SIC BARS

Supplier	Average Coating Thickness (inch)	Number of Specimens	$\bar{\sigma} \pm S.D.$ (ksi)	Weibull (m)	(ksi)	Low σ_f	High σ_f
Control	--	25	48.86 \pm 5.75	8.9	51.49	34.47	60.77
DCI - Coated	0.004	24	43.89 \pm 8.80	4.8	47.91	22.80	59.15
MIC - Coated	0.012	25	47.47 \pm 5.51	9.0	49.70	35.87	55.98
PCI - Coated	0.003	20	52.52 \pm 7.78	6.9	56.04	37.17	63.77
SPL-CNTD	0.004	23	49.68 \pm 14.00	3.0	56.32	18.42	65.59

DCI = Deposits and Composites, Inc.
 MTC = Materials Technology Corporation
 PCI = Refractory Composites, Inc.
 SPL = San Fernando Laboratories

TABLE 18. DETECTION OF DEFECTS IN SEEDED DISKS OF
SINTERED ALPHA SIC BY MICROFOCUS X-RAY

Disk Thickness Inch	Void Size μm		Carbon Inclusion Size (μm)		B_4C Inclusion Size (μm)	
	50-125	125-250	50-125	125-250	50-125	125-250
0.1	D	D	D	D	PI	D
0.125	D	D	D	D	ND	D
0.25	ND	D	--	D	--	D
0.50	--	D	--	D	--	D
<p>D = Detected</p> <p>ND = Not Detected</p> <p>PI = Possible Indication</p>						

The advanced NDE methods, scanning laser acoustic microscopy (SLAM) and scanning photoacoustic spectroscopy (SPAM), were investigated for both sintered alpha silicon carbide and reaction bonded silicon carbide. Although surface roughness of as-fired surfaces causes difficulties for both methods, useful NDE signals can be obtained from both SPAM and SLAM. Complex shape examination seems to be very feasible by SLAM. The SPAM method is also applicable to complex shaped components by appropriate cell design. However, both methods require extensive experience for correct interpretation of NDE signal. In addition, it is not possible to describe the type, size, and location of defects directly from the primary data.

2.3 Mechanical Properties

Failure analysis of baseline strength bars produced by injection molding sintered alpha SiC has indicated that in a majority of cases (60 percent), failure occurred from processing-related volumetric flaws located at or close to the tensile surface. Similar results were observed also with slip cast silicon carbide.

The characteristic strength of 64,700 psi at room temperature of injection molded test bars is among the highest observed at our laboratories, as well as the characteristic strength of 59,400 psi at room temperature for slip cast silicon carbide. The strengths of dry pressed sintered alpha silicon carbide and fine grain reaction bonded silicon carbide are approximately 20-25 percent lower than that reported earlier and have been traced back to processing anomalies. Corrective measures have been implemented. The excellent retention of room temperature strength at 2191°F for all silicon carbide materials investigated in this program is significant. Results are summarized in Figure 79. The time-dependent mechanical properties investigations such as creep and stress rupture were also begun during this reporting period. Compression molded reaction sintered silicon carbide exhibited no time dependent failure in 100 hours at applied stress levels of 40,000 to 56,000 psi in 4-point bend at 1000°C (1832°F). Creep deflections ranging from 3500 to 8000 micro inches were observed. Time-dependent failure in stress rupture occurred at 1200°C (2192°F) for applied stresses of 54,000 psi. Creep deflections ranging from 5900 to 25,900 micro inches were also observed.

Four-point bend creep experiments at 1200°C (2192°F) were completed for this material for three applied stress levels. Minimum creep rates ranged from 2.03×10^{-7} /hr to 9.06×10^{-7} /hr, with an experimental value for stress exponent, $n \approx 3$.

ORIGINAL PHOTO COPY
OF POOR QUALITY

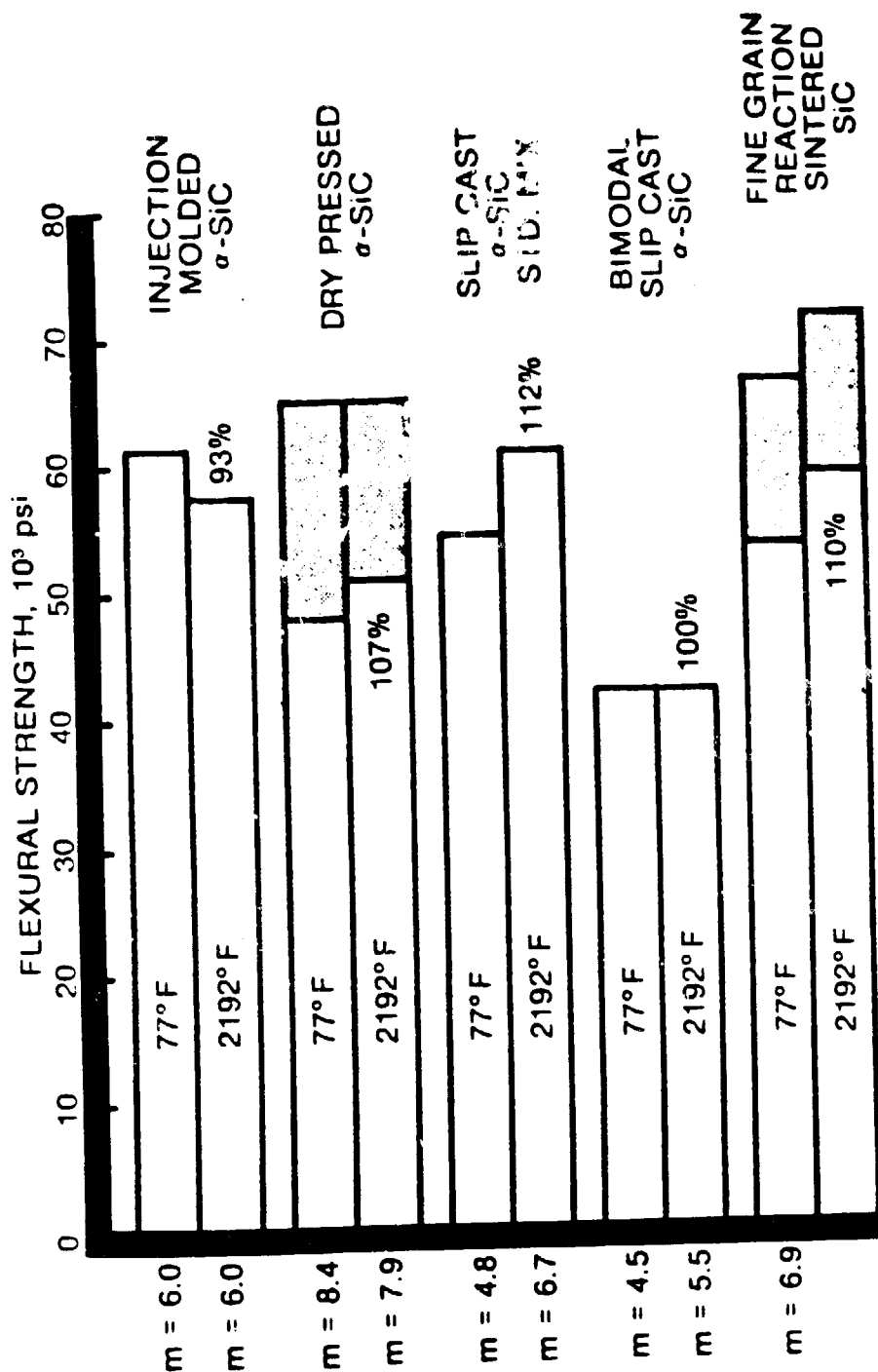
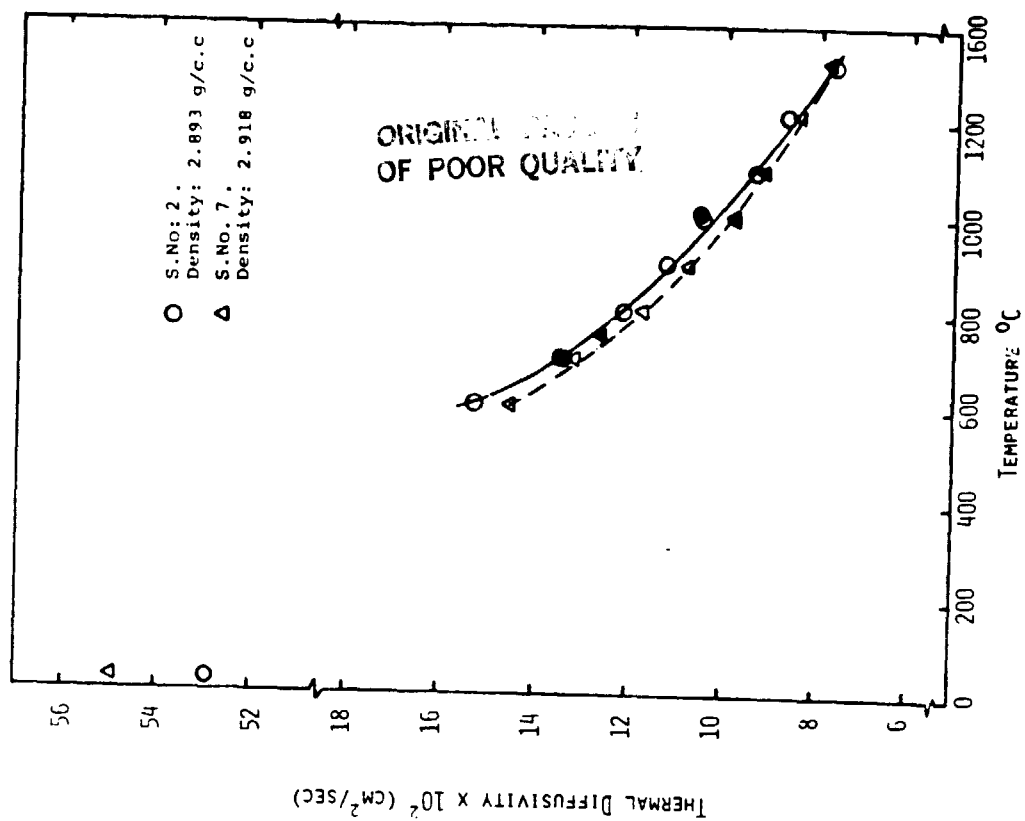


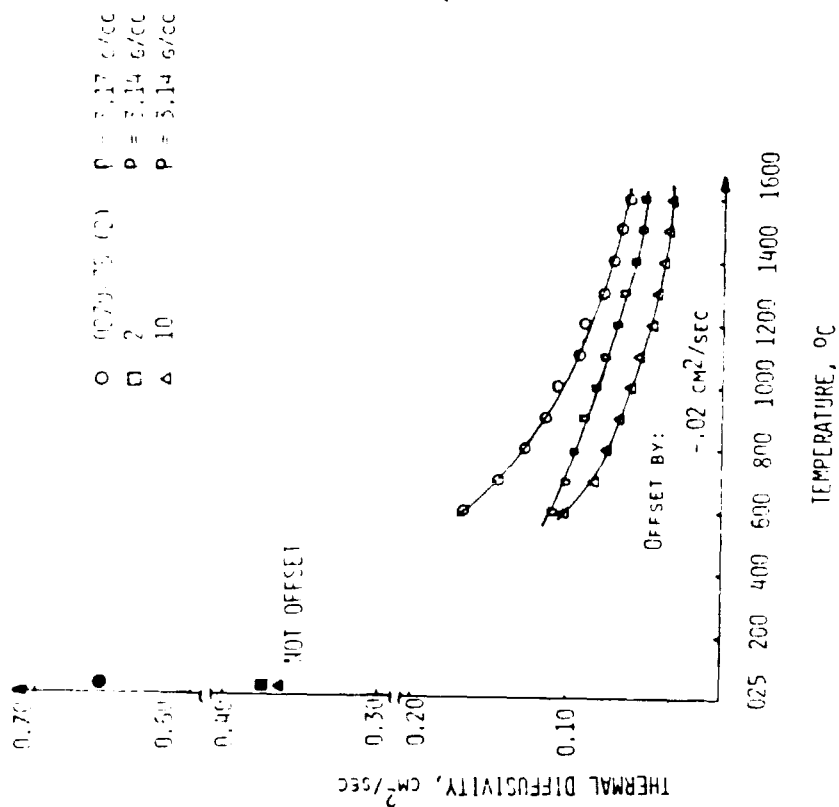
Figure 79. High Temperature Strength Retention of Silicon Carbide Materials.

2.4 Physical Properties

Thermal diffusivity measurements were made as a function of temperature by using the laser flash method for both sintered alpha silicon carbide and fine grain reaction bonded silicon carbide. Results are shown in Figure 80.



(b)



(a)

Figure 80. Thermal Diffusivity Measurements for (a) Sintered Alpha SiC and (b) Reaction Bonded Silicon Carbide.

APPENDIX IV

CARBORUNDUM UNIQUE WORK

ADVANCED GAS TURBINE (AGT) POWERTRAIN PROGRAM
SECOND SEMI-ANNUAL TECHNICAL
PROGRESS REPORT

1. BACKGROUND

This report summarizes the second 6 months work carried out by the Carborundum Company for the Garrett Turbine Engine Company on the Advanced Gas Turbine Powertrain System Development Program authorized under NASA Contract DEN3-167 and sponsored by the Department of Energy.

As a major subcontractor to the program, Carborundum is required to develop silicon carbide components for the hot flow path of the AGT engine. Thus far, injection molding, slip casting, and green machining have been selected for fabrication of these components.

Ceramic injection molding technology has been successfully demonstrated to produce complex shapes economically with a high degree of precision on small items such as turbine blades, stator vanes, and small rotors. At the initiation of this program, maximum cross-sections were limited to components not exceeding 1 inch. Beyond this size, the bake out of organic binders was increasingly difficult. Even when very slow temperature increases over long periods of time were used, cracked parts frequently resulted due to the fine (sub-micron) particle size of the powder and the packing density achieved during molding.

Although recent process advances have significantly extended cross-section capabilities, the rotor designed for the AGT engine still challenges the current state-of-the-art because of its size, which exceeds 3 inches in diameter at the base of the hub.

As a result, alternative approaches based on current technology were evaluated to provide turbine rotors for the early part of the program. These include a variety of ceramic-to-ceramic bonding methods which are applied to the assembly of smaller components. Carborundum's rotor development program emphasized these approaches during the first 12 months of the project.

The current program separates rotor development from static structure development; therefore, the development of static structure is discussed by individual components showing the progress being made towards producing the required deliverables using various fabrication methods.

2. ROTOR DEVELOPMENT

The approach to rotor development encouraged the evaluation of multiple processes at the start of the program. The number was narrowed down to two techniques during this period and evaluation efforts were directed towards producing a non-bladed rotor which is approximately 1/2-inch thicker than the bladed rotor to compensate for the lower centrifugal stress of the unbladed configuration. Based on

future needs to produce a complex bladed rotor, Carborundum selected the injection molding process to produce the part. An injection molding tool was designed with removable cores to produce two shell configurations as well as a solid hub. The shells represent thicknesses within the processing limits of technology available at the start of this program, while the solid hub provides development opportunities for thick section binder removal and subsequent sintering studies.

2.1 Molding Development

Molding activities for the rotor program were carried out on a 250 TG machine equipped with a solid state control incorporating microprocessors for repeatable set-ups via digital inputs. In addition, auxiliary microprocessors were installed for cycle repeatability and fine control adjustment.

2.1.1 Shells

Conditions were determined to produce shells for subsequent bonding studies. Approximately 80 shells were molded. Sixty of these used the standard molding material and the balance used a new molding compound with improved rheological properties and bake out characteristics.

2.1.2 Rotor

A modest effort was maintained to produce the solid simulated rotor. In an effort to eliminate porosity, the injection molding tool was re-worked to provide a secondary compaction step after initial packing. The new molding compound will be evaluated with the modified tool.

2.2 Thixotropic Casting Development

The Garrett AGT rotor hub was the thickest cross-section that had been attempted by thixotropic casting. Earlier difficulties with complete siliconization of these thick sections have been overcome. Material representative of the cast rotors had a mean strength of 43.45 ksi and a Weibull modulus of 8.28 at room temperature (4-point bend test). This is approximately a 40-percent increase in strength since work began on thixotropic casting. Subsequent cast material has shown mean strengths of 49.95 ksi at room temperature.

The development effort resulted in a crack-free, fully siliconized rotor which is available for spin testing. This rotor was cast slightly over-length and machined to a flat surface at the end. Fired density is 2.98 g/cc. No cracks were evident and x-ray examination revealed no internal voids or flaws.

However, based on material properties and projected improvements over the short term, it was decided to curtail development of this approach in favor of the bonded and solid one piece molding approaches.

2.3 Bonded Rotor Development

The goal of the bonded rotor program was to produce a solid simulated rotor having properties equal to or better than the monolithic shape. The major thrust in this development consisted of determining conditions and procedures required to produce a spinnable rotor.

Core material was produced using isopressing and green machining as well as net shape hot pressing. Filling by hot pressing a densifiable SiC powder was also attempted. There were several problems which had to be resolved in order to produce the bonded rotor. These are listed with the corrective action taken:

<u>PROBLEM</u>	<u>ACTION</u>
1. Frequent Mold Breakage	Obtain new graphite mold stock with improved strength.
2. Shell Cracking During Hot Pressing	New mold design using tapered ring to restrict side motion. Optimize pressure, temperature, and time relationship.
3. Porous Interface	Provide a "more flowable" extrudable mix. Use vacuum and isopressing to cold bond segments. Optimize temperature, pressure relationship.
4. Undensified Powder Fill	Increase charge size -- Precompact by isopressing but not yet totally successful.
5. Core Strength Improvement	Hot pressing to net shape. Strengths up to 73,000 psi obtained on 3 inches D x 1/4 inch thick plates.

To date, one bonded simulated rotor was delivered and spin tested at Garrett. The assembly consisted of an isopressed and machined core which had a sintered density of 2.62 g/cc (81.5 percent theoretical), bonded to a sintered injection molded shell. The speed attained at failure was 72,400 rpm. A failure analysis performed by Garrett indicated that fracture originated within the core and that the maximum principal stress attained was 16.3 ksi.

The results from the failure analysis indicated the need to improve the strength of the core material. A concentrated effort was initiated to achieve material improvement using hot pressing techniques since prior work indicated that adequate strengths could be obtained in this manner.

Additional rotors have been produced using hot pressed cores and are available for spin testing.

3. STATIC STRUCTURES

3.1 Turbine Stator

By mutual agreement, the stator configuration being fabricated by Carborundum for the AGT101 engine is segmented. The injection molding process is being used. Tooling was received and initial molding trials were conducted to assess dimensional accuracy and functional quality. Minor gating changes were required and were completed. First articles were produced using a matrix of molding variables from which conditions were selected to produce deliverable components.

3.2 Turbine Shroud

Injection molding was selected to produce the shroud since the part has a variable wall thickness and precise contours. The tool has been completed and delivered to G-W Plastics where molding will be carried out. Since the finished part weighs approximately 10 pounds, it represents the largest single piece ever injection molded in sintered alpha SiC. In order to fill the mold, a flow molding sequence on a 300-ton press will be used. This technique uses the machine screw for partial filling followed by forward screw motion for final packing thereby allowing a large part to be formed in a relatively small press. Approximately 500 pounds of molding compound was prepared for injection molding development.

3.3 Duct Spacer

A total of 30 pieces have been completed and delivered for use in the AGT101 engine.

3.4 Regenerator Shield

Eleven pieces have been delivered to the grinding supplier for finish machining.

3.5 Turbine Backshroud

Billets have been produced for green machining. A template has been designed and procured for final shaping.

3.6 Inner Diffuser

The model for slip casting has been obtained. The mold has been fabricated. Fabrication development has been deferred due to funding limitations.

3.7 Outer Diffuser

The model for slip casting has been obtained and the mold has been fabricated. Fabrication efforts have been deferred due to funding limitations.

APPENDIX V

PURE CARBON COMPANY

ADVANCED GAS TURBINE (AGT) POWERTRAIN PROGRAM
SECOND SEMI-ANNUAL TECHNICAL
PROGRESS REPORT

Pure Carbon Co., acting as British Nuclear Fuel Ltd (BNFL) U.S. distributor, will provide simulated rotors and test bars of Refel reaction-sintered SiC for AGT101 evaluation. Reaction-sintered SiC products are fabricated by a process in which a porous SiC/carbon body is exposed to silicon at elevated temperatures and the carbon is converted to bonding SiC. No material shrinkage occurs during the conversion process. "Green" materials to be reaction sintered may be formed by a variety of routes, e.g., slip casting, injection molding, extrusion, isopressing and warm molding, and the green body may be machined before firing. Requirements of binder removal prior to firing and silicon penetration during firing, however, impose thick section limitations on component geometries. These limitations are determined experimentally, although penetration up to one inch has been demonstrated.

Based on these known limitations, BNFL has performed a study to demonstrate binder bake-out and carbon conversion in the thick rotor sections prior to the initiation of a rotor fabrication development program. For expediency, this study is being performed using isopressed and green machined simulated rotors. One such rotor was fabricated using this method and was evaluated using X-ray NDE techniques. No signs of unreacted region were identified and this rotor was forwarded to Garrett.

Subsequently, six additional simulated rotors have been isopressed, machined, and reacted. Shipment of 3 rotors to Garrett will follow NDE evaluations.

In addition, test plates of isopressed and slip cast Refel materials have been prepared for shipment to Garrett for characterization. Test bars of injection molded material will be prepared as soon as the injection molding tooling is completed.

The following list provides definitions of acronyms as used in this document.

ACC - AiResearch Casting Company
AGT - Advanced Gas Turbine
AOD - Automatic Overdrive Transmission
APU - Auxiliary Power Unit
AS - Aluminum Silicate
BNFL - British Nuclear Fuels Ltd
CBO - Carborundum
CFDC - Combined Federal Driving Cycle
CPS - Cumulative Probability of Success
DARPA - Defense Advanced Research Project Agency
DOE - Department of Energy
DS - Directionally Solidified
EDX - Energy Dispersive X-Ray Analysis
EPA - Environmental Protection Agency
HIP - Hot Isostatic Pressing
HP - High Pressure Side, Air Side
LAS - Lithium Aluminum Silicate
LP - Low Pressure Side, Gas Side
MAS - Magnesium Aluminum Silicate
Mod I - Evolutionary Version of RPD - Metallic Engine
Mod II - Evolutionary Version of RPD - Ceramic Engine
MOR - Modulus of Rupture
ONR - Office of Naval Research

PM	- Powder Metal
PM/PV	- Premixed Prevaporizing
RBSN	- Reaction Bonded Silicon Nitride
RPD	- Reference Powertrain Design
SASC	- Sintered Alpha Silicon Carbide
SEM	- Scanning Electron Microscopy
SI	- Spark Ignition
SiC	- Silicon Carbide
Si ₃ N ₄	- Silicon Nitride
SLAM	- Scanning Laser-Acoustic Microscopy
SPAM	- Scanning Photo-Acoustic Microscopy
SRBSN	- Sintered Reaction Bonded Silicon Nitride
SSN	- Sintered Silicon Nitride
TE	- Trailing Edge
TIT	- Turbine Inlet Temperature
VIGV	- Variable Inlet Guide Vane
VSTC	- Variable Stator Torque Converter
WOT	- Wide Open Throttle (Maximum Power)

REFERENCES

1. "Advanced Gas Turbine (AGT) Powertrain System Development for Automotive Application," Progress Report Number 1 (October 1979 - June 1980), NASA CR-165175, prepared for NASA by Garrett Turbine Engine Co., under Contract DEN3-167, November 1980.
2. Richerson, D. W., Lindberg, L. J., and Dins, C., "Ceramic Gas Turbine Engine Demonstration Program," Garrett Report Interim Report No. 17 (Quarterly), Navy Contract N00024-76-C5352, May 1980.
3. Richerson, D. W., Carruthers, W. D., and Lindberg, L. J., "Contact Stress and Coefficient of Friction Effects on Ceramic Interfaces," to be published in the Proceedings of the Conference on Surfaces and Interfaces in Ceramic and Ceramic-Metal Systems, presented at Berkeley, California, July 30, 1980.
4. Richerson, D. W., Lindberg, L. J., and Carruthers, W. D., "Contact Stress at Ceramic Interfaces," paper presented at Highway Vehicle System Contractor's Coordination Meeting, October 1980.
5. Finger, D. G., "Contact Stress Analysis of Ceramic-to-Metal Interfaces," Final Report, ONR Contract N0014-78-C-0547, September 1979.
6. Carruthers, W. D., Richerson, D. W., and Benn, K. W., "3500-Hour Durability Testing of Commercial Ceramic Materials," Interim Report, NASA CR-159785, July 1980.
7. K. H. Hardtl, "Gas Isostatic Hot Pressing Without Moldes," Bull. Amer. Ceram. Soc., Vol. 54, No. 2, 1975, p. 201.
8. C. D. Greskovich, J. A. Palm, "Development of High Performance Sintered Si_3N_4 ," AMMRC TR-80-46, Sept. 1980.
9. D. C. Larsen, "Property Screening and Evaluation of Ceramic Turbine Engine Materials," AFML-TR-80-4188, Oct. 1979.
10. J. T. Smith, C. L. Quackenbush, "Phase Effects in Si_3N_4 Containing Y_2O_3 or CeO_2 : II Oxidation," Bull. Amer. Ceram. Soc., Vol. 59, No. 5, 1980, p. 533.